Dissertation for Doctoral Degree

Characteristics comparison of SP-LIBS and long-short DP-LIBS for steel measurement

A dissertation submitted to
Tokushima University
in partial fulfillment of the requirements
for the doctor degree

Mechanical engineering
Intelligent structures and mechanics system engineering
Tokushima University
Renwei Liu
Supervisor: Prof. Yoshihiro Deguchi; Prof. Jiping Liu
Co-supervisor: Asso. Prof. Zhenzhen Wang
September 2020

Abstract

Laser induced breakdown spectroscopy (LIBS) has high potential for on-line measurement and is of great significance to the steel industry. On-line steel measurement faces some challenges. During the manufacturing process, the sample temperature will change. There are many lines of iron. These all affect the measurement accuracy and plasma analysis.

In this study, we established an experimental system to evaluate how sample temperature affects LIBS measurement of solid steel. The spectra at different sample temperatures are compared, and the influence of Boltzmann spectra on plasma temperature and the density of Fe atoms in plasma is analyzed. The influence of sample temperature on accuracy was quantitatively analyzed.

The long-short DP-LIBS method was proposed and applied to the measurement of solid steel at different sample temperatures. The aim is to eliminate the influence of sample temperature on plasma. In this way, quantitative measurement results can be obtained.

When the sample temperature increases from room temperature, the plasma temperature does not increase obviously, but the total Fe atom number and Fe+ ion number increase. The plasma temperature calculated by Fe atoms is lower than that calculated by Fe+ ions, and the number of Fe atoms is much larger than that of Fe+ ions. This is consistent with the thermal theory and also shows the inhomogeneity inside the plasma. When the sample temperature changes, the variation of each Fe line is also uneven, which can be observed by Boltzmann diagram.

For the quantitative analysis of Mn, the Mn atom line is more robust than the Mn ion line. Mn atomic wires have less interference with Fe atomic wires and are sensitive to components at the evaluated sample temperature. The second-order multivariate PLS based on Mn atomic lines has higher accuracy, which shows that plasma is a nonlinear system. Adding more information and less interference to the quantitative model is helpful to improve the accuracy.

DP-LIBS method has obvious advantages in the determination of iron. The signal is stable and the fluctuation is small. The sample temperature has less interference to the steel measurement because the surface condition is more stable. The quantitative measurement accuracy of long and short DP-LIBS is higher than that of SP-LIBS.

Keywords: Laser-Induced Breakdown Spectroscopy (LIBS), Sample Temperature Effect, Boltzmann Plot, Quantitative Analysis, Long-Short DP-LIBS

Contents

1 Introduction

1.1 Background and Significance

Steel is one of the most widely used metals in industrial fields, such as architecture, power plant, nuclear industry, ocean applications and so on[1][4]. For different working conditions, the characteristic requirements of steel are very different.

The elemental compositions are one of the most important factors for its characteristics [5][6]. The manufacture processes are important processes to control the steel compositions. The manufacture processes generally include blast furnace, converter, ladle, continuous casting, and finished goods [7]. For the continuous and huge amount production, the rapid on-line analysis of steel components is important to control the quality of steel-making process.

Therefore, advanced control and measurement technologies are required in the steel production line. While traditional chemical analysis method cannot support the fast requirements. Because it comprises a series of steps: take a sample from the processing line, transport to an inspection apparatus or to a laboratory, separation of impurities, preparation for the chemical analysis, and determination of the composition. A series of processes require extra time.

Some laser diagnostic analysis methods of steel have been put forward with more or less success, such as X-ray fluorescence spectroscopy [8], spark discharge-optical emission spectrometry, absorption spectroscopy and spark optical emission spectroscopy [9]. However, due to the need of sample preparation, cost and other aspects, these methods are difficult to be applied for on-line real-time analysis of element compositions of iron and steel products. Laser induced breakdown spectroscopy (LIBS) is an alternative laser diagnostic method to develop on-line qualitative and quantitative multi-element analytical instruments for iron and steel production, which can be used for a variety of materials, such as solids, gas and liquids.

LIBS is an attractive elemental measurement method. For it has some merits such as real-time fast detection, standoff analysis capabilities; quasi nondestructive ablation; low sample consumption; simultaneous all-element detection; safe operation; and necessitating only optical access with little or no sample preparation [10].

1.2 Research Status

LIBS is an element analysis method based on atomic emission spectrometry. Pulse laser is focused on surface of the material to generate plasma, and the emission of plasma is collected by spectrometer and detector. The qualitative and quantitative measurement of sample can be realized by calculating wavelength and emission intensities of the characteristic lines [11].

It has attracted many researchers to study LIBS, and nowadays there are some important achievements in LIBS physics, applications and quantitative measurement.

1.2.1 Increased Research of LIBS

The increasing number of the LIBS research publication indicates LIBS has high potential

and attraction [12][13]. Because LIBS can be applied in many fields, such as coal and fly ash analysis, metal analysis, soil analysis, aqueous solution analysis, nuclear, agricultural product analysis, explosive and gas, and other applications. For metal measurement, the steel, copper and aluminum is the research hotspots for their extensive applications.

The research points of LIBS are mainly focused on plasma physics, measurement apparatus, sample preparation and matrix effects, measurement environment, and quantitative methods [10]. Xu Lin et al. [14] used LIBS to replace the common ICP-MS method in the identification and measurement of iron ore to realize rapid beneficiation. Because LIBS spectral information is noisy, wavelet transform and principal component analysis filter are used to get effective information. K-means and artificial neural network are used to screen five kinds of iron ore respectively. The results show that the k-means method is simple and efficient, while the artificial neural network method has excellent performance. Guo Guangmeng et al. [15] developed a modular compact LIBS measurement system to meet the environmental requirements of soil and liquid pollutant measurement. The detection limit of Cu and Zn in soil is 0.039%, and the RSD is 8%. The detection limit of Cu in liquid is 25 μg/g, RSD is more than 25%. In the actual environmental protection measurement, it is possible to face the solid-phase liquid samples at the same time. Therefore, it is necessary to observe the crystal structure of the samples, and combine LIBS and Raman to obtain the online measurement equipment without mutual interference. The method based on multi variable signal input can improve the measurement ability of trace elements such as Ba and Cr, and support vector machine has higher stability than partial least square method. However, the prediction error of partial least square method for matrix effect is smaller than that of support vector machine, which shows better prediction ability. Takahashi et al. [16] used LIBS to measure Cu, Pb, Zn deposits in 1000ms deep sea, with a relative error of 25%. Because of the interference of the marine environment, the breakdown rate of the plasma fluctuates greatly. The 150ns pulse width laser beam is used to supplement the energy of the plasma, which makes the plasma stable. Fang Fang et al. [17] used LIBS to measure the concentration of heavy metals Cd, Cu, Pb in navel orange peel. Using partial least square method to establish the quantitative model, the relative errors are 9.14%, 8.05 and 6.87% respectively. Cisewski et al. [18] used LIBS to measure whether there were spores of Bacillus anthracis in the suspicious powder. Because of the variability of their composition and the complexity of their signals, they used support vector machine to establish a classification model and realized the classification ability of Bacillus anthracis spores. Gottfried et al. [19] studied the detection of high-energy substances such as explosive residues by LIBS. Due to the existence of N and O in the air, which hindered the measurement accuracy, the Ar gas was used as a buffer to realize remote measurement at distance of 20 m using the double pulse laser beam. The partial least square method is used to classify and prove the ability to identify high energy materials. Bottom et al. [20] reviewed the application of LIBS in cultural heritage and archaeology. Because LIBS has the advantages of low damage to the tested samples, good environmental adaptability, and portable equipment, it can be used to measure cultural relics such as bronzes, stone carvings or water sinks. Because it is difficult to prepare standard samples, it is necessary to use LIBS without standard samples for quantitative measurement, which is called Calibration-Free LIBS. Using fs laser can realize the thickness layered detection of cultural relics.

1.2.2 LIBS Measurement of Steel Sample

The analytical tasks of LIBS for the steel industry can be classified into two groups [7]: 1, bulk analysis of the elements compositions. 2, maps of elementals distributions on surface [21]. Besides the measurement of steel sample, the top gas of the furnace and the slags are also the important targets for measurement. Compared with the other targets, the measurement of the steel in manufacture process has some unique challenges. The situations of steel have various change during manufacture processes, the remote distance measurement is required for hot sample temperature, the complex of Fe lines also have some interferences with other target element lines, and so on. Therefore, to improve LIBS measurement accuracy, many scholars studied the application in the steel-making process.

Aragón et al. used LIBS method to detect the carbon content of molten steel samples in a laboratory induction furnace and proved that this method can be used for the direct determination of alloy melt composition [22]. Palanco et al. designed an open-path laser-induced plasma spectrometer (OP-LIPS) and proved it is a reliable technology to identify the composition changes of hot-solid and liquid stainless steel [23]. Sun et al. used LIBS method to carry out multi-element quantitative analysis of steel sample and obtained good measurement results, and BPNN quantitative model helps to increase the measurement accuracy [24]. Li et al. also applied LIBS to quantitative analysis of phosphorus both in pig iron and low alloy steel in air atmosphere [25].

In recent years, in order to improve the industrial application of LIBS, many researchers developed LIBS technique to enhance and stabilize laser-induced plasma, in which the use of external energy is an effective method and has been widely studied. Andrey M. Popov et al. developed a small chamber to maintain plasma temperature for higher breakdown [26]. Sobral H et al. added a fast high voltage square-shaped electrical pulse to enhance the analytical capabilities of LIBS [27].

The process of steel production is extremely complicate. The changes of sample temperature and morphology are involved in this process, which will greatly affect the real-time measurement accuracy of LIBS. Some researchers have studied the influence of steel sample temperature on LIBS measurement results.

Palanco et al. analyzed the influence of steel temperature on LIBS measurements for high alloy steel samples heated up to 1200°C. The results shown that the signal emission intensity was obviously affected by sample temperature. When the temperature was above 600°C, the surface composition changes due to the formation of variable thickness slag layer, which will have an impact on the measurement results [28]. Zhigilei et al. found that the increased sample temperature can decrease the ablation threshold and increase the intensity of the spectral line according to simulation calculations [29]. Eschlböck-Fuchs et al. studied the effect of sample temperature on the laser-induced plasma dynamics and emission intensity for different solid sample [30]. The results shown that spectral intensity of all samples increased with the increase of sample temperature. The other researchers also emphasized that sample temperature can change the ablated craters and the signal intensities [31]-[33].

1.2.3 Improvement of DP-LIBS

The above study shows that the complicate sample situations, especially the sample temperature affects the signal intensity and plasma stability, which will affect the application of LIBS on-line measurement of steel. Therefore, a method is necessary to stabilize the plasma and improve the LIBS ability to measure steel on-line. Double-pulse LIBS is a promising way to enhance the analytical performance in practical application.

The experimental results have proved that double-pulse LIBS is an effective method to enhance the signal intensity and improve the plasma stability. Jiang. X et al. have investigated the steel lines in the shorter wavelength vacuum ultraviolet regions, the signal was enhanced using nanosecond double-pulse lasers [34]. Lu Y, Zorba V et al. applied the combination of fs-laser and ns-laser to improve the analytical capabilities of LIBS, and the limits of detection (LOD) was also improved [35]. Rizwan Ahmed et al. coupled first 1064nm laser and second 532nm laser for double pulse configurations to measure aluminum, and the signal intensity was enhanced three hundred times [36].

V. I. Babushok et al. emphasized the basic rule of using DP-LIBS [37], the configurations are flexible, such as collinear, orthogonal pre-spark, orthogonal pre-heating and dual pulse crossed beam modes. In addition, combinations of laser pulses with different wavelengths, different energies and durations were studied, thus providing flexibility in the choice of wavelength, pulse width, energy and pulse sequence. Usually, the double pulse technique leads to a better coupling of the laser beam with the plasma plume and target material, thus providing a more temporally effective energy delivery to the plasma and target. So the enhancement of signal intensity can be up to two orders of magnitude greater than a conventional single pulse laser.

R. Sanginés et al. has compared the orthogonal double pulse method and the single pulse method on sample temperature heated [38]. And they proposed that the double pulse method is like the method of improving sample temperature, which will increase the ablated mass.

1.3 Contents and Structure of This Dissertation

In this study, two experimental systems were established to measure the solid steels under different sample temperatures. Plasma states were calculated and the quantitative analysis was adopted. Fe occupies the maximum content in steel, so use Fe lines to calculate plasma states. Mn element is the target element in steel, to evaluate the quantitative measurement accuracy.

Firstly, the basic LIBS system was set up for the properties evaluations. Chemical standard steel samples were measured. By using Boltzmann Plot, the plasma states were calculated. The quantitative behaviors of Mn ion lines and atom lines were compared.

To improve the steel measurement behavior, the collinear long-short DP-LIBS was employed to discuss the sample temperature effect on steel measurement for the improvement of LIBS technique. The standard bulk steel samples with different sample temperature were measured by single pulse LIBS (SP-LIBS) and collinear long-short DP-LIBS respectively to systematically study the sample temperature effects for steel measurement. Furthermore, the comparative analysis has been carried out from several aspects between SP-LIBS and long-short DP-LIBS to evaluate the detection ability of collinear long-short DP-LIBS at different sample temperature.

Finally, the quantitative measurements using SP-LIBS and DP-LIBS method were compared.

2 Theory of Laser-Induced Breakdown Spectroscopy

2.1 LIBS Measurement Processes

During LIBS measurement, the plasma generation and cooling down follow a series of processes [10][39]. The processes are presented as Fig.2-1. After laser beam is coupled with sample surface, a part of surface is vaporized, and then the material vapor is atomized and ionized, after plasma is generated, it expands to excite the surrounding gas breakdown. After the laser pulse, the plasma cannot obtain energy for reheating, and it cools down. The electron in plasma includes the free electron and excited electron in atoms. When the plasma cools down, the free electrons become slow and combine with ions, which will make the continuous backgrounds emissions. When excited atoms cool down, the electrons at higher energy levels fall to lower energy levels, making the characteristic lines emissions. Different elements have different spectral lines, for their energy levels structure inside atoms are different, so the spectral lines of different elements are different.

Usually, the continuous backgrounds emissions have faster cooling down speed than the characteristic lines, so set an operate delay time is necessary, to discard the continuous backgrounds emissions and maintain the obvious characteristic emissions. For research, different delay time are set, to record the plasma cooling down processes.

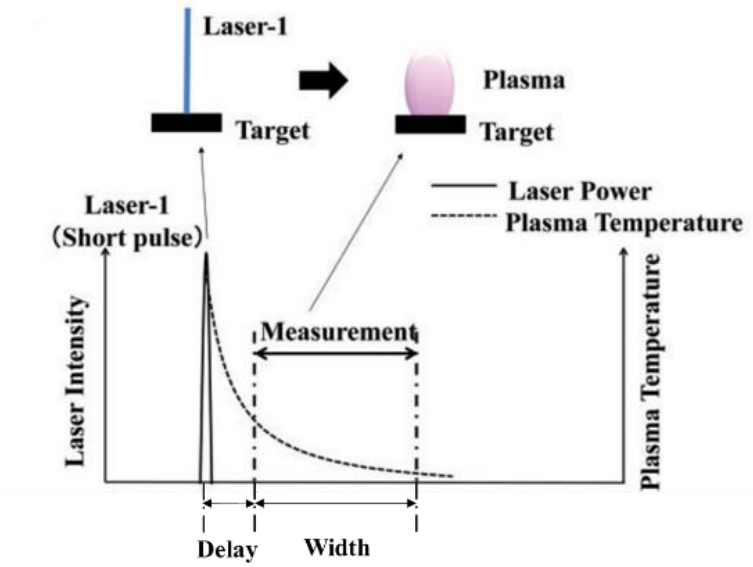

Fig.2-1 The basic process of plasma and LIBS measurement (SP-LIBS)

2.2 Spectral Lines and Boltzmann Plot Analysis

The reason why sample temperature changes the LIBS signal is that it changes plasma states. So the analysis of plasma states is necessary. Boltzmann Plot is an important analysis method for plasma [40][43]. It is based on the local thermal equilibrium (LTE) theory [44][46]. The intensity I of spectral lines of the same emission particles obey the relation as following

equation Eq.(2-1).

$$I_{s,i} = K\frac{hc}{\lambda_i}A_i\frac{N_s}{Z_s(T)}g_i\exp\left(-\frac{E_i}{kT}\right) \qquad \text{Eq.(2-1)}$$

$$\begin{aligned}\ln\left(\frac{I\lambda_i}{A_i g_i}\right) &= \ln(Khc) + \ln\left(\frac{C_s}{Z_s(T)}\right) - \frac{E_i}{kT} \\ &= \ln(Khc) + \ln(C_s) - \frac{n}{2}\int\partial\left[\ln(T)\right] - \frac{E_i}{kT} \\ &\approx \ln(C_s) - \frac{E_i}{kT}\end{aligned}$$

Where K is the light sensitivity coefficient of sensor; h is the Plank constant; c is the speed of light; λ_i is spectral line wavelength; A_i is the transition probability of the spectral line; C_s is the atoms or ions number of corresponding emission species; $Z_s(T)$ is the partition function of corresponding emission species; g_i is the degeneracy of the high energy level of spectral line; E_i is the upper energy level of the spectral line; T is plasma temperature; k is the Boltzmann constant. n is a coefficient has the relation with heat capacity of emission species gas [44], and when the atoms and ions number of the emission element is big enough, the other part of the intercept can be ignored. Therefore, by using the Boltzmann Plot, T and C_s can be estimated.

For practical analysis, the precise plasma temperature is difficult to calculate for each point of Boltzmann Plot may have some fluctuations. So the plasma temperature factor is defined, as the ratio of two spectral lines from the same element. The definition of plasma temperature is as following formula Eq.(2-2). When the upper energy levels of two spectral lines are of larger differences, the plasma temperature factor is more sensitive to the plasma temperature change. When the ratio is the higher upper level to lower upper level, the ratio is larger when plasma temperature is higher.

$$\frac{I_{s,i1}}{I_{s,i2}} = K'\frac{A_{i1}g_{i1}\lambda_{i2}}{A_{i2}g_{i2}\lambda_{i1}}\exp\left(-\frac{E_{i1}-E_{i2}}{kT}\right) \qquad \text{Eq.(2-2)}$$

Some researchers also pointed out that the Boltzmann Plot can also be applied for quantitative measurement [47]. But it requires the enough numbers of spectral lines and accuracy.

Free electron number density is also an important plasma states factor, which is connected with the line broadening (Full Wave at Half Maximum, FWHM) of spectral lines. The calculation of electron number density is as following Eq.(2-3).

$$\Delta\lambda_{specline} = \Delta\lambda_{measured} - \Delta\lambda_{equipment}$$

$$\begin{aligned}\Delta\lambda_{specline} = \Delta\lambda_{FWHM} &= 2\omega\left(\frac{N_e}{10^{16}}\right) + 3.5\alpha\left(\frac{N_e}{10^{16}}\right)^{1/4}\left(1-\frac{3}{4}N_D^{-1/3}\right)\omega\left(\frac{N_e}{10^{16}}\right) \\ &\approx 2\omega\left(\frac{N_e}{10^{16}}\right)\end{aligned} \qquad \text{Eq.(2-3)}$$

Where N_e is the number density of electrons, and ω is the electron collision coefficient. The calculation of the spectral line FWHM should consider the line broadening of the equipment,

which is a fixed number for a spectrometer. ω is also fixed for a certain characteristic spectral line. Therefore, for convenient discussion, the FWHM of spectral line can be the electron number density factor. When the FWHM of line is larger, the electron number density is higher.

2.3 Long-Short Dual-Pulse LIBS Method

The collinear long-short dual-pulse laser-induced breakdown spectroscopy (long-short DP-LIBS) method has been studied to measure steel sample. The collinear configuration of lasers is very suitable for the steel on-line, for it can be applied for the remote measurement. It demonstrated the feasibility and enhanced detection ability of long-short DP-LIBS method due to pre-heating and re-heating effects of long pulse. Yoshihiro Deguchi, Wang et al. have proposed the structure of long-short DP-LIBS lasers configuration [48]. Signals enhancement for steel measurement and aluminum under water was testified. Plasma temperature was more stable with long-short DP-LIBS. Cui have applied the long-short DP-LIBS in the measurement of steel [49][50]. Signal enhancement and plasma states were compared, and the plasma photo were analyzed. For SP-LIBS, plasma is near the sample surface, while for long-short DP-LIBS, plasma has more abundant expand, while free-running long pulse laser cannot induce plasma.

The schematic diagram of laser pulse configuration of long-short DP-LIBS is shown in Fig.2-2, where the conventional DP-LIBS laser configuration is also presented for explanation. For long-short DP-LIBS, the laser-induced plasma was generated by the short pulse-width laser and the external energy was supplied by the long pulse-width laser with the pulse width of 60ms under free running (FR) conditions, which means the Q value of optical resonant cavity does not change during laser pulse formation, to sustain the plasma to improve the detection ability and feasibility in the real applications due to its collinear configuration.

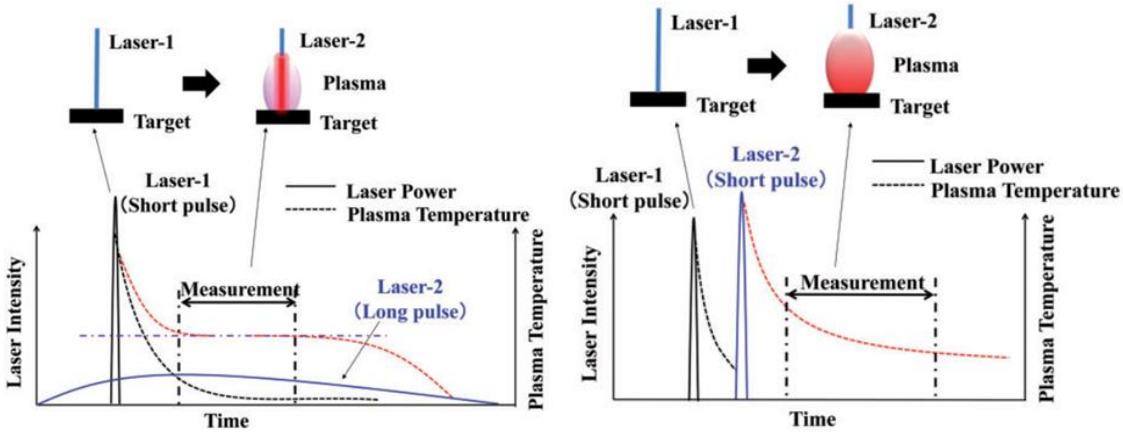

(a) long-short DP-LIBS (b) conventional DP-LIBS

Fig.2-2 The basic process of plasma and LIBS measurement (SP-LIBS)

Generally, DP-LIBS can enhance the signal intensities and plasma existing time. The plasma temperature is usually not uniform according to the spatial and temporal distribution. While conventional DP-LIBS makes the temperature distribution not uniform and fluctuated. In the case of long and short DP-LIBS, the plasma temperature can be maintained at a certain higher level along the long pulse-width laser path without obvious undesirable effect. The plasma

generated by the short pulse-width laser is stabilized and maintained at a high temperature during the plasma cooling process by long pulse-width laser radiation. It is significant for laser-induced plasma processes. Besides, long-short DP-LIBS also may have the other merits. Firstly, long-pulse width laser radiation has the cleaning and pre-treatment effects of the target surface while the short-pulse laser is to induce the plasma. Secondly, optical fiber delivery is easy for the long pulse-width laser radiation because peak laser intensity is low. Thirdly, the self-absorption effect is supposed to be reduced by restricting the hot plasma region by the long pulse-width laser radiation.

2.4 Quantitative Analysis Methods

The qualitative measurement of LIBS is relative easy, while the quantitative measurement is usually affected by the matrix effect and surrounding environment influence. Many research testified the LIBS quantitative measurement ability for both solid and liquid steel, with certain calibration methods such as experimental conditions optimization and data processing [51][59]. The key process of quantitative method is to establish a function between the mass fraction of element and LIBS signal intensity. According to Eq.(2-1), LIBS target element signal has the linear increase with the element mass component, as following Eq.(2-4).

$$C_s = C_0 + a_{s,1} I_s \qquad \text{Eq.(2-4)}$$

Because of LIBS signals instability, and the inhomogeneity of plasma, the quantitative measurement based on only the target spectral line is always not enough [60]. The quantitative method based on the machine learning theory is commonly applied in LIBS measurement, such as Partial Least-Square (PLS), Artificial Neural Network (ANN) and Support Vector Machine (SVM). Different kinds of samples, or different target elements of samples, have their own suitable model types. Quantitative models also need to be matched with pretreatment methods to achieve better robustness and measurement accuracy [61].

The multivariate method is always preferred, and PLS method is one of the common applied method for LIBS [62][65]. According to the dominant factor theory in PLS method, one of the common accepted model is as following Eq.(2-5). In this function, besides the target element signals, the other elements signals in samples are also considered, which means the multi-variates. When in major research work only the linear terms are considered, the second order intensity can be also considered, for plasma in LIBS is always not a linear system. The non-linear factor should be considered.

$$C_s = C_0 + a_{s,1} I_s + a_{s,2} I_s^2 + \sum_i a_{i,1} I_i + a_{i,2} I_i^2 \qquad \text{Eq.(2-5)}$$

There are many forms of ANN, the most basic of which is the back propagation neural network (BPNN), which refers to the training method of adjusting the weight of each neuron with the error of the output actual value and the target value when training the model. The basic neuron structure consists of summation node and activation function. The summation node and activation function are shown in formula Eq.(2-6). F function is a classical sigmoid function. When constructing neural network, multiple neurons can be used to form a multi-level and multi structure form in the hidden layer. Due to the nonlinearity of activation function, neural network is nonlinear in physical sense. At the same time, because of the flexibility of the hidden

layer structure, it is difficult to solve directly, so it is necessary to set the initial weight network and learning rate. The difference between the predicted value of the model and the actual value is gradually corrected by reverse transmission, and the response ratio to the error is the learning rate. The lower the learning rate is, the slower the fitting speed is, but the accuracy will be improved.

$$\begin{cases} SUM: \quad v=\alpha_1 x_1+...+\alpha_1 x_1+b \\ F: \qquad\quad F=\dfrac{1}{1+e^{-v}} \end{cases} \qquad \text{Eq.(2-6)}$$

The structural parameters of BPNN model need to be determined first are the number of layers of hidden layer and the number of neurons in each layer. The purpose of model training is to determine the synaptic weight of each neuron node, α_n. The training result of BPNN model is also related to the training process. The parameters of training process to be determined are initial weight and learning rate.

In SVM, the definition of support vector is the segmentation boundary of the sample maximum interval in the two classification model, and the reciprocal of the spacing of the segmentation boundary is $1/2\|\omega\|$ [66][67]. The kernel function is used to map the independent variables of samples to a hyperplane, so that different types of samples have convex boundaries in the hyperplane. The support vector is obtained by quadratic programming. After development, SVM method has developed C-SVM for classification and ε-SVM for quantitative fitting. When classifying, the form of C-SVM is to construct an objective function, such as formula Eq.(2-7), to minimize the value of the objective function, so that the divided data set has the maximum interval.

$$\phi(\omega,\xi)=\frac{1}{2}\|\omega\|^2+C\sum_{i=1}^{N}\xi_i \qquad \text{Eq.(2-7)}$$

In the formula, ξ is the relaxation factor, which refers to the number of samples allowed to be mistakenly divided; C is the normal number of constraint error range, which is called the penalty factor; N is the number of training set samples. The Lagrange multiplier method is used to rewrite the objective function into a programming problem as shown in formula Eq.(2-8). In formula, α_n is the coefficients to be determined through model training. *K* is the kernel function, which determines the property of the model. The wide used *K* is listed in Eq.(2-9)[68].

$$\begin{cases} \max \sum_{i=1}^{N}\alpha_i-\frac{1}{2}\sum_{i=1}^{N}\sum_{j=1}^{N}\alpha_i\alpha_j y_i y_j K\left(X_i,X_j\right) \\ \quad s.t. \quad 0\le\alpha_i\le C \quad i=1,2,...\mathrm{N} \\ \qquad\qquad \sum_{i=1}^{N}\alpha_i y_i=0 \end{cases} \qquad \text{Eq.(2-8)}$$

Linear kernel function: $K\left(x_i, x_j\right) = x_i^T x_j$

Polynomial kernel function: $K\left(x_i, x_j\right) = \left(\gamma\left(x_i^T x_j\right) + r\right)^q$ Eq.(2-9)

Radial basis kernel function: $K\left(x_i, x_j\right) = \exp\left(\frac{-\left|x_i - x_j\right|^2}{2R^2}\right)$

Therefore, to evaluate the training effect of the quantitative model, we need to evaluate the effect of fitting training and the prediction ability of other samples [69][71]. The specific indexes of fitting performance are: *Slope*, R^2, root mean square error of calibration (RMSEC); the specific indexes of predicting performance are: average relative error (ARE), root mean square error of prediction, RMSEP), average relative standard deviation (ARSD). *Slope* is the slope of the calibration curve of the fitting point, and the other factors are calculated as Eq.(2-10).

$$R^2 = \left(\frac{\sum_{i=1}^{n}\left(x_i - \bar{x}\right)\left(c_i - \bar{c}\right)}{\sqrt{\sum_{i=1}^{n}\left(x_i - \bar{x}\right)^2 \mathrm{g}\left(c_i - \bar{c}\right)^2}}\right)^2 \quad \text{Eq.(2-10)}$$

$$RMSEC = \sqrt{\frac{\sum_{i}^{n}\left(x_i - c_i\right)^2}{n}}$$

$$ARE = \frac{1}{m}\sum_{i=1}^{m}\frac{\left|y_i - v_i\right| \times 100\%}{v_i}$$

$$RMSEP = \sqrt{\frac{\sum_{i}^{m}\left(y_i - v_i\right)^2}{m}}$$

$$ARSD = \frac{1}{m}\sum_{i=1}^{m} RSD_i = \frac{1}{m}\sum_{i=1}^{m}\frac{1}{y_i}\sqrt{\sum_{j=1}^{t}\frac{\left(y_{ij} - \bar{y}_i\right)^2}{t-1}}$$

Where, x is the calculated value of the model of the fitting point, c is the stoichiometric value of the fitting point, n is the total signal number of the fitting point, y is the calculated value of the model of the prediction point, v is the stoichiometric value of the prediction point, m is the total signal number of the prediction point, and t is the number of experimental repetitions corresponding to the target element content.

The higher the R^2 is (maximum is 1), the better regression quality the model is. The smaller the *RMSEP* is, the better prediction quality the model is. Sometimes, it is not easy to select which sample is good for validation, and the total prediction ability of the model should be considered. Limit of detection (LOD) is calculated for this evaluation. As following definition Eq.(2-11).

$$LOD = 3\frac{ASTD}{Slope} \quad \text{Eq.(2-11)}$$

ASTD is the average standard deviations of all regression points, and *Slope* is the calibration curves of the quantitative model

The quantitative model obtained in machine learning method has its limitation. For the fixed model category and training sample set, selecting a set of optimized model parameters can get better quantitative results, but such optimization often has no physical explanation. The trained quantitative model is also expected to have good component prediction ability for other unknown samples. However, due to the lack of physical explanation, it is difficult to determine the applicability of the quantitative model to unknown samples. Therefore, in this study, in addition to optimizing the parameters of the model to get better results, we also need to analyze the plasma state, and explain the reasons that limit the accuracy and application range of the quantitative model. At the same time, based on the plasma state, the method of optimizing the quantitative model should be analyzed to make the optimization method more universal.

Up to now, there are many research of PLS, ANN and SVM on LIBS measurement. PLS is a simple model form, and its physical meaning is easy to understand. Yao et al.[64] Pointed out that when measuring the ash content of coal, using C, Si, Al, Fe, Ca, Mg, Na, Ti and K signals as multiple input vectors and PLSR as model, the relative error of ash content was 6.94% and the detection limit was 1.73%. Zhao et al.[72] summarized the improvement methods of PLS, including using quadratic polynomial PLS, adding dominant factor PLS, combining with wavelet transform PLS, plasma state standardization PLS, mixing with main element or support vector machine PLS, and so on.

Zhang et al.[73] Used SiO_2, Al_2O_3, Fe_2O_3, Cao, MgO, MnO_2, TiO_2 and graphite C to configure 45 kinds of imitated fly ash samples, and used WNN with main element analysis function to realize the screening of abnormal spectral lines and the classification of coal, which has better fitting effect than the traditional artificial neural network. He et al.[74] used BPNN to measure C element in steel, because C line is easy to be interfered by Fe line, use genetic algorithm (GA) to optimize the input signal structure, reduce the interference of C signal, after correction, the linear correlation increases significantly. Farhadian et al. [75] used the method of principal element analysis combined with ANN to improve the input vector when only ANN was used in LIBS measurement of high energy materials such as TNT, which significantly reduced the fitting residual. Lu et al.[76] used ANN to establish the corresponding relationship between LIBS spectral data and coal calorific value, because there is no unified theory to explain the model structure setting method, ANN's neuron structure often needs repeated trial and error to ensure the fitting accuracy and prediction accuracy at the same time. Genetic algorithm is used to optimize the network structure and construct a composite neural network, so that the average error of calorific value prediction is 0.39mj/kg, which meets the requirement of 0.8mj/kg in the national standard GB / T 29161-2012.

Dastjerdi et al. [77] used LIBS measurement to classify PVC, PE, PP, PS, PVC, etc. based on SVM model. By comparing the kernel functions, it was found that the kernel functions of quadratic polynomials had better classification effect, and the accuracy was more than 90%. Lin et al. [78] applied the least square SVM to LIBS measurement of steel, and identified 40 kinds of steel samples, the accuracy was more than 96.25%. It can be seen that SVM can be

used in all kinds of LIBS measurement samples. Chen et al. [79] used LIBS to measure Cr in pork. Compared with PLS and ANN, SVM has better prediction accuracy. The root mean square error of SVM is 0.6961% after optimization of structural parameters by particle swarm optimization. The accuracy can reach the same accuracy of atomic absorption spectrum. Zhang et al. [80] used LIBS to detect coal quality in the power plant, and used PCA and SVM to reduce RMS error of calorific value prediction from 1.23mj/kg to 0.85mj/kg, and relative error from 5.4% to 3.68%. Peng et al [81] proposed a hybrid classification method based on LIBS, K-means and support vector machine (SVM). First, K-means are used to group the data independently, and then SVM is used to classify the data. The accuracy can reach 98%. Compared with the single SVM classification model, the hybrid classification model can save 58.92% operation time while ensuring the classification accuracy.

In this study, MATLAB R2019a software platform is used to establish the quantitative model, and the training and testing of the model are realized by self-programming. The MATLAB platform is built-in with the regress() function for PLS fitting, and the feedforwardnet() function and train() function for BPNN fitting. The SVM model uses libsvm software package recognized by other scholars and embedded in MATLAB, then it can call svmtrain() function to adjust model parameters and build SVM model.

2.5 Summary

Basic knowledge necessary for this dissertation is introduced. Plasma is the observation target in LIBS measurement, and its states can be easily interfered by the environments and sample situations. The change of plasma states induces the change of LIBS signals. Based on the theory, plasma states can be analyzed through LIBS signals. The common analyzed plasma states are plasma temperature and free electron number density.

Long-short DP-LIBS is a kind of double pulses of laser configurations. Different from conventional double-pulse LIBS, the pulse width of two lasers are very different. Long pulse width laser beam exits before and after the short pulse-width laser beam. It supplies energy during different periods of plasma evolution.

Machine learning is a kind of method to build function between LIBS signals and target element component. There are many types of models used for LIBS in previous research, while for a specific target there is the specific optimization ways. In this study, we should study how to improve the model quality for steel measurement.

3 Experimental Systems

3.1 LIBS Measurement of Chemical Steel Samples for Basic Plasma Analysis

The experimental set up of SP-LIBS system for particle steel samples measurement is presented in Fig.3-1. It contains the optical part and sample processing part. The optical part contained a laser, a spectrometer, an ICCD camera and other accessories, the computer and pulse generator controlled the action of the ICCD camera.

The emission signals were delivered by optical fiber and detected by spectrometer and ICCD camera, and then data were transmitted to computer for analysis. The spectrometer (SOL NP250-2) has two channels with different resolutions, which can measure two pieces of spectra at the same time. For the low-resolution channel, the grating number is 600l/mm, and the resolution is 0.076nm/pixel, and the central position of the grating was set as 280nm, so the wavelength region was 240~320nm. For the high-resolution channel, the grating number is 3600l/mm, and the grating resolution is 0.012nm/pixel, and the central position of the grating was set as 252nm, so the wavelength region was 246~258nm. The ICCD camera (Andor iStar 334T) recorded following the laser Q-switch action through pulse generator, and the signal gain was fixed as 2500, and the gate width time was fixed as 300ns. The ICCD exposure time was set as 5s, so each time of measurement was the accumulation of 100 (5s×20Hz) times of laser shots. ICCD can set different delay time after laser pulse, varying as 1000ns, 2000ns, 3000ns, and 4000ns, which can reflect the plasma evolution process after its formation. The Nd:YAG laser (Quantel Brio) has the fixed frequency of 20Hz, with the pulse width of 6ns, the beam diameter of 9mm. It was operated at 1024nmn, and the pulse energy was controlled as 31mJ/pulse. The Lens 1 with the focus distance of 800mm concentrated the laser beam onto the sample surface, and Lens 2 with the focus distance of 100mm concentrated the plasma signal onto the fiber. The long-pass filter, with cut-off wavelength of 400nm, separated the laser beam and the plasma signal.

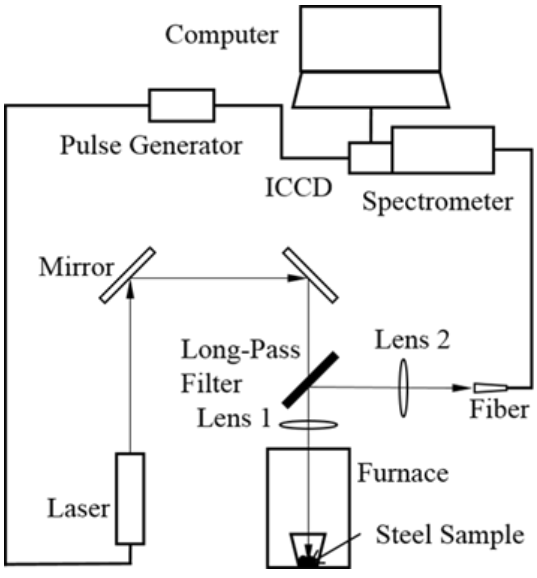

Fig.3-1 SP-LIBS system for particle steel samples measurement

In the above wavelength 246~258nm region, the obvious Mn wavelength is the ion line, and there are many Fe lines crowded with high interference, so the other wavelength region was also measured for the Mn atom line and less Fe lines. The Nd:YAG laser (LOTIS TII, LS-2134UTF) has the fixed frequency of 10Hz, with the pulse width of 5-8ns, the beam diameter of 6mm. It was operated at 1024nmn, and the pulse energy was controlled as 52.0mJ/pulse. The spectrometer 0.012nm/pixel channel shifted its central wavelength to 405nm, so the wavelength region was 400-410nm. ICCD has the fixed 5s exposure time, 300ns gate width, so each time of measurement was the accumulation of 50 (5s×10Hz) times of laser shots. ICCD varied delay time as 1000ns, 2000ns, 3000ns and 4000ns, and the corresponding gain was 2000V, 2300V, 2500V, 3000V.

3.2 Experimental System for Comparison of SP-LIBS and Long-Short DP-LIBS

The experimental setup of collinear long-short DP-LIBS and SP-LIBS for bulk steel samples measurement is presented in Fig.3-2. The system includes two lasers, a digital delay generator, a spectrometer, an ICCD camera, optical fiber, computer and other auxiliary optical devices. Spectrometer and ICCD camera are of the same brands and models as the Fig.3-1. A long pulse laser with wavelength of 1064 nm, pulse width of 60μs, pulse energy of 200mJ and frequency of 10 Hz is generated by the Laser (LOTIS TII, LS-2137U) in the free-running (FR) mode. The laser oscillation is free to output in a relatively long duration. Thus FR laser pulse has lower energy density which is not enough to produce an observable plasma emission. A short pulse laser with wavelength of 1064 nm, pulse width of 5–8 ns, pulse energy of 24.5mJ and frequency of 10Hz is generated by the Laser (LOTIS TII, LS-2134U). The reflected short pulse laser beam combined with the long pulse laser beam by polarization prism to realize the collinear long-short DP-LIBS. The inter-pulse delay time between long pulse and short pulse was adjusted by a digital delay generator and was set to 30μs in this study. When the long pulse laser did not work and only short pulse laser passed through polarization prism, it can realize the SP-LIBS. The combined laser beams or short pulse laser beam was reflected by the mirror and then focused on the steel sample by the lens with focal length of 800mm to generate plasma. The plasma emission was collected and focused on entrance of the optical fiber by a lens with focal length of 100mm.

The delay time was the record start time after the short pulse was triggered, which can be adjusted by ICCD camera. ICCD has the fixed Gain of 3500V, exposure time of 5.05s, and width time of 1000ns. The delay time of ICCD camera varied as 2000ns, 3000ns and 4000ns.

3.3 Samples

The sample processing part contained a muffle furnace to heat the steel sample to different temperature and maintain it. The muffle furnace has a hole with the diameter of 10mm on the top to pass through the laser beam and plasma signals. The powder steel samples were placed in a ceramic crucible, and the bulk steel samples were placed on a ceramic plate. Then the samples were put into the furnace one species by one species. The powder samples were measured in the Fig.3-1 system and bulk samples were measured in the Fig.3-2 system. An X-

Y moving stage supported the muffle furnace, and after each time of LIBS measurement, it has a slight move to avoid the repeat measurement on the same surface. The X-Y moving is necessary to avoid the ablation accumulation crater effects.

When measure samples at room temperature, muffle furnace doesn't work. When measure at elevated temperatures, set the muffle furnace and it will increase to the settings. After reaching the setting, maintain 30 minutes before LIBS measurement, to achieve the thermal balance in the steel samples.

The compositions of the chemical standard powder steel are listed as Table 3-1, following Japanese Iron and Steel Certified Reference Material standard. For powder samples, sample temperature varied as 20℃, 300℃, 700℃, 1000℃. The melting point of steel is usually up to 1600℃, so steel kept in solid phase during the experiment.

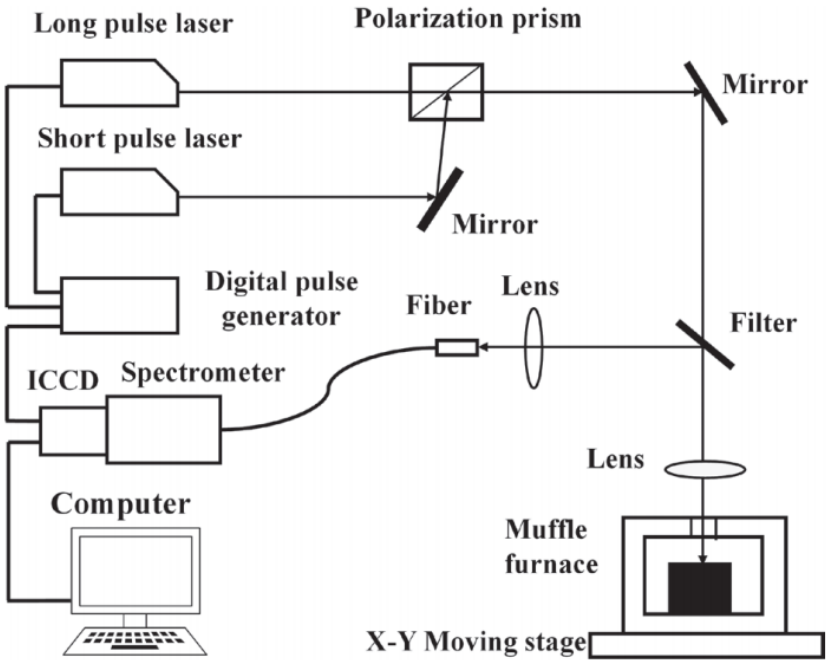

Fig.3-2 Collinear long-short DP-LIBS and SP-LIBS for bulk steel samples measurement

Table 3-1 Compositions of the chemical standard powder steel (Mass compositions %)

	Species	C	Si	Mn	Fe	Mn/Fe
JSS030-9	Carbon steel	0.195	0.237	0.750	98.72	0.007597
JSS050-7	Carbon steel	0.378	0.190	0.498	98.86	0.005037
JSS057-9	Carbon steel	0.529	0.182	0.759	98.45	0.007709
JSS120-1	Pig iron	2.85	1.32	0.70	94.37	0.007418
JSS168-8	Low alloy steel	0.0399	0.201	0.417	99.08	0.004209
JSS653-15	Stainless steel	0.0563	0.616	1.572	61.00	0.02577

The compositions of the bulk steel are listed in Table 3-2, following the spectral standard of China, and all the steel is of low carbon cast steel species. For bulk samples, sample temperature varied as 20℃, 300℃, 500℃, 700℃, 1000℃.

For one experimental condition (one sample, one sample temperature, one delay time), 5 times measurements were repeated. To judge whether the spectral line in the steel is Fe line or not, a bulk of standard pure iron sample was measured. The compositions of the pure samples are listed as Table 3-3. The iron sample is also heated as 20℃, 300℃, 500℃, 700℃, 1000℃.

Table 3-2 Compositions of the bulk steel samples (Mass compositions %)

Species	C	S	Si	Mn	P	Cr	Ni	Fe
ZG10#	0.085	0.032	0.217	0.44	0.042	0.104	0.134	98.755
ZG25#	0.233	0.033	0.354	0.472	0.034	0.216	0.046	98.479
ZG45#	0.454	0.044	0.444	0.752	0.041	0.141	0.122	97.72
ZG60#	0.586	0.042	0.471	0.778	0.037	0.131	0.114	97.575
28CrNiMo	0.276	0.028	0.56	0.842	0.032	0.362	0.432	96.996
35CrNiMo	0.34	0.027	0.779	0.957	0.029	0.408	0.614	96.348
20MnMo	0.192	0.026	0.363	1.12	0.031	0.201	0.246	97.517
30SiMn	0.297	0.028	0.47	1.23	0.029	0.203	0.11	97.423
35SiMn	0.332	0.029	0.716	1.36	0.031	0.154	0.148	97.007

Table 3-3 Compositions of pure iron sample

Species	C	S	Si	Mn	P	Cr	Ni	Fe
Pure iron	0.0032	0.0049	0.0031	0.032	0.0037	0.0053	0.016	99.7419

The muffle furnace is the important equipment, and steel samples were heated inside it. The photo of it is presented in Fig.3-3. The particle chemical samples were placed in the crucible. The photo of the chemical samples before and after the heating are presented in Fig.3-4. The bulk spectral standard steel and iron samples are presented in Fig.3-5.

3.4 Summary

In this chapter, two experimental systems were established. One is the conventional system measuring chemical samples, which can change the measurement wavelength regions, and increase the sample temperature. The basic LIBS measurement properties on steel can be obtained in this system. The other one is long-short DP-LIBS system, which has the special configurations of two lasers. This design is aimed to improve the LIBS quality on steel, and whether it works should be testified in this study. The bulk spectral standard samples were measured in this

The variations of sample temperatures and sample species are listed for both experimental systems. The influence of sample temperature and quantitative measurement are two key points in this study.

(a) The working system (b) The outlook of furnace (c) the crucible

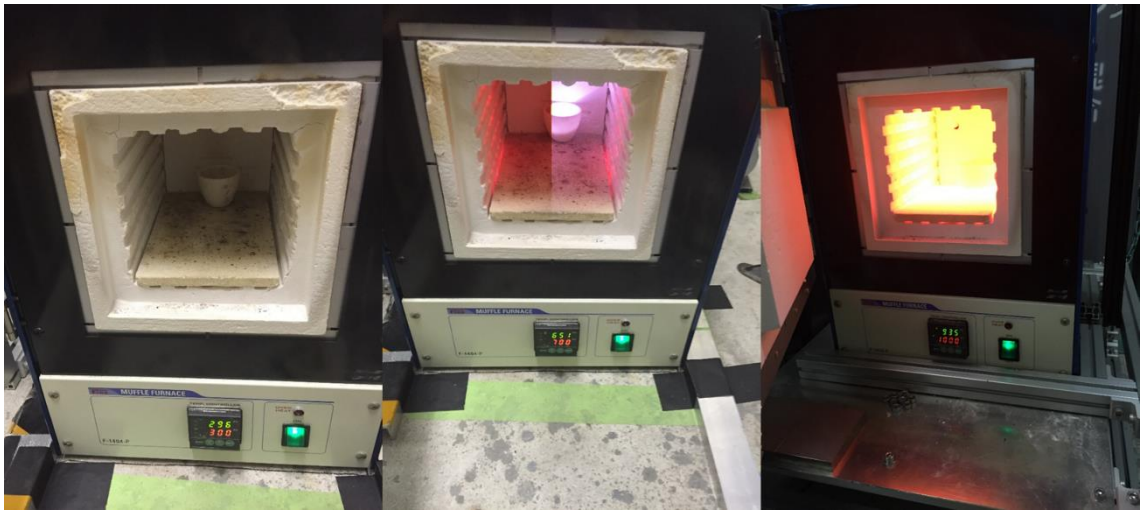

(d) The inner side of furnace at different settled temperature

Fig.3-3 The photo of the muffle furnace

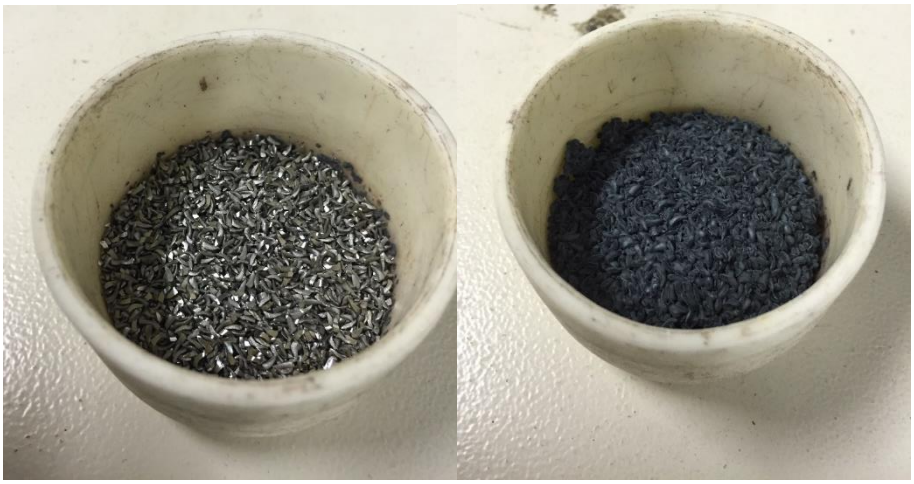

(a) Before heating (b) After heating

Fig.3-4 The photo of the chemical samples before and after the heating

(a) Bulk steel sample (ZG25#) (b) pure iron

Fig.3-5 The photo of the bulk spectral standard samples

4 Plasma Analysis of Steel at Different Sample Temperatures

The chemical standard samples were measured in the system Fig.3-1, while samples are in particle form. Two wavelength regions of 246-258nm and 400-410nm were selected for analysis. Fe lines in this two regions were identified, which is basic for analysis. The plasma states were analyzed based on Boltzmann Plot or some factors. The quantitative analysis under different conditions is analyzed, and the factors affecting the accuracy of measurement are pointed out. The results of this chapter help to build the basic overview of LIBS measurement on steel samples, including the plasma states analysis and quantitative analysis.

4.1 Steel Spectra in Wavelength of 246-258nm

Fig.4-1 presented the normalized spectra, the comparison of pure iron and steel samples, and the delay time was set as 1000ns. When Fig.4-1 (a) is enlarged as Fig.4-1 (b), it can be observed that different samples have differences, but the identification of the spectral lines are difficult. Fe lines are very crowded for its complicate atom structure, and spectral lines informnation can be reffered in NIST database [82]. In the same wavelength region, the spectrum of high-resolution grating is as shown in Fig.4-1 (c). More spectral lines are detected for lower instrumental broadening. For more accurate analysis, high resolution grating is necessary.

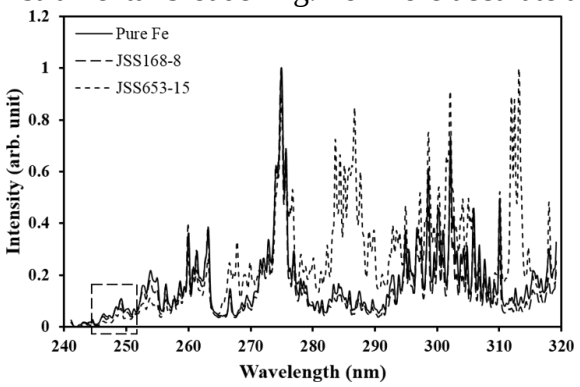

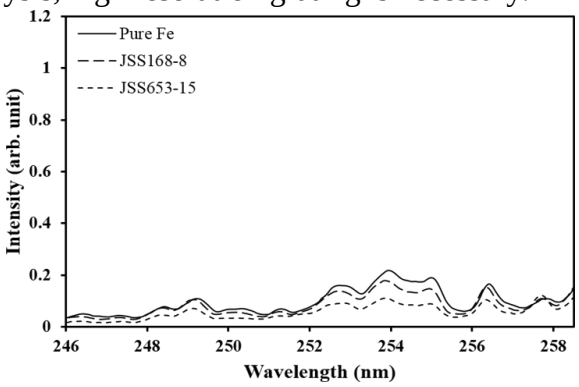

(a) Spectra with the resolution of 0.076nm/pixel(b) The enlarged figure of selected wavelength in (a)

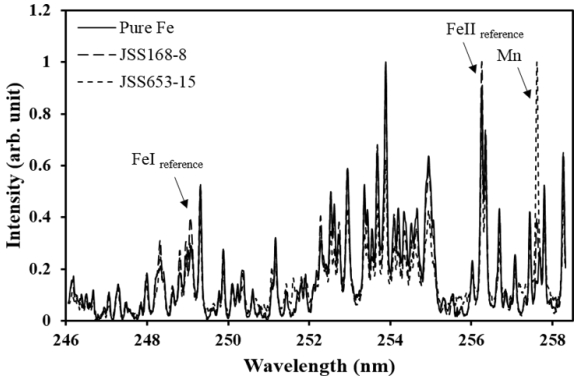

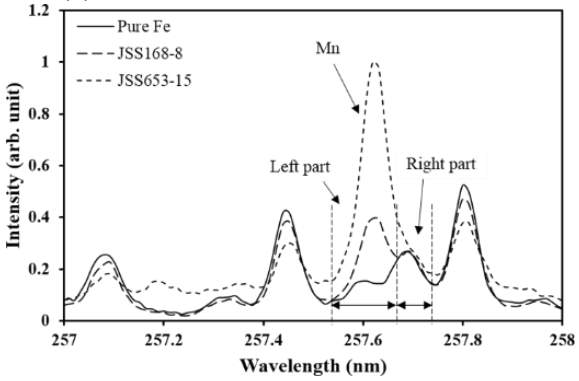

(c) Spectra with the resolution of 0.012nm/pixel (d) The enlarged figure of Mn line in (c)

Fig.4-1 Spectra comparison between pure iron and steel samples at 20℃ in 246-258nm region (delay time: 1000ns; normalization: the highest point of the spectrum itself)

One Mn ion line can be observed in this region, which is precisely shown in Fig.4-1 (d), there are the interference Fe line at the neighbor of Mn line. Among the other more than 50 lines in the spectrum, there are mainly Fe atom lines and Fe^{+} ion lines, and it is difficult to judge the ionization levels based on database only. Select the most obvious atom line and ion line for analysis, named as "FeI reference" and "FeII reference" respectively, shown in Fig.4-1 (c). They have relative low interference with their neighbor lines, and kept obvious among all delay time. The spectral information of Mn ion line and two Fe reference lines are listed in Table 4-1.

Table 4-1 The spectral lines information in Fig.4-1 (c)
(W.L.: wavelength, I.L.: ionization level)

No.	W.L. (nm)	I.L.	A (s^{-1})	gk	E (cm^{-1})
FeI $_{reference}$	249.0644	I (atom)	3.44E08	3	40842.154
FeII $_{reference}$	256.2535	II (ion)	1.79E08	2.5	46967.4751
Mn	257.6104	II (ion)	2.80E08	4	38806.691

For analysis, all the spectral line intensity was defined as the area, meaning the integration intensity. Mn line intensity was calculated by subtracting Fe interference, as Eq.(4-1).

$$I_{Mn} = A_{left} - \alpha A_{right} \qquad \text{Eq.(4-1)}$$

Where A is the area, and α is the ratio of left part to right part of pure iron spectra. When delay time increased, α changed as measured in pure iron spectra. When delay time was 1000ns, α was 0.766; when delay time was 2000ns, α was 0.351; when delay time was 3000ns, α was 0.227; when delay time was 4000ns, α was 0.146.

According to theory, the spectral lines of different energy levels from the same element can form a plasma temperature factor. The ratio of FeII $_{reference}$/ FeI $_{reference}$ is also a plasma temperature factor. According to theoretical database, the relation between FeII $_{reference}$/ FeI $_{reference}$ and plasma temperature is shown in Fig.4-2. As it indicates, FeII $_{reference}$/ FeI $_{reference}$ increases when plasma temperature increases.

The change of plasma temperature factor FeII $_{reference}$ /FeI $_{reference}$ with sample temperature is shown in Fig.4-3. As it is shown, among different samples, the distributions of FeII/FeI are almost same, both the value and the change trend are basically the same. That means, the differences of the target species are not the crucial factors of the plasma temperature change. Besides, for the same sample and same sample temperature, as the delay time increases, the value of FeII/FeI decreases. This is following the common sense, for as the plasma develops, it will not get the input energy and gradually decay, and in this way the plasma temperature continuously goes down.

However, the surprising results are that, when the sample temperature increases, there is no obvious increase of the FeII/FeI. This is also contrast to the common sense of the plasma forming process. Under higher sample temperature, the sample surface and the surrounding gas has a higher energy level, it is easier to be ablated and less laser beam energy will be used to form the plasma. Therefore, it is reasonable to suppose that the formed plasma during LIBS process can absorbs more energy from the laser beam under higher temperature, and the plasma

has a higher energy level. Secondly, because the surrounding gas has a higher energy, it is reasonable to assume that the plasma is able to decay slower for the energy transfer rate with the surrounding gas is smaller. Further explanation is discussed later.

Because the ionization energy for Fe atom is up to around 762.5kJ/mol≈7.9eV, which is higher than the most of upper energy levels of atom lines, so the fade speed of ion lines are faster than that of atom lines. For each the other target Fe line, Fe target/FeI reference was calculated, and the evolution speeds of Fetarget/FeI reference and FeII reference/FeI reference were compared. If Fe target/FeI reference has the similar fade speed with FeII reference/FeI reference, the target Fe line can be regarded as ion line. If the fade speed of Fe target/FeI reference is much slower than FeII reference/FeI reference, the target Fe line can be regarded as atom line. The example of spectral line ionization judgement is shown in Fig.4-4, taking the sample of JSS030-9 as example.

Two neighbor Fe lines in Fig.4-4 (b) and (c) were checked in Fig.4-4 (d) and (e), and their fade speed were different. For Fe line in 252.188~252.3439nm, it had a lower fade speed than FeII reference, while Fe line in 252.4278~252.5597nm, it had a similar fade speed with FeII reference. So Fe line in 252.188~252.3439nm is more likely to be an atomic line while Fe line in 252.4278~252.5597nm is more likely to be an ion line. The high possible theoretical line is the one with relative low upper energy level, high transition probability A_i and high degeneracy g_i. Check the NIST atomic spectra database, it can observed that the most possible line in 252.188~252.3439nm is FeI line 252.2849nm; while the most possible line in 252.4278~252.5597nm is FeII line 252.5388nm. Other lines were also judged in this way.

Similarly, the other spectral lines can also be analyzed. Following the step that first judge the ionization levels and the search the lines in the database, their information can be judged. The theoretical Fe lines information in spectra were listed in Table 4-2 of Fe atom lines and Table 4-3 of Fe^+ ion lines. Which helps to build the Boltzmann Plot.

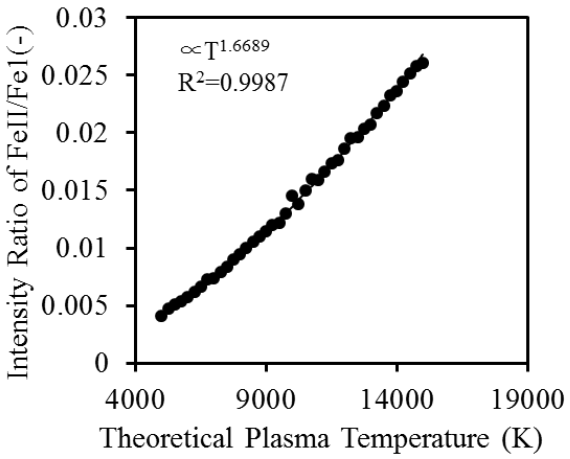

Fig.4-2 The theoretical relation between FeII $_{reference}$ /FeI $_{reference}$ and the plasma temperature

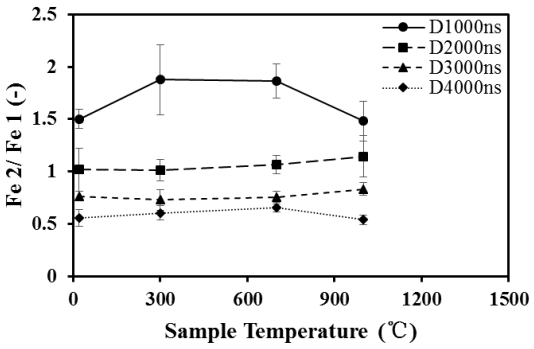

(a) JSS030-9

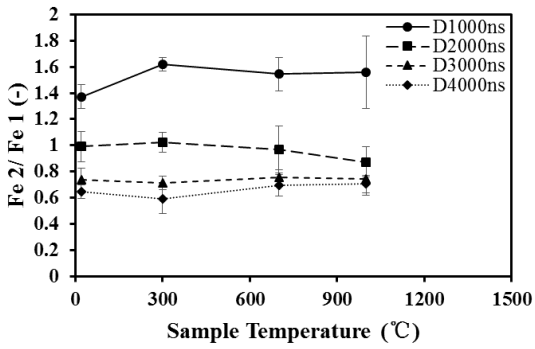

(b) JSS050-7

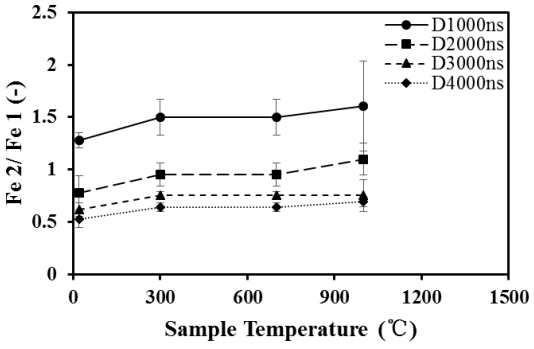

(c) JSS057-9

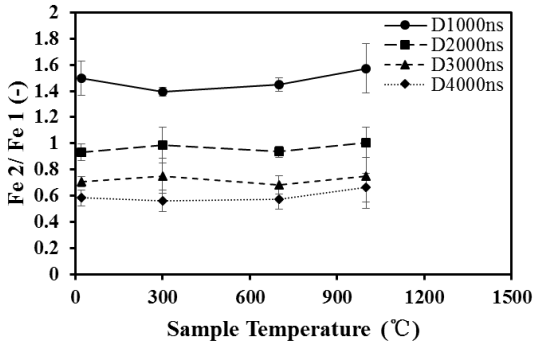

(d) JSS120-1

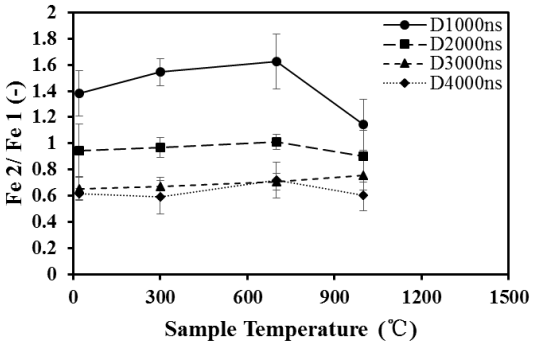

(e) JSS168-8

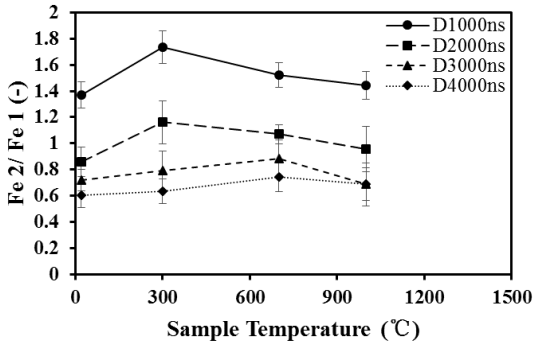

(f) JSS653-15

Fig.4-3 The change of plasma temperature indicator Fe II $_{reference}$/FeI $_{reference}$ among different samples, sample temperature and delay time

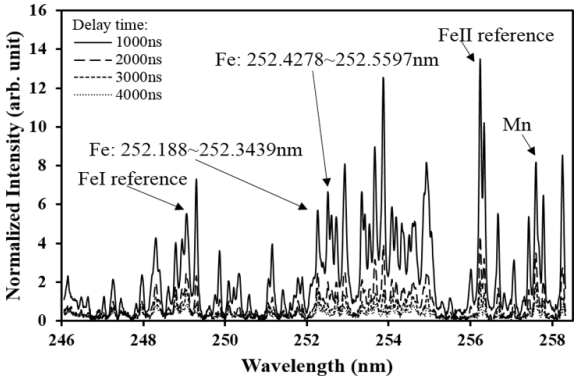

(b) The spectra at 20℃ with different delay time

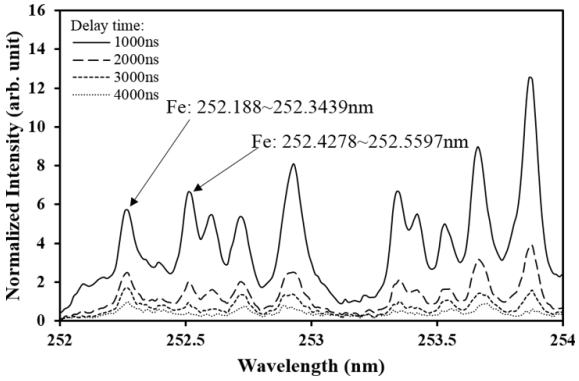

(c) The enlarged figure of Fe target lines in (b)

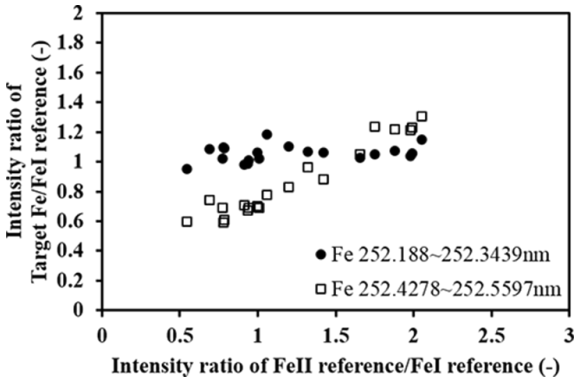

(d) The change of Fe target lines at 20℃

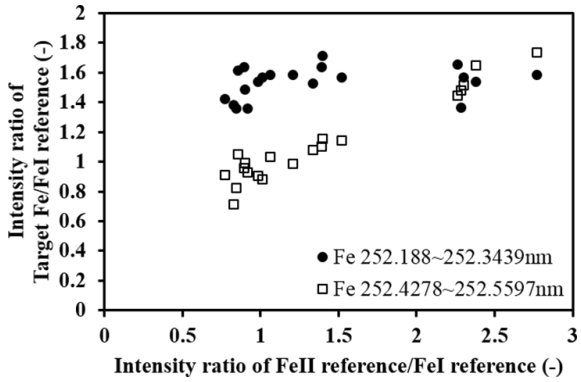

(e) The change of Fe target lines at 700℃

Fig.4-4 The example of Fe line ionization levels judgement (Sample: JSS030-9; Spectra normalization standard: the highest intensity in the spectrum of 4000ns)

Table 4-2 The Fe atom spectral lines (FeI) information in 246nm-258nm

Wavelength (nm)	A (s^{-1})	g_k (-)	E_k (cm^{-1})	Wavelength (nm)	A (s^{-1})	g_k (-)	E_k (cm^{-1})
246.2181	1.10E+07	2	41018.05	250.1132	6.75E+07	3	39969.85
246.373	1.64E+07	2	48304.64	250.6572	2.04E+07	4	60757.6
246.5149	4.35E+07	4	47930	251.0835	1.29E+08	2	40231.34
246.888	2.40E+07	5	47420.23	251.2365	2.00E+06	3	40207.91
247.0965	2.36E+06	5	47834.55	251.6571	1.71E+06	4	47452.72
247.2871	2.10E+07	1	41130.6	251.7661	1.58E+07	3	47693.24
247.4814	6.13E+07	3	48122.93	252.2849	2.13E+08	4	39625.8
247.9776	1.74E+08	2	41018.05	254.3922	4.70E+08	5	59085.83
248.4188	2.26E+08	1	41130.6	254.5978	7.16E+07	3	39969.85
248.6373	3.08E+06	3	40207.09	255.2606	6.19E+05	2	40052.04
248.8142	4.20E+08	4	40594.43	256.8865	2.04E+06	1	46901.83
248.9752	2.31E+08	1	41130.6	256.9597	1.01E+06	4	45833.23
249.0644	3.44E+08	3	40842.15	257.2755	2.48E+06	3	51825.77
249.6534	2.15E+07	5	47420.23				

Table 4-3 The Fe ion spectral lines (FeII) information in 246nm-258nm

Wavelength (nm)	A (s^{-1})	g_k (-)	E_k (cm^{-1})	Wavelength (nm)	A (s^{-1})	g_k (-)	E_k (cm^{-1})
249.3184	2.02E+08	6.5	61527.61	254.3378	6.70E+07	5.5	60887.61
249.7714	1.00E+07	3.5	66377.32	254.8744	2.40E+08	0.5	61035.29
249.8897	2.12E+08	5.5	61587.21	254.9083	1.89E+08	3.5	69606.57
250.3874	2.23E+08	4.5	70314.62	254.9394	1.65E+08	1.5	62244.52
251.9047	2.10E+08	2.5	67000.53	255.0683	1.07E+08	5.5	65363.61
252.1091	2.05E+08	1.5	67273.83	255.5067	1.96E+07	3.5	62065.53
252.5388	1.91E+08	6.5	60837.56	256.0282	1.77E+08	1.5	64834.07
252.6294	2.47E+08	2.5	60402.33	256.2535	1.79E+08	2.5	46967.48
252.7455	1.23E+08	2.5	73054.91	256.3475	1.51E+08	1.5	47389.81
252.9545	2.20E+08	4.5	62158.13	256.622	2.61E+08	4.5	83871.21

253.3627	1.92E+08	5.5	60887.61	256.6401	2.29E+08	2.5	83868.45
253.4418	1.83E+08	3.5	61156.83	257.0849	1.84E+08	2.5	69650.48
253.5485	7.50E+07	3.5	62065.53	257.4366	2.40E+08	1.5	59663.44
253.7138	1.44E+08	4.5	77861.65	257.6864	1.32E+08	5.5	72261.74
253.8204	1.26E+08	5.5	72261.74	257.7922	1.20E+08	0.5	47626.11
254.0661	1.70E+08	3.5	75600.9	258.2584	8.80E+07	1.5	47389.81
254.1835	8.20E+07	2.5	61041.73				

4.2 Sample Temperature Effects

4.2.1 Change of Spectra

Fig.4-5 showed the change of spectra with sample temperature, and each figure was normalized by its corresponding 20℃ spectrum. When sample temperature was higher than 20℃, the spectra were more excited. However, at high sample temperature, the increase of spectra intensity didn't have proportional increase with sample temperature. For JSS030-9, in Fig.4-5 (a), from 300℃ to 1000℃, the total intensity decreased; for JSS653-15 in Fig.4-5 (c), 700℃ and 1000℃ had almost the same intensity. Besides, the spectra shape at different sample temperature were also different. Some spectral lines had higher excitation rates than the others, indicating the inhomogeneity of sample temperature influence on spectral lines. When delay time changed from 1000ns to 4000ns, the fluctuation of the backgrounds became more obvious.

This is quite opposite to the results in Fig.4-3. The spectra behavior indicate that there is a big change of LIBS signal from room temperature to 300℃, however, from Fig.4-3, it shows that there is no obvious plasma temperature difference among the sample temperature regions. Besides, under higher sample temperature, when the delay time goes on, the decay speed of FeII/FeI is almost same as that under room temperature, this means that the higher sample temperature doesn't help to maintain the plasma temperature.

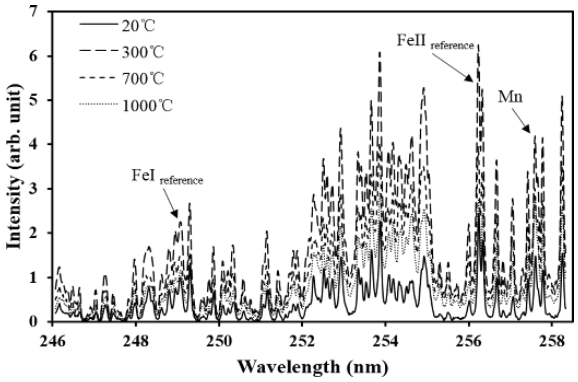

(a) Sample: JSS030-9, Delay time: 1000ns

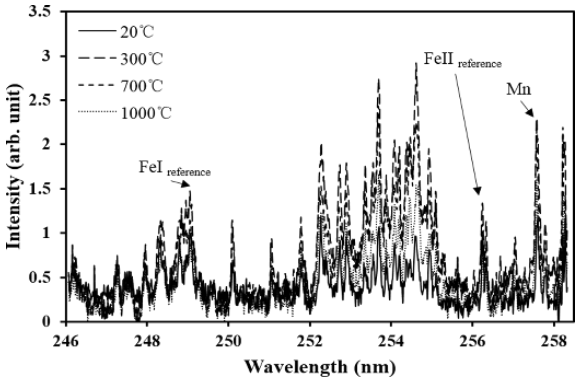

(b) Sample: JSS030-9, Delay time: 4000ns

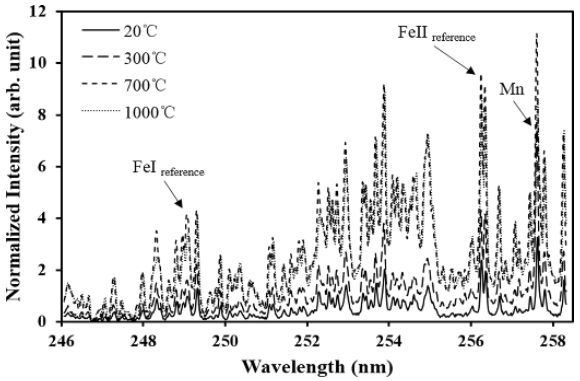

(c) Sample: JSS653-15, Delay time: 1000ns

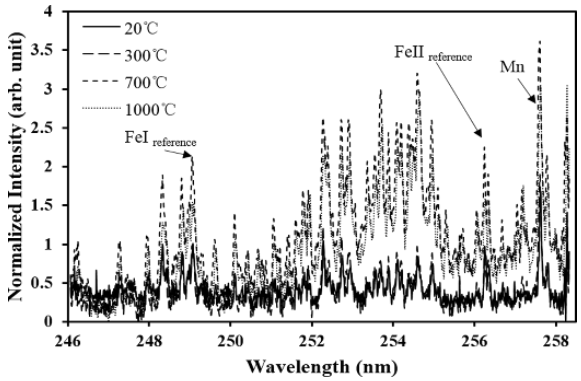

(d) Sample: JSS653-15, Delay time: 4000ns

Fig.4-5 Normalized steel spectra at different sample temperatures (normalization: FeI reference at 20℃)

The spectra total absolute emission ability is related with not only the sample temperature, but also the delay time. The absolute total emission ability of JSS030-9, with the change of delay time is shown in Fig.4-6.

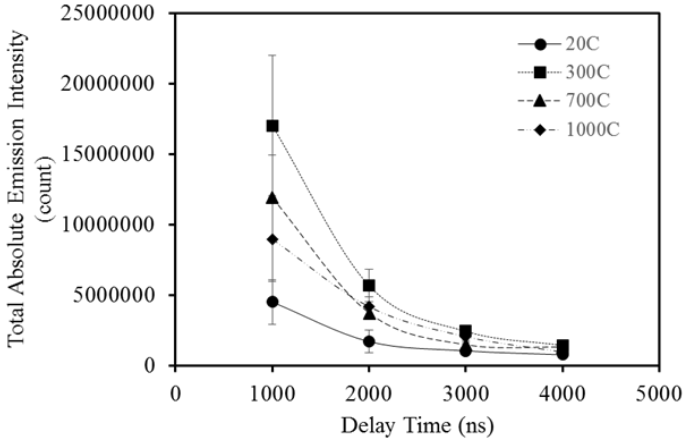

Fig.4-6 The relation between absolute emission intensity and delay time (Sample: JSS030-9)

As it is shown in Fig.4-6, the total absolute emission ability decays as delay time goes on. Until the delay time of 4000ns, the emission abilities under different sample temperature are almost same. The LIBS signal emission ability has the relation with both the sample temperature and delay time. When the delay time is long, meaning that plasma temperature is low, the emission ability is low, and emission ability under different sample temperatures are almost same. However, when delay time is 1000ns, the plasma temperature is high, the emission ability difference between different sample temperatures is obvious. For all of samples, the emission ability under room temperature is obviously smaller than that under higher temperatures. However, for other temperature regions, the highest emission intensity of different samples is distributed in different temperature.

Besides, it can be observed from Fig.4-5 and 4-6, signal stability does not increase as sample temperature increases. On the contrast, the error bars somehow become larger as sample temperature increases. There are two factors can induce the increase of signals intensity. One is the increase of plasma temperature, according to Eq.(2-1), the increase of the plasma temperature will induce the increase of intensity. The other one is the increase of the atom or

ion number inside plasma. When the breakdown volume on the sample surface is different, the number of atoms or ions is different.

No matter the increase of the plasma temperature or the breakdown volume, it means the increase of the plasma thermal states. When sample temperature increased, it is supposed that the plasma thermal states increase, for less laser energy is cost for the breakdown of the samples. However, intensity at 300℃ had higher intensity than the other elevated temperatures, meaning the higher plasma thermal states. It means the change of plasma with sample temperature is not uniform.

4.2.2 Change of Plasma States

Fe lines were adopted for the Boltzmann Plot calculation for Fe occupies the biggest compositions in steel samples. The Boltzmann Plot at room temperature of the sample JSS030-9 is shown in Fig.4-7. The structure complicity of Fe atom induces have many spectral lines of Fe atoms and Fe^{+} ions, so there are not only one partition function inside plasma. So there are not one Boltzmann Plot inside the plasma, and the selection of spectral lines for Boltzmann Plot is necessary.

After knowing all spectral lines information, the typical Boltzmann Plot was built as Fig.4-7, using the sample of JSS030-9 at 20℃, with delay time 1000ns. As explained in Theory, one Boltzmann Plot line is the fitting line of the spectral lines that have the same partition function. Several Boltzmann Plot lines exist at the same time because of the complexity of Fe atom electronic orbits structure and plasma inhomogeneity, so several partition functions exist at the same time. If the corresponding points of the fitting lines are different under different conditions, the subsequent analysis will be not accurate. Therefore, it is necessary to set the standard states, and the corresponding points of each Boltzmann Plot lines were fixed later. In this study, set the plasma at 20℃ with delay time 1000ns as the standard state, as in Fig.4-7; because at room temperature Mn signals had high linear dependency with the compositions, and when delay time was 1000ns, the fluctuation of backgrounds was small, shown in Fig.4-5. For other conditions, even though the corresponding partition function of each spectral line changed, its corresponding Boltzmann Plot line didn't change. Some points don't belong to these fitting lines, because the wavelength of spectra is limited, and the information is not enough to build a Boltzmann Plot line for them.

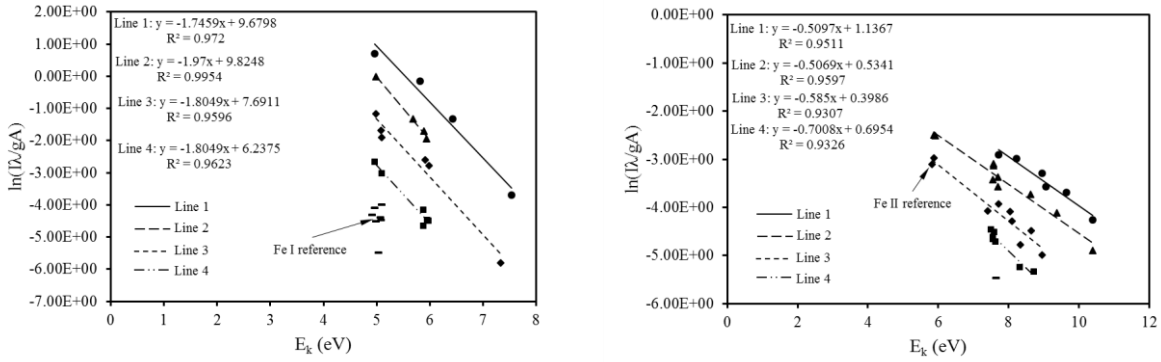

Fig.4-7 The typical Boltzmann Plot at 20℃ with delay time 1000ns (Sample: JSS030-9)

Noll showed that the Boltzmann Plot line can be drawn in one line [41], corresponding to the dominant partition function. The Line1 has the highest intercept, meaning the biggest number of Fe atoms or ions are corresponding to this states. So it belongs to the dominant partition function. The change of Boltzmann Plot with different delay time and sample temperatures were presented in Fig.4-8 and Fig.4-9. The distribution of the Boltzmann Plot lines describes the plasma thermal states, for each line has the information of its corresponding plasma temperature and atoms or ions number.

The change of the Boltzmann Plot should consider three factors of slope, intercepts and linear dependency together. At different situations, the linear dependency of the Boltzmann Plot almost kept more than 0.9, and it kept at the top position of all points, meaning the dominant partition function occupies the biggest number of Fe atoms or ions. The slope of the ion line is larger than atom line, meaning the ions have the higher plasma temperature than atoms. The intercept of ion line is smaller than atom line, meaning the number of Fe ions is lower than Fe atoms. This is consistent to the LTE theory.

When delay time increased, the slope of has some decrease, meaning the decrease of plasma temperature. Compared with delay time of 1000ns, the intercept at the increased delay time has a lower intercept, meaning the decrease of atoms and ions. When delay time increased, plasma temperature decreases and the number of Fe atoms and ions decreased. When sample temperature is elevated from room temperature, the slope didn't have obvious increase, while the intercept has obvious increase from room temperature. It means the plasma temperature doesn't increase at elevated temperatures, while the Fe atoms and ions have obvious increase at elevated temperatures. During the sample temperatures of 300℃, 700℃, 1000℃, the atom or ion numbers also didn't have obvious increase. In addition to the spectral lines belonging to dominant partition function, other spectral lines also have their changes, it can be seen that some points have different distributions in elevated temperatures from room temperature. All this indicates that the plasma doesn't have uniform change with sample temperature increase. The increase of sample temperature doesn't induce a uniform increase of plasma thermal states.

By analyzing Boltzmann Plot, the detail change of plasma states can be observed. Besides, the total change of the plasma states can also be estimated. The total Fe atoms or Fe+ ions number and the average plasma temperature can be calculated as Eq. (2-1), and the atoms or ions number is relative number that can only indicate the change of them, but not the absolute number. Because of the limitation of wavelength, the spectral information cannot be all included, average plasma temperature is also not the exact value of plasma, but it can reflect the plasma thermal states change among different conditions. The change of relative total Fe atoms and Fe^{+} ions number and average plasma temperature are shown in Fig.4-10 and Fig.4-11, taking JSS030-9 and JSS653-15 as examples, while other samples had a similar change with them.

According to the Fig.4-10, the Fe atoms and Fe+ ions number had obvious change with delay time and sample temperature. When sample temperature was higher than 20℃, the atoms and ions number had an obvious increase. From 300℃ to 1000℃, different samples had different change of Fe and Fe+ number. Comparing Fig.4-10 and Fig.4-5, the total atoms and ions number had the corresponding relation with the spectra intensity. Comparing Fig.4-10 (a) and (b), it can be observed that the number of Fe+ ions was much lower than that of Fe atoms. It indicated that the ionization level of the Fe atom was low, which corresponded to the relative

low laser pulse energy of 31mJ/pulse and cold environment temperature for plasma. When delay time increased, the particle of Fe atoms and Fe+ ions had obvious decrease, corresponding to the plasma fade process. And when delay time was 4000ns, the number differences between 20℃ and other temperatures were not obvious. The average plasma temperature kept at a relative stable level in Fig.4-11. The Fe atoms kept at around 6000K and Fe+ ions kept at around 20000K. Plasma temperature didn't increase when sample temperature increased. As delay time increased, plasma temperature had a little decrease generally, but not as obvious as atoms or ions number change. The number change was more sensitive to the delay time increase than that of plasma temperature. It can be understood that when plasma fades from delay time 1000ns to 40000ns, a part and a part of particles cooled down, while the rest particles in plasma should kept the temperature to remain the plasma.

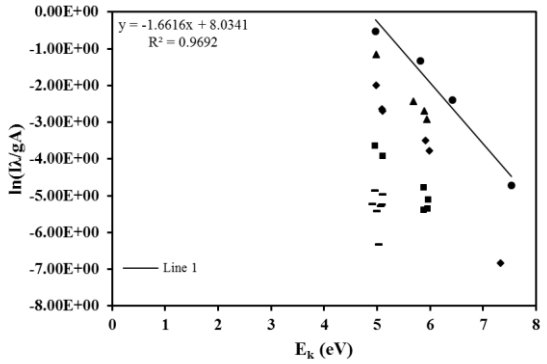

(a) atom lines, delay time: 2000ns

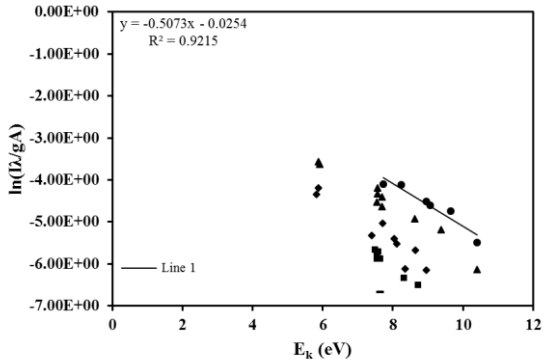

(b) ion lines, delay time: 2000ns

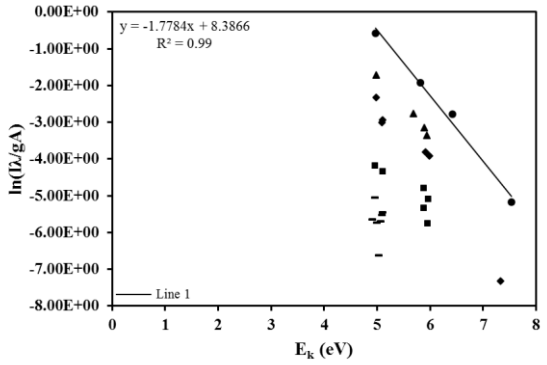

(c) atom lines, delay time: 3000ns

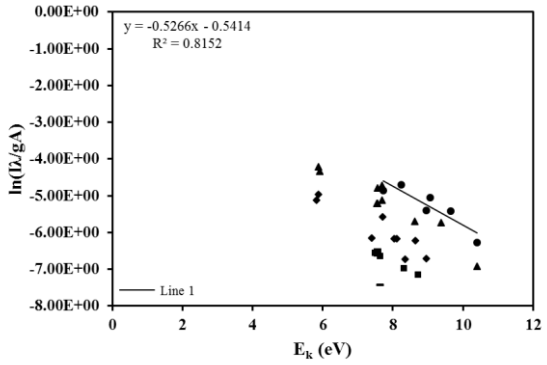

(d) ion lines, delay time: 3000ns

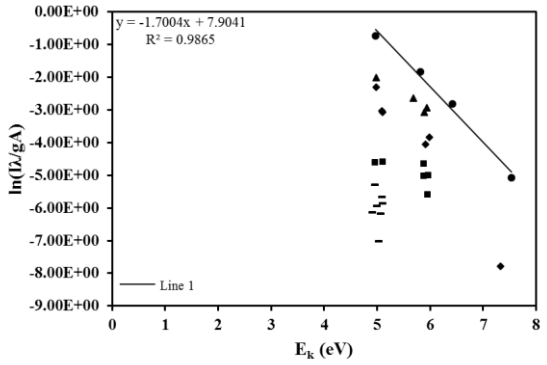

(e) atom lines, delay time: 4000ns

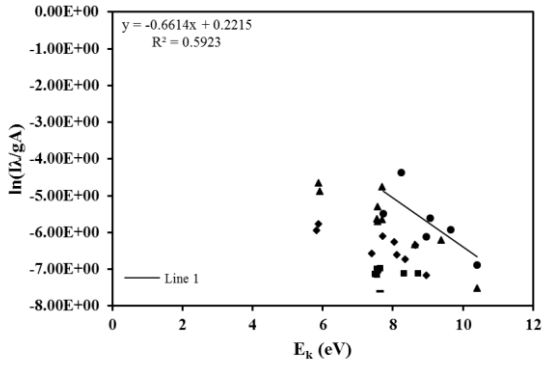

(f) ion lines, delay time: 4000ns

Fig.4-8 The change of Boltzmann Plot with different delay time (Sample: JSS030-9, 20℃)

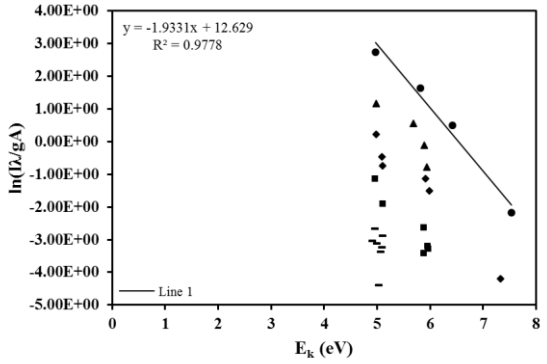

(a) atom lines, sample temperature: 300℃

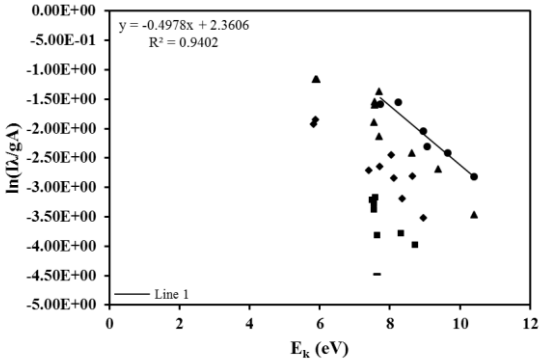

(b) ion lines, sample temperature: 300℃

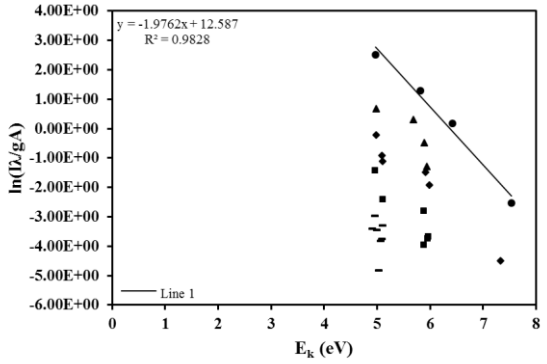

(c) atom lines, sample temperature: 700℃

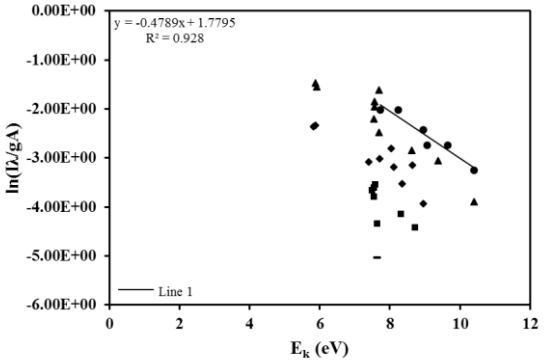

(d) ion lines, sample temperature: 700℃

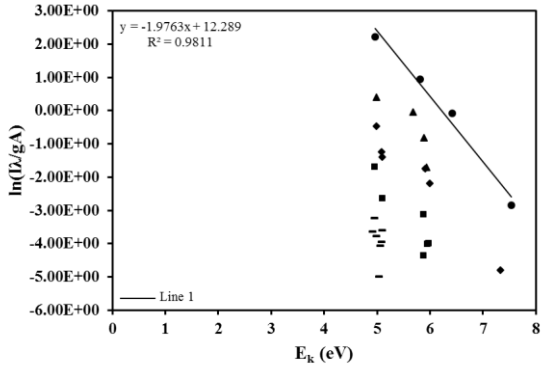

(e) atom lines, sample temperature: 1000℃

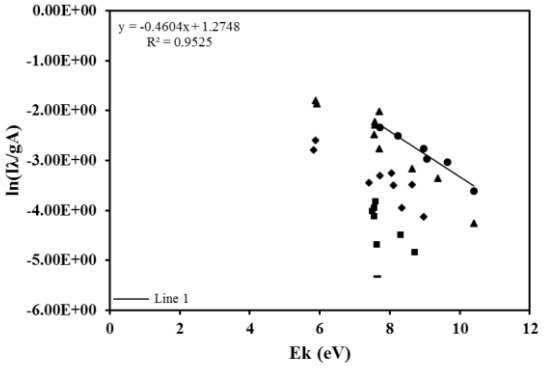

(f) ion lines, sample temperature: 1000℃

Fig.4-9 The change of Boltzmann Plot with different sample temperatures (Sample: JSS030-9, delay time: 1000ns)

Laser beam pulse supplies the energy for the processes, including the solid surface vaporization, material vapor atomization and ionization, and plasma reheating. When the total laser pulse energy remains, if one process saves the energy cost, it will flow to the other processes. When sample is heated, the energy cost for the breakdown per mass sample decreases. As the results indicated, the saved energy induces more solid surface breakdown rather than the reheating of the plasma. So the plasma temperature almost kept the same, while the Fe atom and ions density have obvious increase with sample temperature increasing.

From Fig.4-3, Fig.4-10 and Fig.4-11, the answer to how energy flow can be obtained. When sample temperature is higher than 20℃, the energy cost for solid breakdown per sample mass decreases, the saved energy flows to induce more solid breakdown, other than to reheat the plasma. The more solid breakdown makes the increase of atoms and ions number in plasma, but the average plasma temperature and ionization rates don't have obvious change. When sample temperature increases from 300℃ to 1000℃, the microstructure phase of the steel also changed, and different species of the steel have different phase change, so the binding energy of the steel microstructure is different, inducing the difference of solid breakdown. So not all the samples will increase its solid breakdown when the sample temperature increased from 300℃ to 1000℃. This explains in Fig.4-6, the reason why signal intensity at 300℃ is higher than the other elevated temperature.

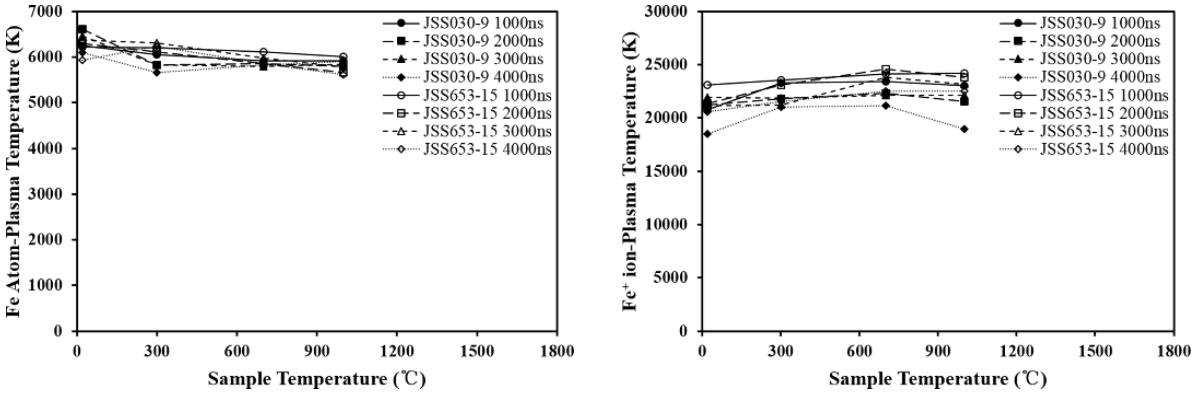

(a) Fe atoms (b) Fe^+ ions

Fig.4-10 The average plasma temperature calculated from Boltzmann Plot of Fe atoms and Fe^+ ions

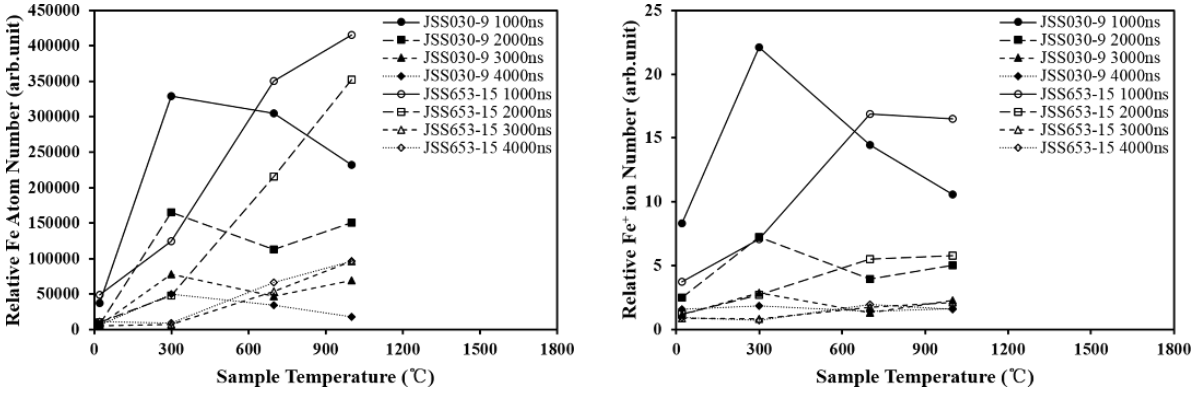

(a) Fe atoms (b) Fe^+ ions

Fig.4-11 The Fe atoms and Fe^+ ions number calculated from Boltzmann Plot

When plasma temperature in Fig.4-10 shows to be similar at different sample temperatures, the reasons why spectra in Fig.4-5 show the different shapes at different sample temperatures should be explained. Compared with Fig.4-7, distributions of points in Fig.4-9 are different. When the points belonging to the dominant Boltzmann Plot didn't change, the other points changed their positions. At room temperature, 4 layers of the Boltzmann Plot can be observed, as sample temperature elevated, the layers became not clear, for some points are scattered. It

means, some spectral lines are more sensitive to the sample temperature than the others. So the change of the spectral lines of Fe lines are not uniform with sample temperature, which also indicates the complicacy of Fe plasma.

At different sample temperature, the cooling down speed of the plasma temperature is also different. The change of plasma temperature with delay time is presented as Fig.4-12. Fig.4-12 is also based on the calculation of Boltzmann Plot of Fe atom lines. As it can be observed, plasma temperature has faster cooling down speed at room temperature, while at elevated sample temperature, the cooling down is not obvious during the delay time of 1000ns to 4000ns. It is because when surrounding gas and environments is at higher temperature, the heat transfer between plasma and environments become slower.

In Fig.4-3, FeII/FeI has obvious drop down at all sample temperatures, which is different with the results in Fig.4-12. It is because the elevated surrounding temperature doesn't help to maintain the ions number in plasma. At different sample temperature, the ionization levels decreased along with delay time. Therefore, the plasma temperature evaluated through FeII/FeI and Boltzmann Plot shows different behaviors.

Plasma is very complicated. For LIBS, because plasma exists in a very cold environment for it, the inhomogeneity is very serious. Plasma states evaluated through one or two factors are always not enough. So more detail effects and spectral lines should be carefully considered.

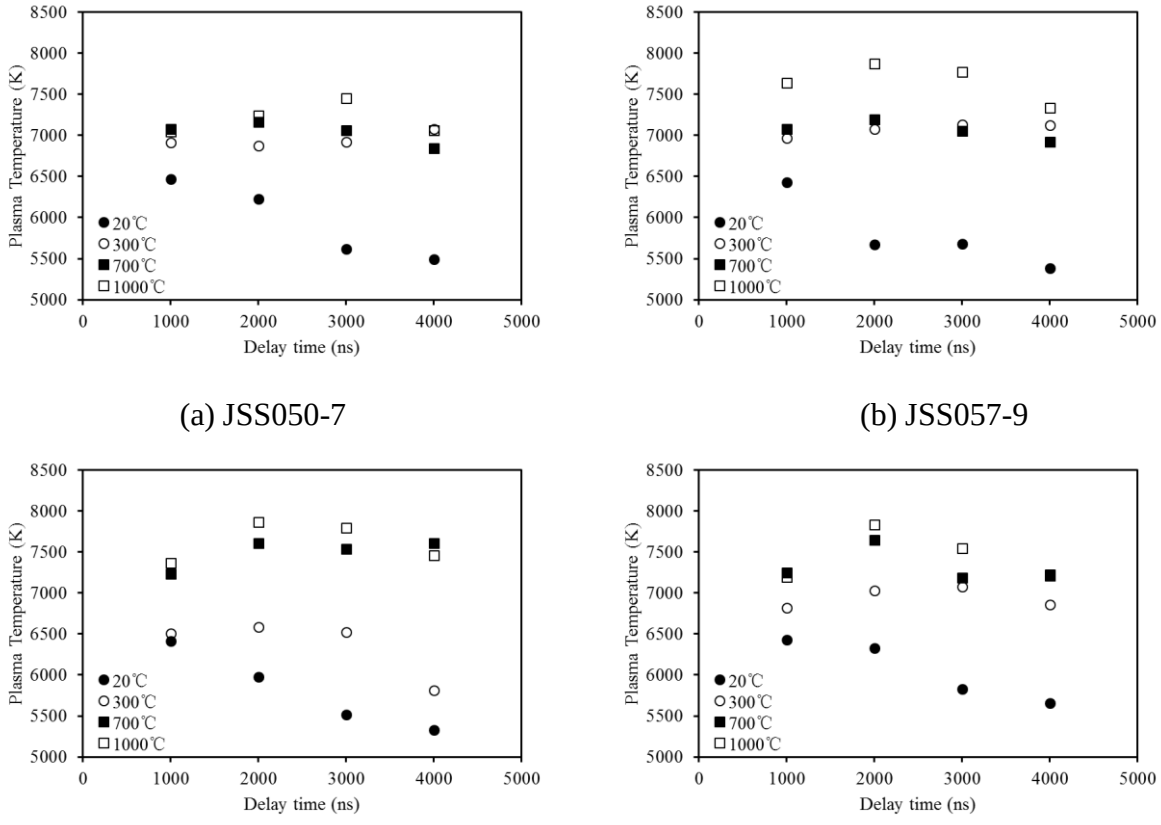

(a) JSS050-7 (b) JSS057-9

(c) JSS120-1 (d) JSS653-15

Fig.4-12 The change of plasma temperature with delay time (Based on Boltzmann Plot)

4.3 Sample temperature effects on Mn ion line

4.3.1 Measurement at Room Temperature

To evaluate the situation change influence onto the quantitative measurement, in this study, the line ratio of Mn ion line/FeII reference is selected as the quantitative factor; this is because FeII reference line has the same ionization level as the Mn line, and it is the most obvious one among FeII lines. And the dependence of the I_{Mn}/I_{Fe} on the components ratio under different delay time is shown in Fig.4-13.

At room temperature, the when delay time increased, the interference gradually increased. It means the spectral backgrounds have more obvious effects on the signals. One of the possible reasons is that when delay time increases, the intensity of spectral lines decreases. When backgrounds remains at a stable levels, the interference becomes high. As delay time increased, the error bars also became higher. It means the fluctuations become higher.

The phenomenon is hard to explain is that the conflict between the emission ability and the LIBS signal quality. In LIBS measurement, one of the main target is to improve the signal intensity. This is because when the emission ability is high, it means that the plasma is more stable, the characteristic lines are more obvious and stable, and this is helpful for the quantitative measurement. However, in this study, experimental results show that, when the emission ability is strong, the signal fluctuation rate increases, and the relation with the Mn mass components decreases.

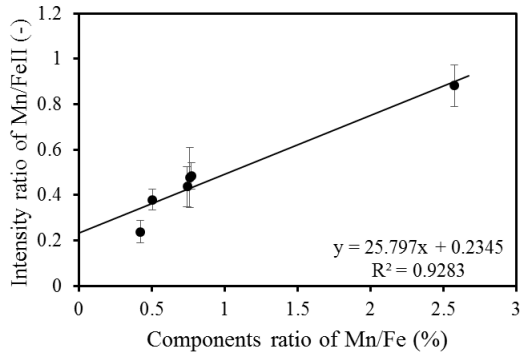

(a) D1000ns

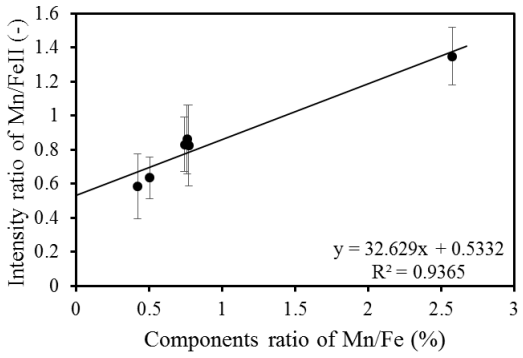

(b) D2000ns

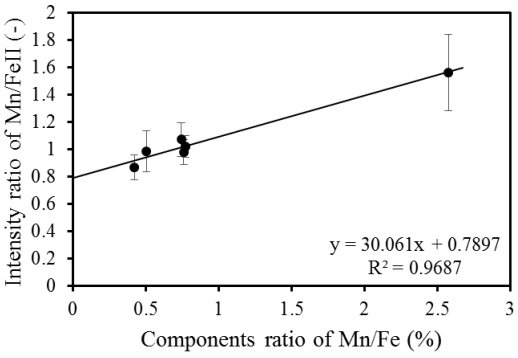

(c) D3000ns

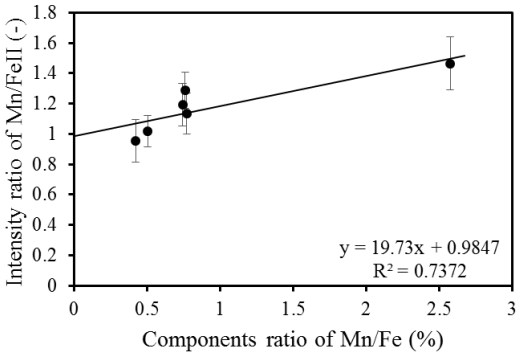

(d) D4000ns

Fig.4-13 The relation between Mn ion line/FeII reference and mass ratio of Mn/Fe at room temperature

4.3.2 Measurement at Elevated Temperature

The sample temperature does not only affect the spectra shape and the emission ability, but also the quantitative measurement signal. The calibration of Mn/FeII at different sample temperature is presented in Fig.4-14. From Fig.4-13(a) and Fig.4-14 (a), (e), (g), when sample temperature is under the room temperature, 300℃, 700℃, the relation between the signal intensity and Mn components are almost following the linearity relation; And the linearity correlation is more than 0.90. Under 1000℃, the intercepts increased and slope decreased obviously. According to Chapter 4.2 discussion, 1000℃ has a similar plasma parameters with 300℃ and 700℃, it means the change of plasma with sample temperature is not uniform, and the analysis based on one or two factor is not enough.

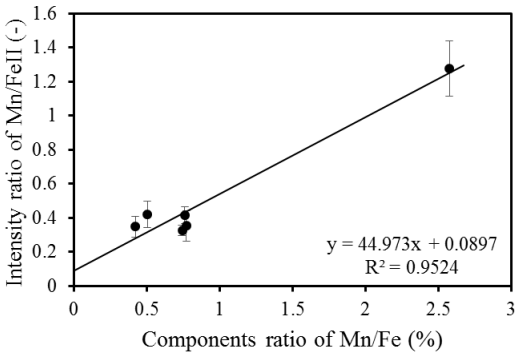

(a) 300℃ D1000ns

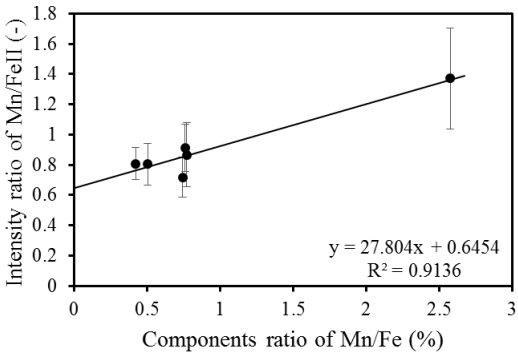

(b) 300℃ D2000ns

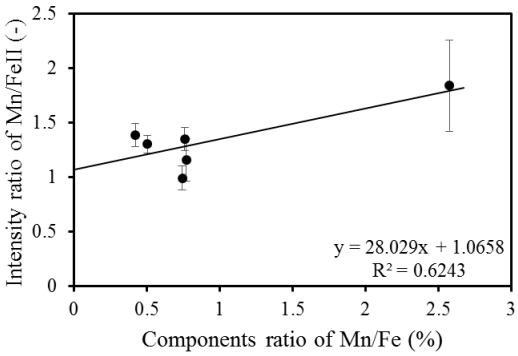

(c) 300℃ D3000ns

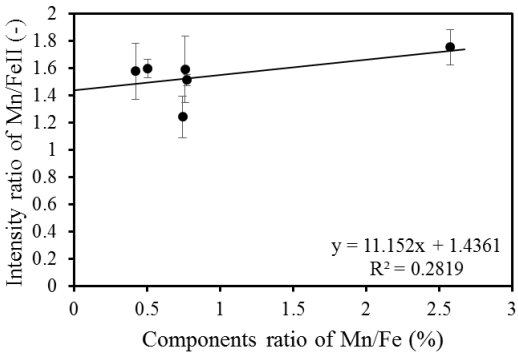

(d) 300℃ D4000ns

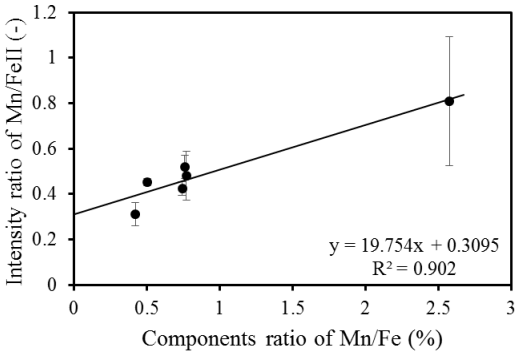

(e) 700℃ D1000ns

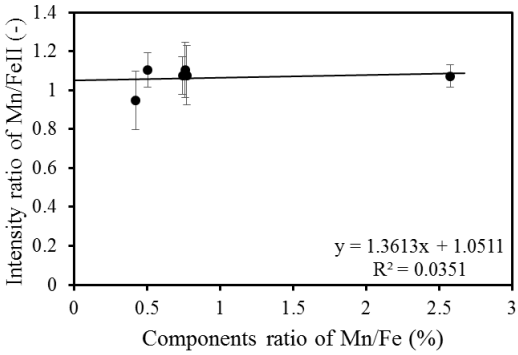

(f) 700℃ D2000ns

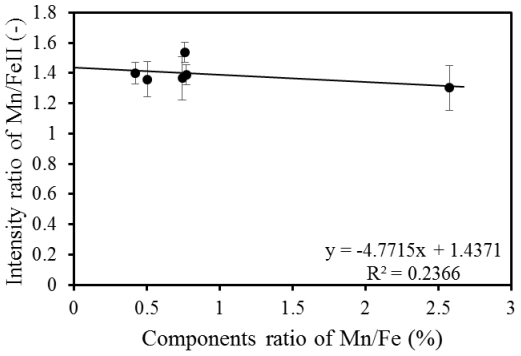

(e) 700℃ D3000ns

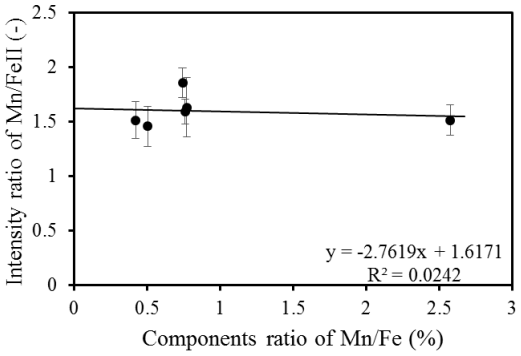

(f) 700℃ D4000ns

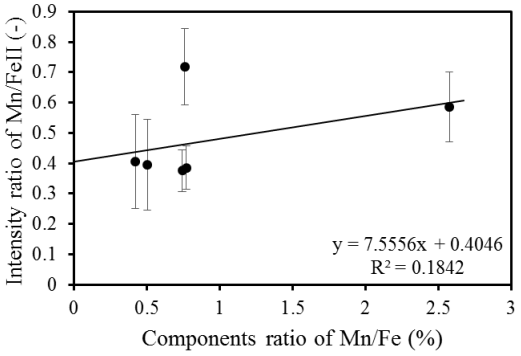

(g) 1000℃ D1000ns

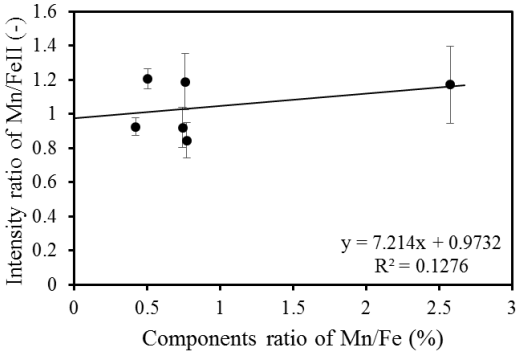

(h) 1000℃ D2000ns

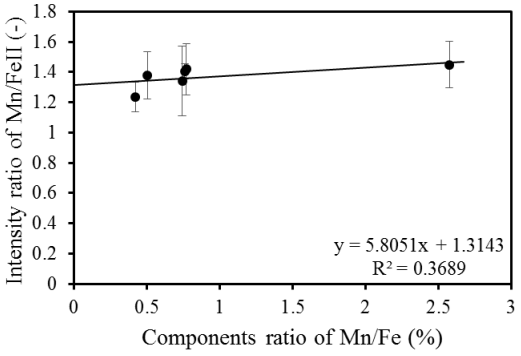

(i) 1000℃ D3000ns

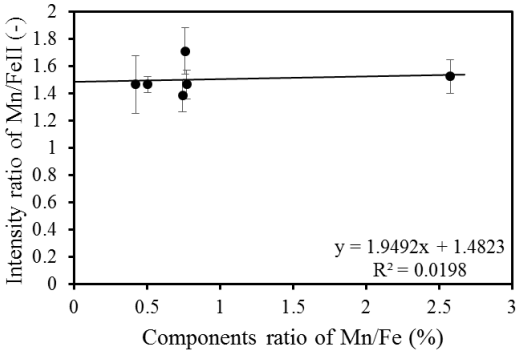

(j) 1000℃ D4000ns

Fig.4-14 The relation between MnII /FeII reference and mass ratio of Mn/Fe at different sample temperatures

According to the other delay time, generally, MnII/FeII loss its relation with the mass component as sample temperature increased. The slope decreased and R^2 decreased. Considering the discussion in Secession 4.2, one of reason is that the change of Fe lines is not uniform, the interference between MnII line and Fe lines are not uniform, and the evaluation of MnII line becomes not correct. Because the change of Fe lines in this wavelength regions cannot be simply described by plasma states, and MnII line is easily interfered by neighbor Fe line, so the wavelength region of 246-258nm is not suitable for quantitative analysis of Mn line.

4.4 Steel Analysis in Wavelength of 400-410nm

4.4.1 Spectra at Different Sample Temperatures

There are abundant Fe lines in the wavelength region of 246-258nm, which is good for plasma states analysis for Boltzmann Plot. But the interference of the Fe lines and the instability of Mn ion line, is not good for quantitative measurement. So we turned to the measurement of 400-410nm wavelength regions. The spectra in the wavelength of 400-410nm are shown in Fig.4-15. As it can be observed, at different conditions, the noise are different, higher delay time generally has higher noise. But the interference of Fe lines are small, each spectral line can be observed and identified in different conditions. Besides, the change of spectral lines in different conditions seems to be smaller, indicating a more stable quality when sample temperature changes.

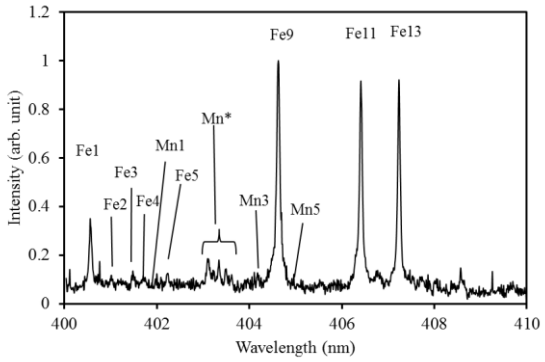

(a) 20℃ D1000ns

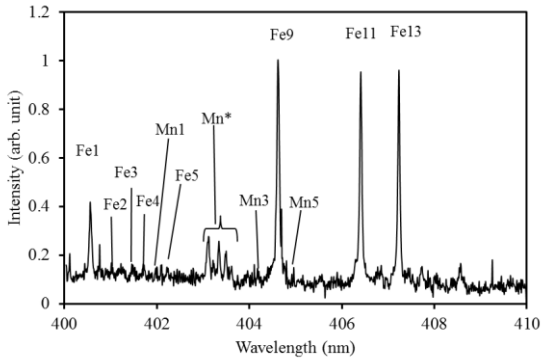

(b) 20℃ D2000ns

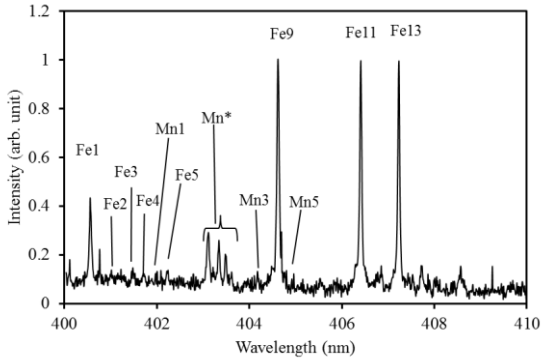

(c) 20℃ D3000ns

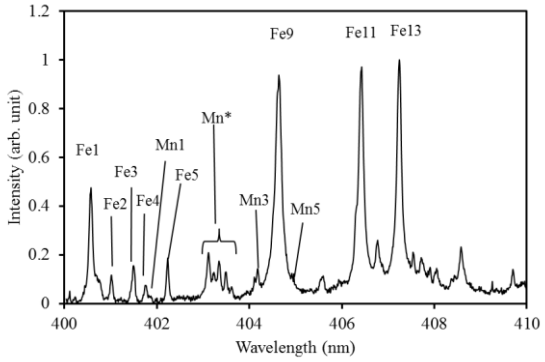

(d) 300℃ D1000ns

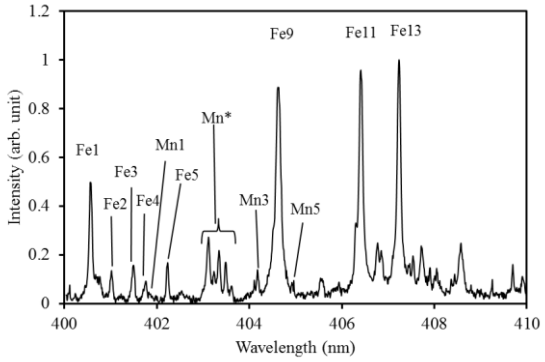

(e) 300℃ D2000ns

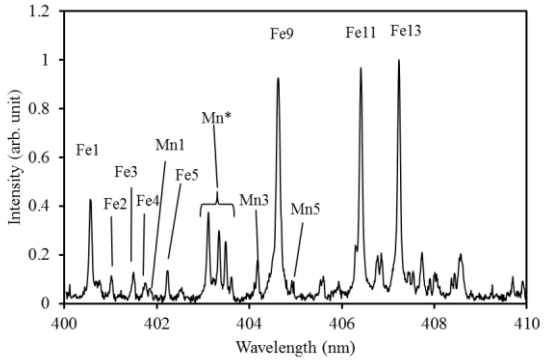

(f) 300℃ D3000ns

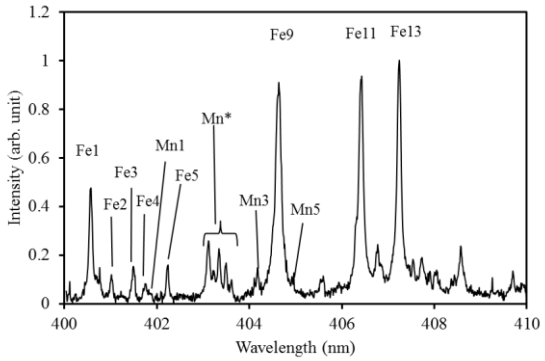

(g) 700℃ D1000ns

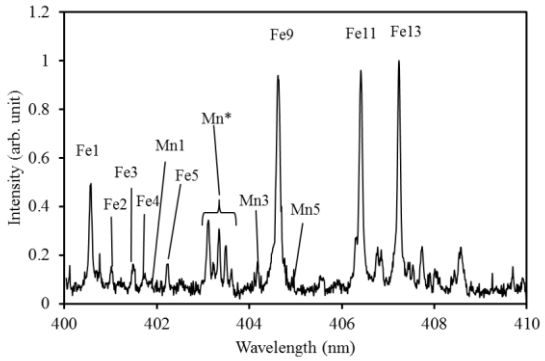

(h) 700℃ D2000ns

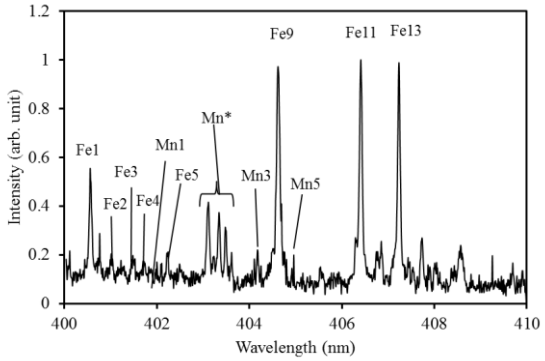

(i) 700℃ D3000ns

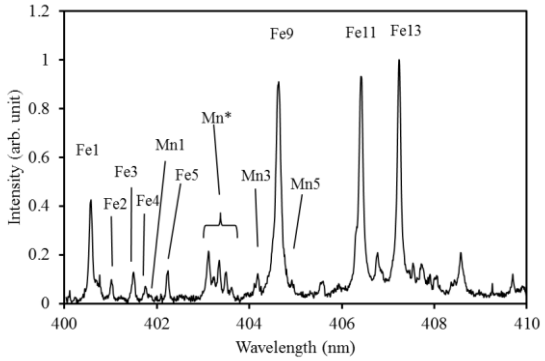

(j) 1000℃ D1000ns

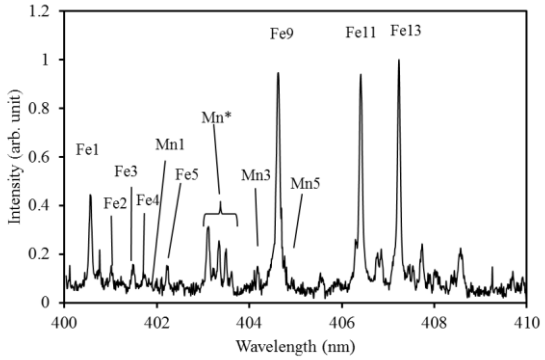

(k) 1000℃ D2000ns

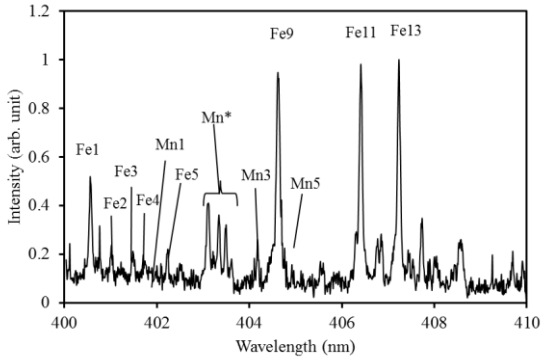

(l) 1000℃ D3000ns

Fig.4-15 Spectra of JSS050-7 at different sample temperature in 400-410nm region (normalization: the highest point of the spectrum itself)

There are two merits for measuring at this wavelength regions. One is the less interference between Mn lines and Fe lines. The other is the identification of spectral lines become easier, because spectral lines are not crowded, and the background noises is not serious during the measurement conditions. As it can be observed in Fig.4-15, both the signal intensities and the FWHM of spectral lines changed at different sample temperature. How sample temperature changes plasma states should be analyzed later.

The identification of the spectral lines are presented in Table 4-4, based on NIST database. All spectral lines are atom lines, and several Mn lines can be observed.

Table 4-4 Spectral lines information in the wavelength region of 400-410nm (Atom lines)

Element	Wavelength (nm)	A (s^{-1})	g_k (-)	E_k (cm^{-1})
Fe1	400.5242	2.04E+07	5	37521.161
Fe2	400.9713	4.64E+06	5	42859.778
Fe3	401.4531	1.53E+07	7	49477.127
Fe4	401.7148	3.25E+06	11	49460.902
Fe5	402.1866	8.55E+06	9	47106.484
Fe9	404.5812	8.62E+07	9	36686.16
Fe11	406.3594	6.65E+07	7	37162.746
Fe13	407.1738	7.64E+07	5	37521.161
Mn1	401.81	2.54E+07	8	41932.64
Mn3	404.136	7.87E+07	10	41789.48
Mn5	404.876	7.80E+07	4	42143.57
Mn*1	403.076	1.70E+07	8	24802.25
Mn*2	403.307	1.65E+07	6	24788.05
Mn*3	403.449	1.58E+07	4	24779.32

4.4.2 Plasma States Evaluation

In this wavelength region, set the ratio of Fe5/Fe1 as plasma temperature factor. It increases when plasma temperature increases. It is not suggested to draw Boltzmann Plot in this wavelength regions because Fe lines have higher energy levels having relative small differences with each other. The fluctuation of signals will introduce big errors to Boltzmann Plot. The change of Fe5/Fe1 with sample temperature is shown in Fig.4-16. As it can be observed, Fe5/Fe1 is a little increased at elevated sample temperature compared with room temperature. In 300,700,1000℃, however Fe5/Fe1 didn't have obvious differences. Fe5/Fe1 had some decrease when delay time increased. This results also shows that plasma thermals states do not change uniformly with the sample temperature increase. Which is consistent with the results of Fig.4-3. At some conditions, when delay time increased, Fe5/Fe1 didn't decrease continuously. It is because the upper energy levels differences between Fe5 and Fe1 line is not large enough, as shown in Table 4-4. The fluctuations of the signals may bring the errors in the factor.

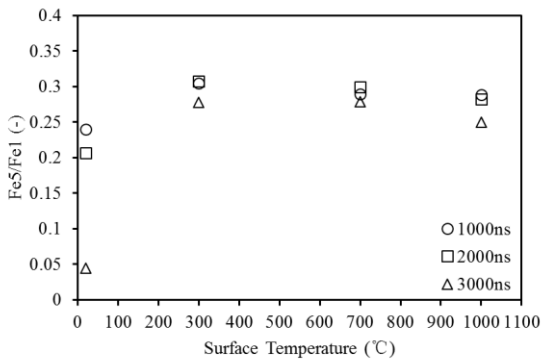

(a) JSS030-9

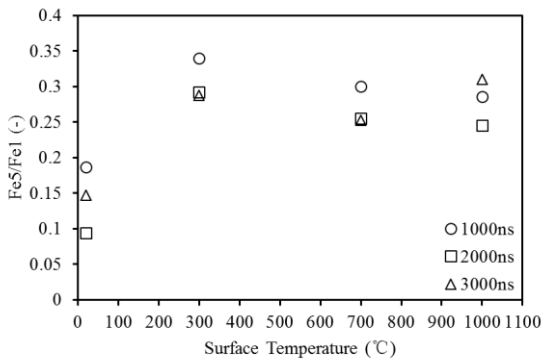

(b) JSS050-7

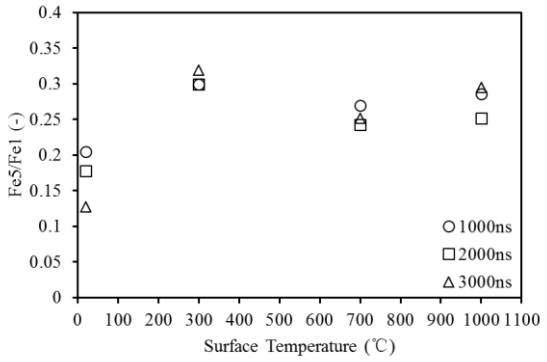

(c) JSS057-9

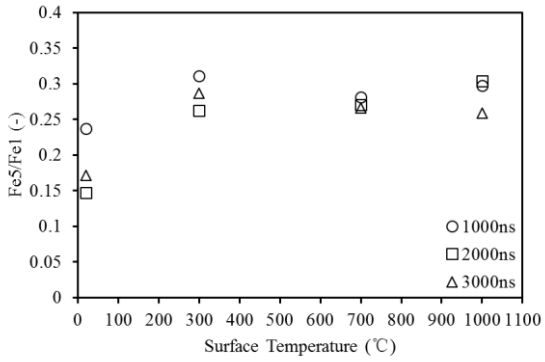

(d) JSS120-1

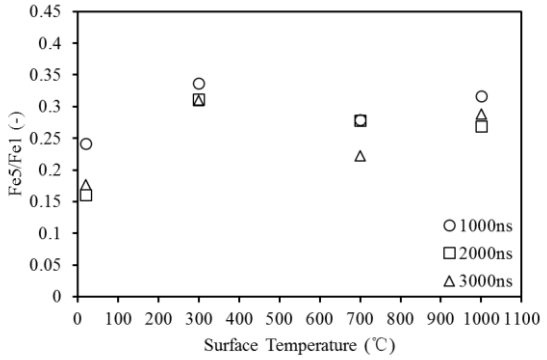

(e) JSS168-8

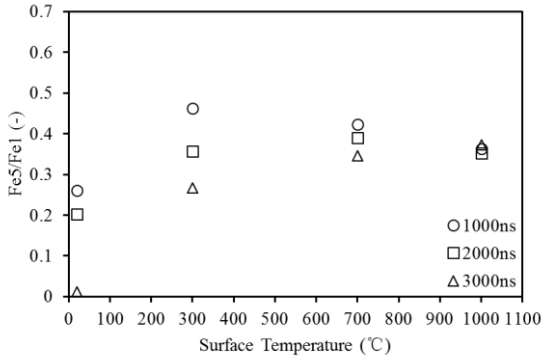

(f) JSS653-15

Fig.4-16 The dependence of Fe5/Fe1 on sample temperature

The other commonly calculated plasma states factor is free electron density, which is based on the full width at half maximum (FWHM) of the spectral lines. For the accurate calculation of free electron density, the equipment broadening of the spectrometer should be considered, which is not easy. But according to theory, FWHM is high when free electron density is high. The change of FWHM of Fe9 line with sample temperature is shown in Fig.4-17. As it can be observed, FWHM of Fe9 had obvious decrease with delay time, meaning the decrease of free electron density. While for sample temperature, 300℃ has the highest free electron density than the other sample temperature. It is consistent with the results in Fig.4-11.

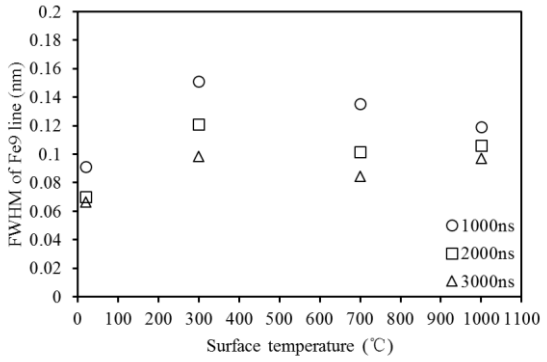

(a) JSS030-9

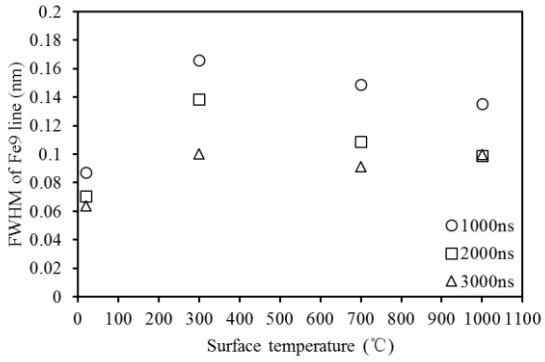

(b) JSS050-7

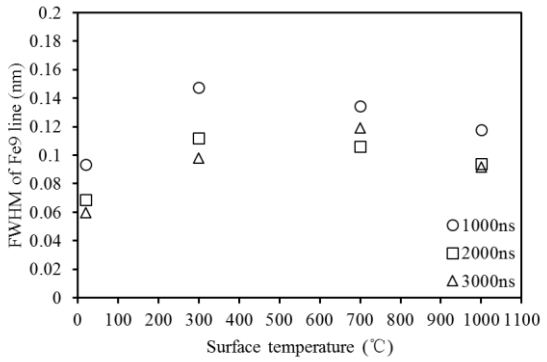

(c) JSS057-9

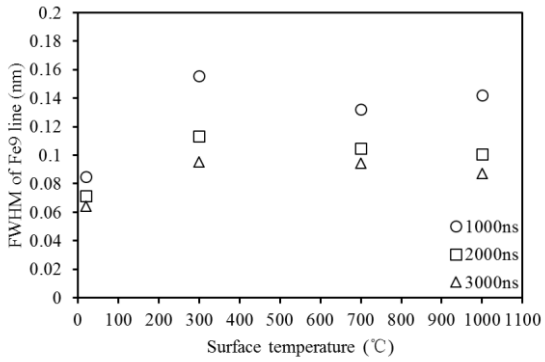

(d) JSS120-1

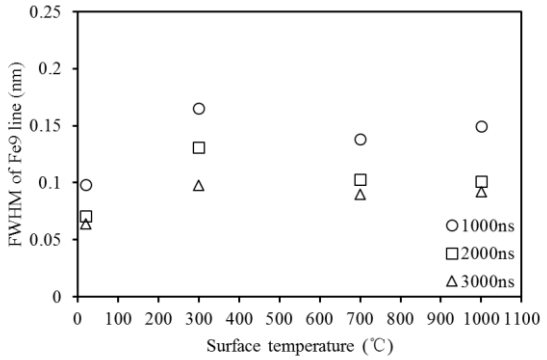

(e) JSS168-8

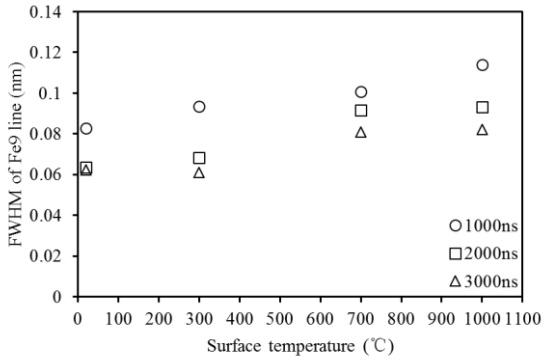

(f) JSS653-15

Fig.4-17 The dependence of FWHM of Fe9 on sample temperature

Both the higher plasma temperature and higher electron density indicate the higher plasma thermal states. Based on Fig.4-16 and Fig.4-17, generally for chemical standard steel samples, plasma states are highest at 300℃.

Because plasma states have inhomogeneous change with sample temperature, and there is some fluctuations interfering the single spectral lines. The analysis based on Boltzmann Plot is also necessary to testify the above conclusions, for more spectral lines are analyzed. The Boltzmann Plot based on Fe lines in Table 4-4 is shown in Fig.4-18. As it can be observed, the Boltzmann Plot is scattered at some conditions, which will introduce errors to the plasma temperature evaluation. It is not easy to find the Boltzmann Plot of dominant partition function for Fe lines are not enough. The Boltzmann Plot analysis should also be careful.

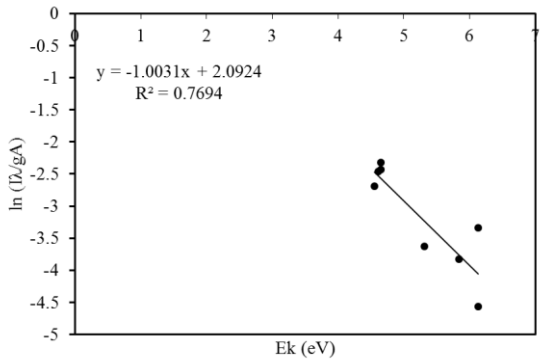

(a) 20℃ D1000ns

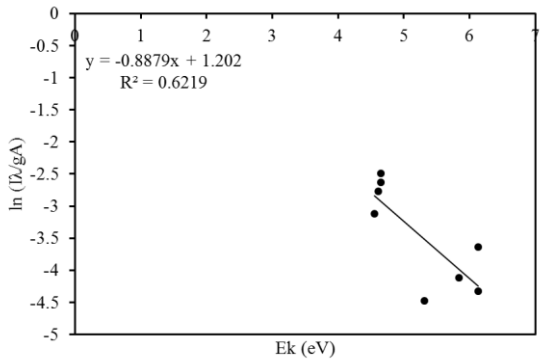

(b) 20℃ D3000ns

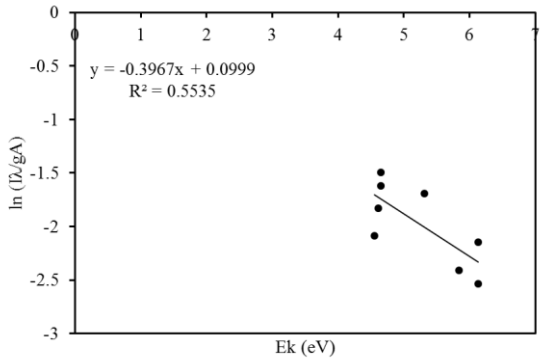

(a) 700℃ D1000ns

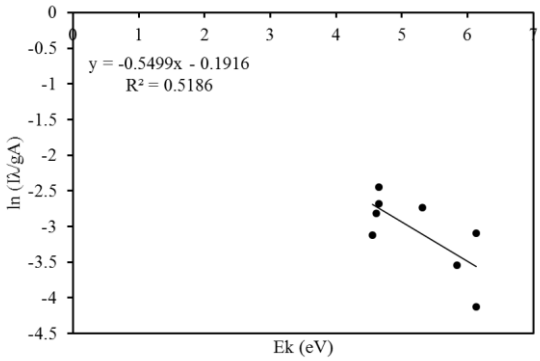

(b) 700℃ D3000ns

Fig.4-18 Boltzmann Plot based on Fe lines in Table 4-4 (Sample: JSS050-7)

4.4.3 Sample temperature effects on Mn atom line

The signal ratio of Mn*/Fe9 is the component factor of Mn element. The calibration curve of Mn*/Fe9 at different sample temperature is presented in Fig.4-19. As it can be observed, the linear correlation kept at relative high levels at different sample temperature and delay time, which proves that the interference of Mn spectral line is less. This is consistent with the spectra that Mn line can be identified at different conditions. Besides, when sample temperature increased, the slope of calibration curves gradually decreases its value. It means the Mn signal becomes less sensitive to the Mn component when sample temperature increased. It is consistent with the results in Fig.4-14.

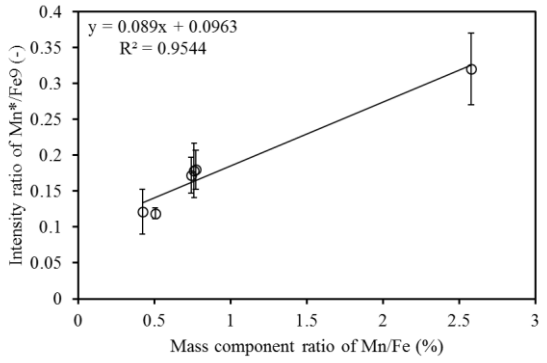

(a) 20℃ D1000ns

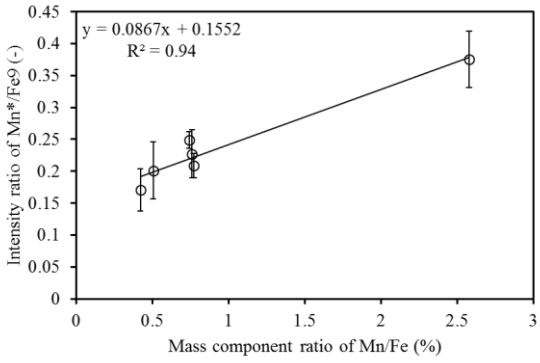

(b) 20℃ D2000ns

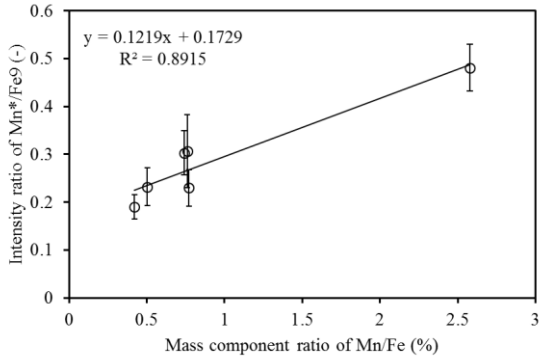

(c) 20℃ D3000ns

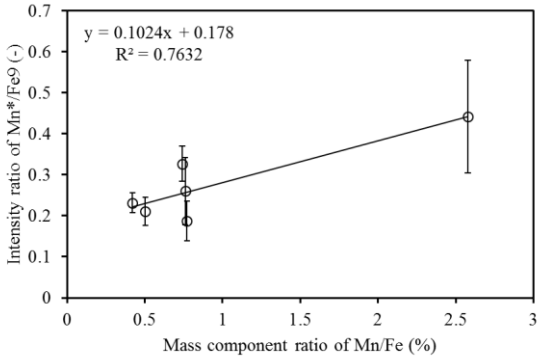

(d) 300℃ D1000ns

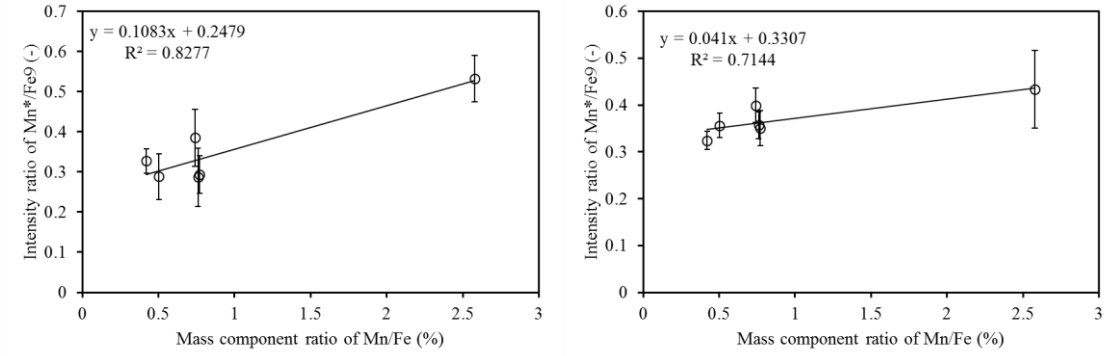

(e) 300℃ D2000ns

(f) 300℃ D3000ns

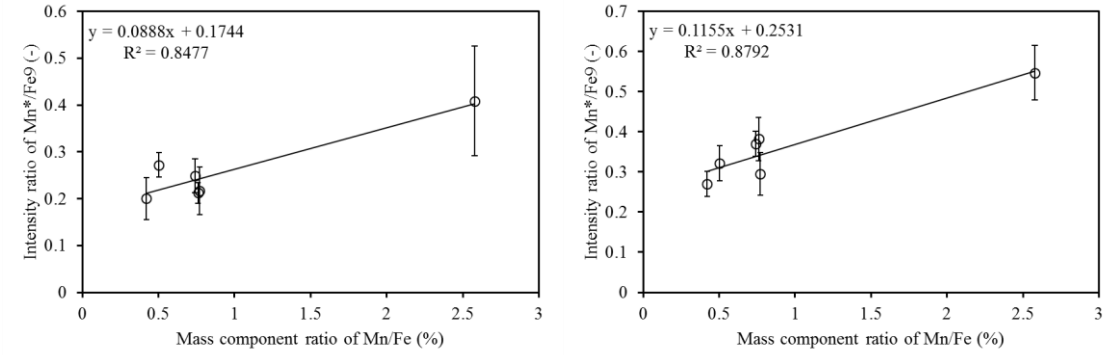

(g) 700℃ D1000ns

(h) 700℃ D2000ns

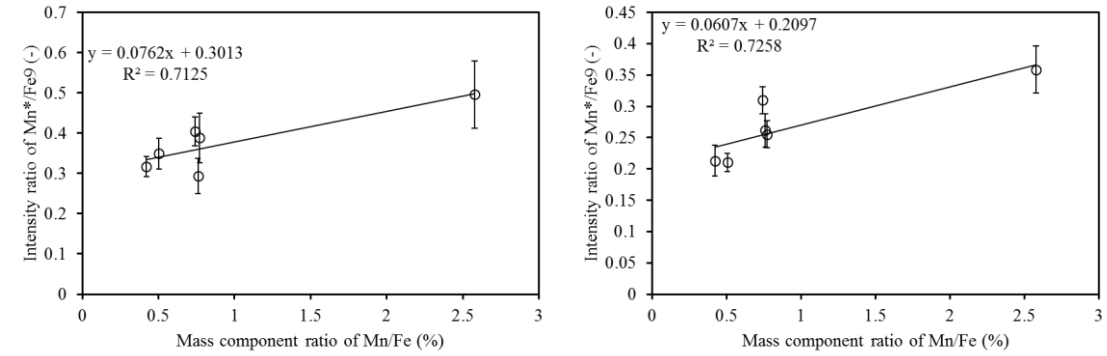

(i) 700℃ D3000ns

(j) 1000℃ D1000ns

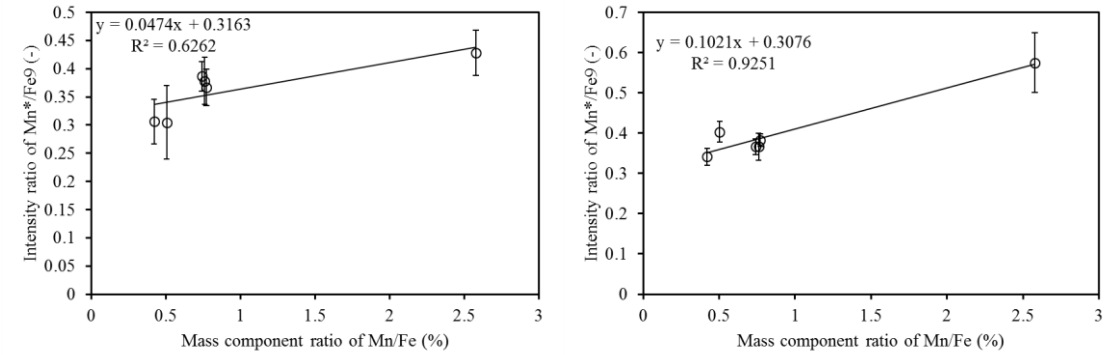

(k) 1000℃ D2000ns

(l) 1000℃ D3000ns

Fig.4-19 Calibration curve of signal ratio of Mn*/Fe9 at different sample temperature

When sample temperature increases, the quantitative measurement ability decreases. The sample temperature effects cannot be ignored. As it shows in spectra, spectral line is easy to be

identified at high sample temperature, but the quantitative ability becomes worse. It means as sample temperature increased, there is some complicate factors affecting the Mn line intensity.

4.4.4 Quantitative models Analysis

As it can be considered, when sample temperature increases, the plasma states have very complicate change, which is not easy to be evaluate through only one or two factors. Besides, when sample temperature increases, even though spectral line has higher intensity, it is disturbed and has less relation with component.

Therefore, for quantitative measurement, the machine learning methods are proposed, which is wildly used in LIBS measurement now. The theory of common used machine learning PLS is explained in Chapter 2. The principle of machine learning is not based on the physical theory, but it is to establish an approximate relationship between independent variables and dependent variables. Considering the complicate Mn signal intensity change with unclear plasma factors, it is reasonable. In this secession, we are discussing about the structure parameters of quantitative models.

Because MnII line has serious interference with Fe lines, and is easy to be interfered by measurement conditions, MnI lines in the wavelength region of 400-410nm are more suitable for quantitative measurement. Because the calibration curves usually had higher linear correlations when delay time is 2000ns, and the spectra have less noises at this delay time, so all the quantitative models are based on delay time of 2000ns. Set JSS057-9 as the validation sample for quantitative analysis. Based on the single variate linear PLS method, the type of the model is Eq.(4-2)

$$C_{\frac{Mn}{Fe}} = a\frac{I_{Mn^*}}{I_{Fe1}} + b. \qquad \text{Eq.(4-2)}$$

And the quantitative models at different sample temperature are shown in Fig.4-20. The RMSE for regression of Fig.4-20 are (a) 2.815‰, (b) 4.392‰, (c) 3.786‰, (d) 3.541‰ respectively. The RMSEP for prediction of Fig.4-20 are (a) 1.706‰, (b) 2.165‰, (c) 1.906‰, (d) 3.867‰ respectively.

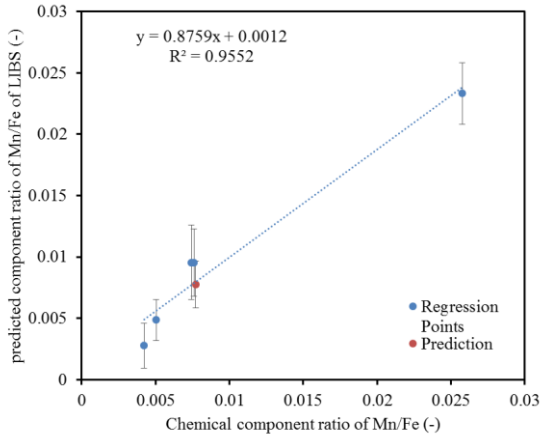

(a) 20℃

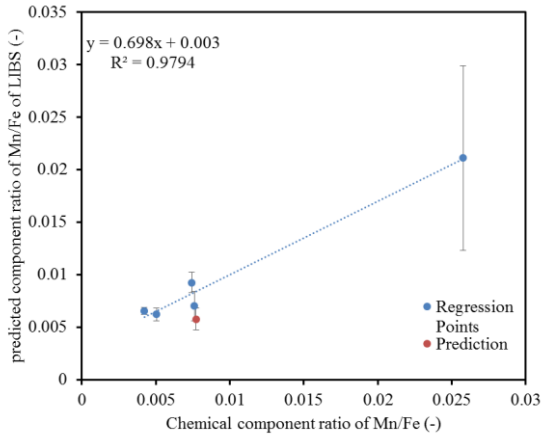

(b) 300℃

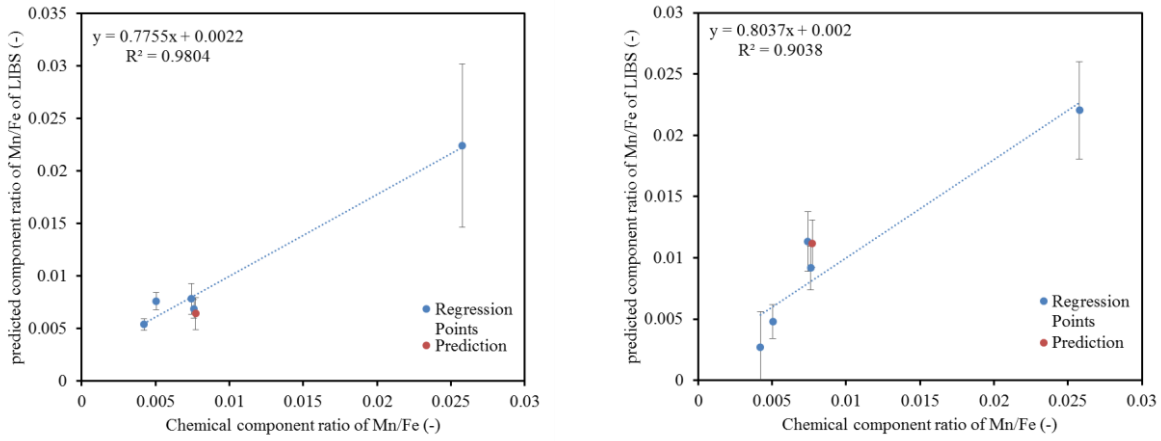

(c) 700℃ (d) 1000℃

Fig.4-20 The single variate linear PLS quantitative models at different sample temperature (Fixed delay time: 1000ns)

Generally, compared with the results in Fig.4-13 and Fig.4-14, the quantitative measurement hear is better in elevated sample temperatures, the slope is higher while the intercept remains small, which means the lower backgrounds interference. It can be observed that at room temperature, the measurement accuracy is higher, with better slope, R^2, RMSEP and smaller error bars. How to discard sample temperature effects on LIBS should be further considered.

Compared with calibration curves, the PLS models have improve the accuracy of models a lot. The slope of the calibration curves increased. It means the decrease of LOD, which means the increase of models precisions. At high sample temperature, the slope is still far away from 1. And the error bars are high. This is consistent with the previous results that Mn line lost its quantitative ability at high sample temperature. PLS model can only just decrease this errors. So the calibration of the models are necessary.

Because plasma is not a linear system, the emission of the spectral lines may also not be linear, so whether the spectral lines have non-linear relation with element component should be considered. The multiple variate 2^{nd} order PLS method is tried. The type of the model is as following equation. And the quantitative model is as following Fig.4-21.

As it can be observed, at all sample temperatures, the 2^{nd} order PLS have increased the slope and the linear correlations. The regression accuracy became better. Considering the input Mn signals didn't change, it means the 2^{nd} order system is more near with the plasma system. It testifies the plasma is not a linear system, and the non-linear quantitative model is better for the regressions. This also indicates that, to obtain a good quantitative model, the model type is one of the key factors.

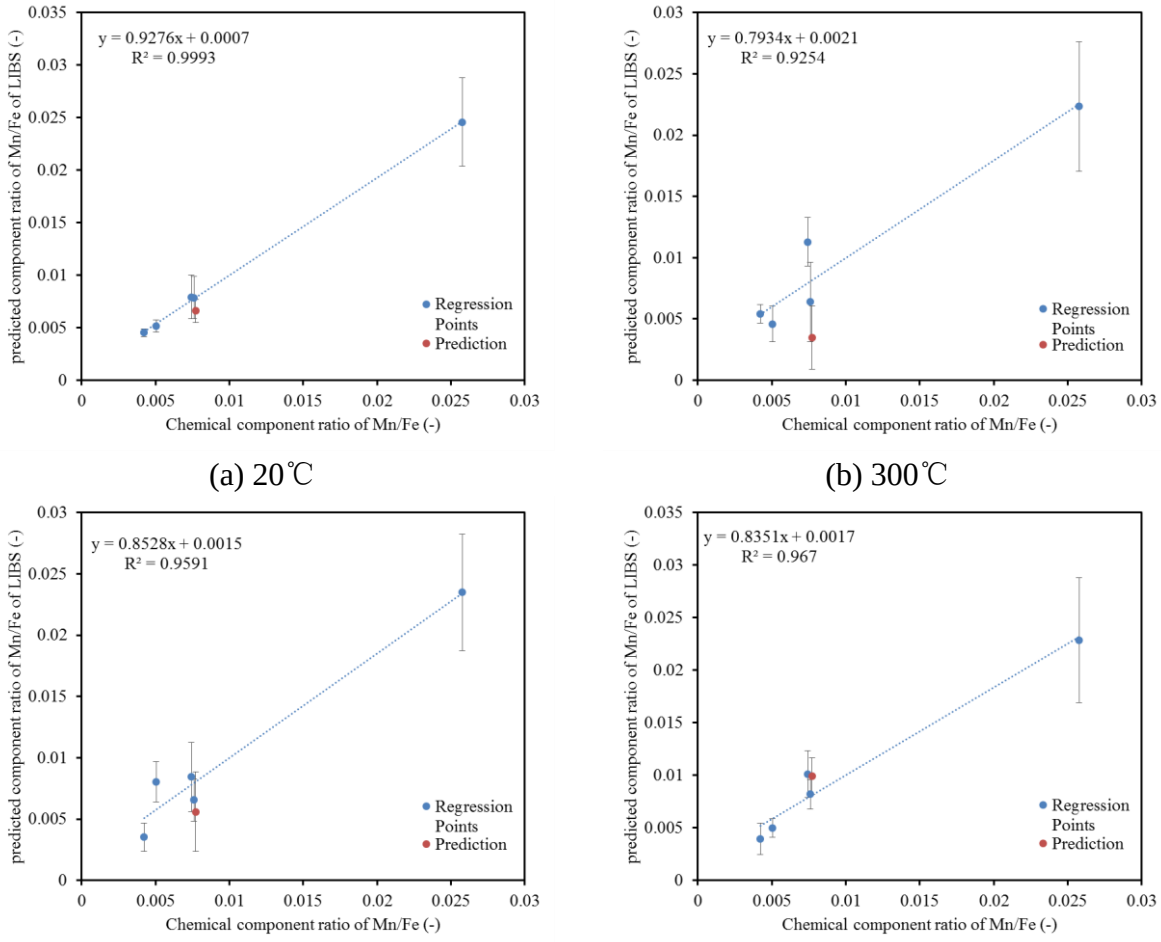

Fig.4-21 The single variate 2nd order PLS quantitative models at different sample temperature (Fixed delay time: 1000ns)

When the plasma temperature factor Fe5/Fe1 and electron number density factor FWHM of Fe9 cannot describe the change of plasma states with the sample temperature, it can partially reflects such kind of effect. It is proposed that, put such kind of information into the quantitative models, and it will help to increase the quantitative models quality. The calibration of the PLS model by adding this two factors are presented in Fig.4-22. No matter adding one factor or adding two factors, the model is optimized. Compared with adding only one factor, adding two factors together induces a more accurate model. The RMSE for regression is 1.968‰, and RMSEP for prediction is 1.704‰. By using the multiple variate 2nd order PLS, slope and R^2 are increased, and RMSEP decreased. Quantitative analysis accuracy is increased.

Therefore, the single variate linear PLS method is usually not so accurate, for plasma is not a linear system, and some other effects also influence the accuracy. By adding the plasma states evaluation factors into the model, the accuracy increased, and the good form of PLS is as following Eq.(4-3).

$$C_{\frac{Mn}{Fe}} = a_{11}\left(\frac{I_{Mn*}}{I_{Fe1}}\right)^2 + a_{12}\left(\frac{I_{Mn*}}{I_{Fe1}}\right) + a_{21}\left(\frac{I_{Fe5}}{I_{Fe1}}\right)^2 + a_{22}\left(\frac{I_{Fe5}}{I_{Fe1}}\right) + a_{31}FWHM^2_{Fe9} + a_{32}FWHM_{Fe9} + b$$

Eq.(4-3)

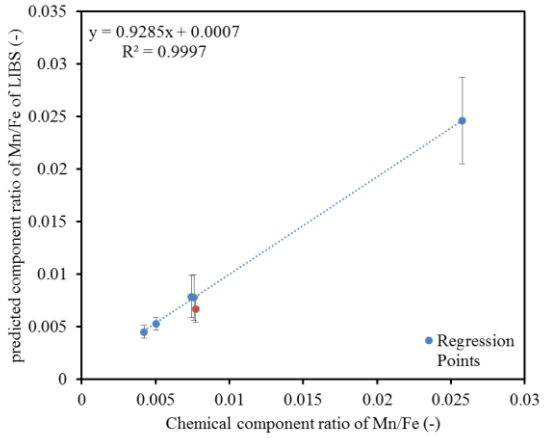

(a) adding only Fe5/Fe1

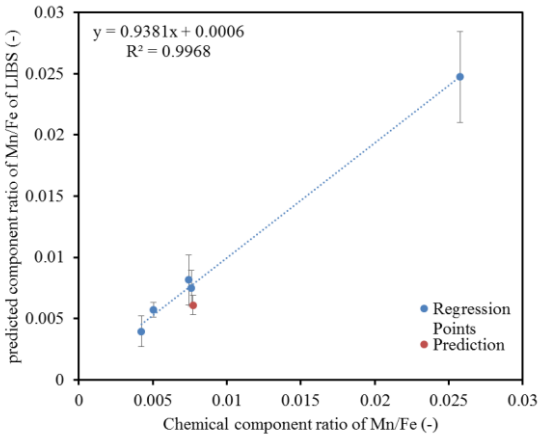

(b) adding only FWHM of Fe9

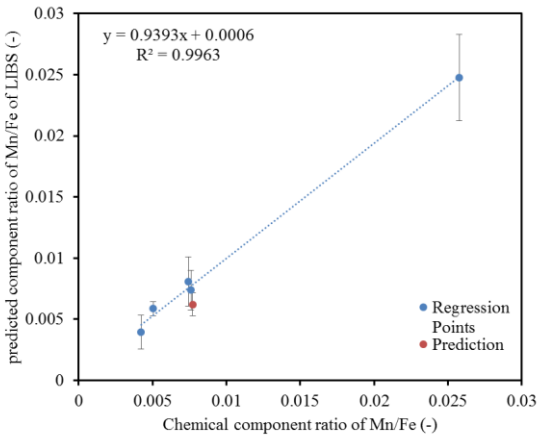

(c) adding both Fe5/Fe1 and FWHM of Fe9

Fig.4-22 The multiple variate 2nd order PLS quantitative models at 20℃

Based on this model types, the quantitative models at elevated sample temperature is also presented in Fig.4-23. The corresponding RMSE is (a) 2.611‰, (b) 1.950‰, (c) 2.218‰. RMSEP is (a) 5.332‰, (b) 5.892‰, (c) 2.788‰. Compared with previous results, the models accuracy increased.

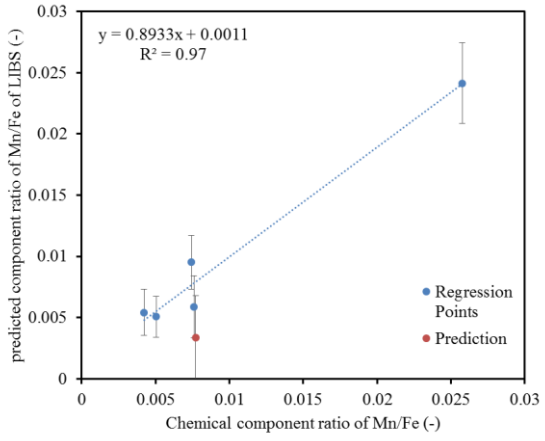

(a) 300℃

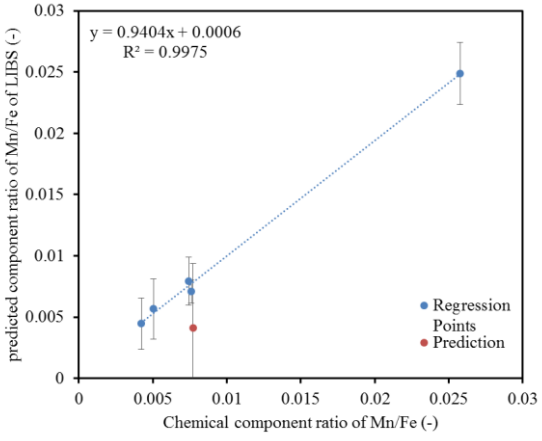

(b) 700℃

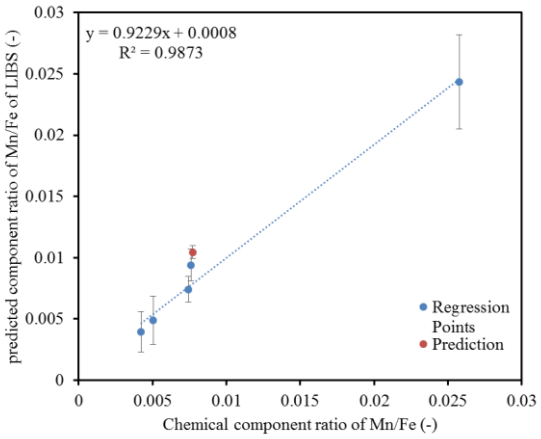

(c) 1000℃

Fig.4-23 The multiple variate 2nd order PLS quantitative models at 20℃

There is no certification that plasma is a strict 2nd order non-linear system. For non-linear system, there are many different function types. BPNN method is also a good for regression, because it has complicate internal structure, it can fit any type of function. When the input vectors are fixed as the Mn signal and Fe5/Fe1 and FWHM of Fe9, the results of BPNN is presented as Fig.4-24.

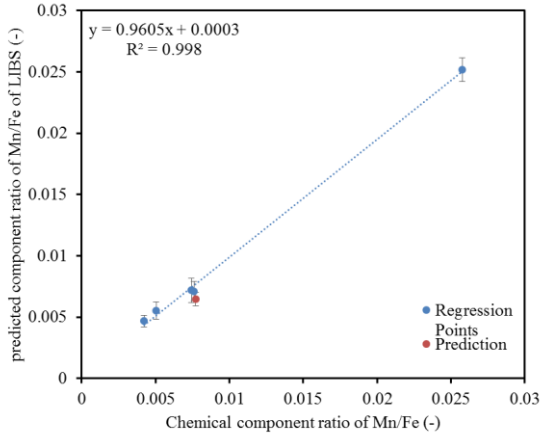

(a) 20℃ 1st time training

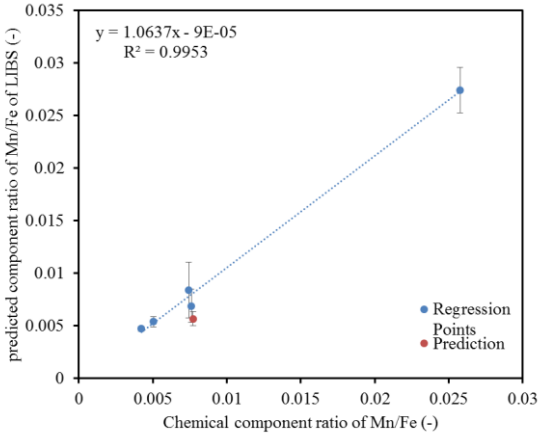

(b) 20℃ 2nd time training

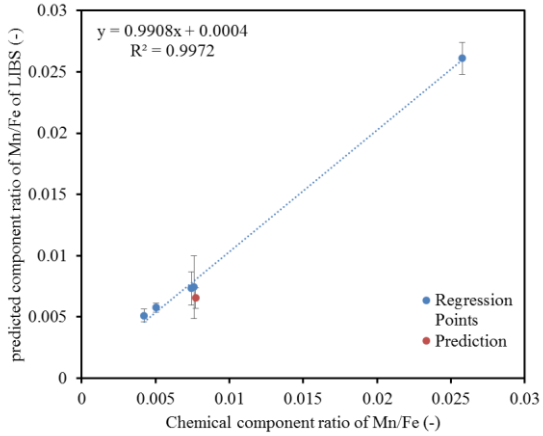

(c) 20℃ 3rd time training

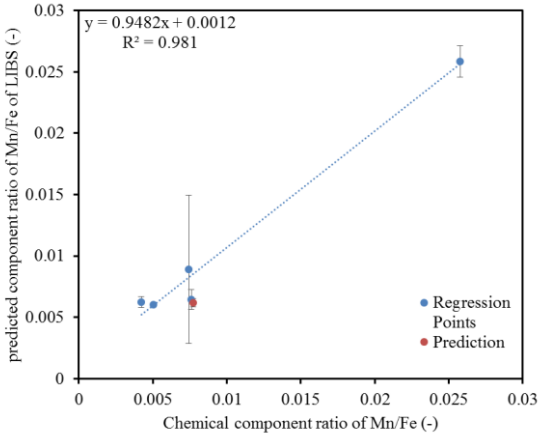

(d) 300℃ 1st time training

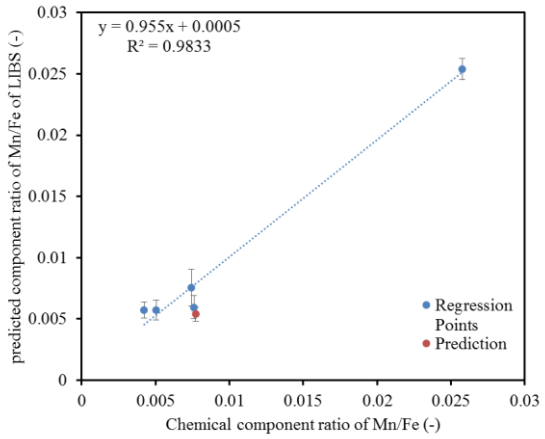

(e) 300℃ 2nd time training

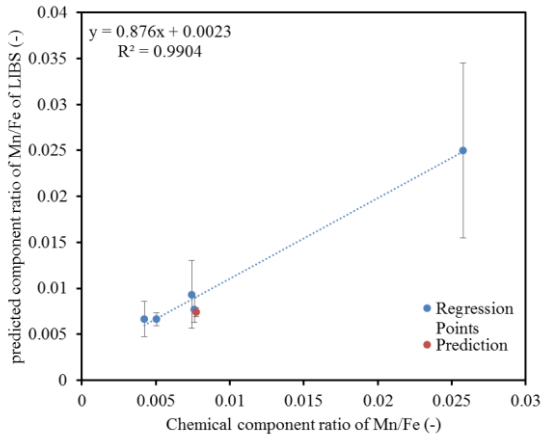

(f) 300℃ 3rd time training

Fig.4-24 BPNN model with multiple variates input vector

As it can be observed. The error bars of both the regression points and the verification point became smaller. And the slope and linear correlation became near to 1. This indicates BPNN is more reliable, which can even decrease the fluctuation errors of LIBS measurement. However, BPNN method is dependent on not only the model types, but also the regression processes, such as the initial conditions. So (f) shows the bad results, and the other figures cannot fixed its model numbers. Besides, BPNN method is difficult for physical explanation. The application of BPNN method should be very careful.

4.5 Summary

When sample temperature is elevated from room temperature, the general plasma temperature doesn't have obvious increase, while the total Fe atoms and Fe^+ ions numbers are improved. The plasma temperature calculated from Fe atoms is lower than that from Fe^+ ions, while the number of Fe atoms is much bigger than Fe^+ ions. Which is consistent with the thermal theory, while it indicates the inhomogeneity inside plasma. When sample temperatures change, the change of each Fe line is also not uniform, which can be observed in Boltzmann Plot.

For Mn quantitative analysis, Mn atom line is more robust than Mn ion line. The Mn atom line has less interference with Fe lines, and it is sensitive to the components at evaluated sample temperature. Through the discussion of PLS model, the Mn lines have non-linear relation with the component, which is different from the theory equations, but it is reasonable for the complicity of plasma. Based on Mn atom lines, the multi-variates PLS using 2nd order has higher accuracy, it means that the plasma is a non-linear system, and put more information with less interference in to the quantitative models help to increase the accuracy. Plasma is a non-linear system, and the emission of elements are also not following just a simple linear theory. Based on the 2nd order PLS, the accuracy of the model increased. When adding the plasma temperature factor Fe5/Fe1 and electron number density factor FWHM of Fe9, the quantitative model increased the quantitative quality.

Because the plasma is non-linear system, BPNN method is also good for the quantitative model regression. The results shows that it can obtain the better regression accuracy. However, BPNN method accuracy relies on not only the training dataset, but also the training processes.

There is no general theory for the most correct training processes, so the BPNN model may have the danger to be in bad regression, which is not good for quantitative measurement.

5 Comparison of SP-LIBS and Long-Short DP-LIBS

In the other research, DP-LIBS has proven its merits for LIBS to enhance its application regions, stabilize the thermal states of plasma, and increase the reproducibility [83][87]. Long-short DP-LIBS is a kind of new proposed method of two lasers configuration. We are going to testify whether it can improve the behavior of LIBS measurement on steel.

Based on the discussion in Chapter 4, atom line of Mn is better for analysis than ion line. The wavelength region of 400-410nm was selected for following analysis. The plasma analysis of long-short DP-LIBS requires less of other effects interference, so the bulk samples were measured, replacing particle samples, because it has less surface effects.

5.1 Sample Temperature Effect Using SP-LIBS

In section 5.1 and 5.2, the plasma states analysis is based on the sample 20MnMo in Table 3-2. Fig.5-1 shows the measurement results at different sample temperature of 20°C, 300°C, 500°C and 700°C using SP-LIBS. Measured spectra were the average of five measurements and normalized by maximum signal from SP-LIBS measurement, as shows in Fig.5-1 (a), (b), (c), (d). The measured spectral wavelength range was 400–410 nm, from which many manganese and iron emission lines can be identified. The specifications of these emission lines were checked using NIST database and has been shown in previous work. By observing the spectra, it can be found that the spectra at each sample temperature can be clearly distinguished and the signal intensity of each spectra line was obviously different with sample temperature variation, which means that sample temperature would have a significant impact on the spectra measured by SP-LIBS. Fig.5-1 (e) shows the sample temperature dependence of Fe 400.524 nm, Mn 404.136 nm and Fe 402.187 nm signal intensity. As the sample temperature increased from 20°C to 700°C, the emission intensity of Fe 400.524 nm, Mn 404.136 nm and Fe 402.187 nm increased and reached maximum value around 700°C. In addition, signal intensity variation of this three spectral lines had similar trend with increasing sample temperature. It indicates that the sample temperature has significantly effect on signal intensity measured by SP-LIBS and the influence mechanism on each spectral line is similar.

In the sample temperature increased from 20°C to 700°C stages, the measured signal intensity increased with the increase of sample temperature, and the change of ablation mass had an important contribution for this phenomenon. The intensity of spectral line has obvious relationship with the total ablation mass of the sample, which depends on many factors, such as specific heat, partial reflectance of the sample surface, sample temperature, etc. High sample temperature is an effective way to improve total ablation mass. The maximum ablated amount of sample M was calculated by following Eq.(5-1).

$$M = \frac{E_c}{C_p\left(T_b - T_0\right) + l} \qquad \text{Eq.(5-1)}$$

Where, E_c is the laser energy coupled to the sample, C_p is the specific heat, T_b is the boiling temperature, T_0 is initial sample temperature and l is latent heat.

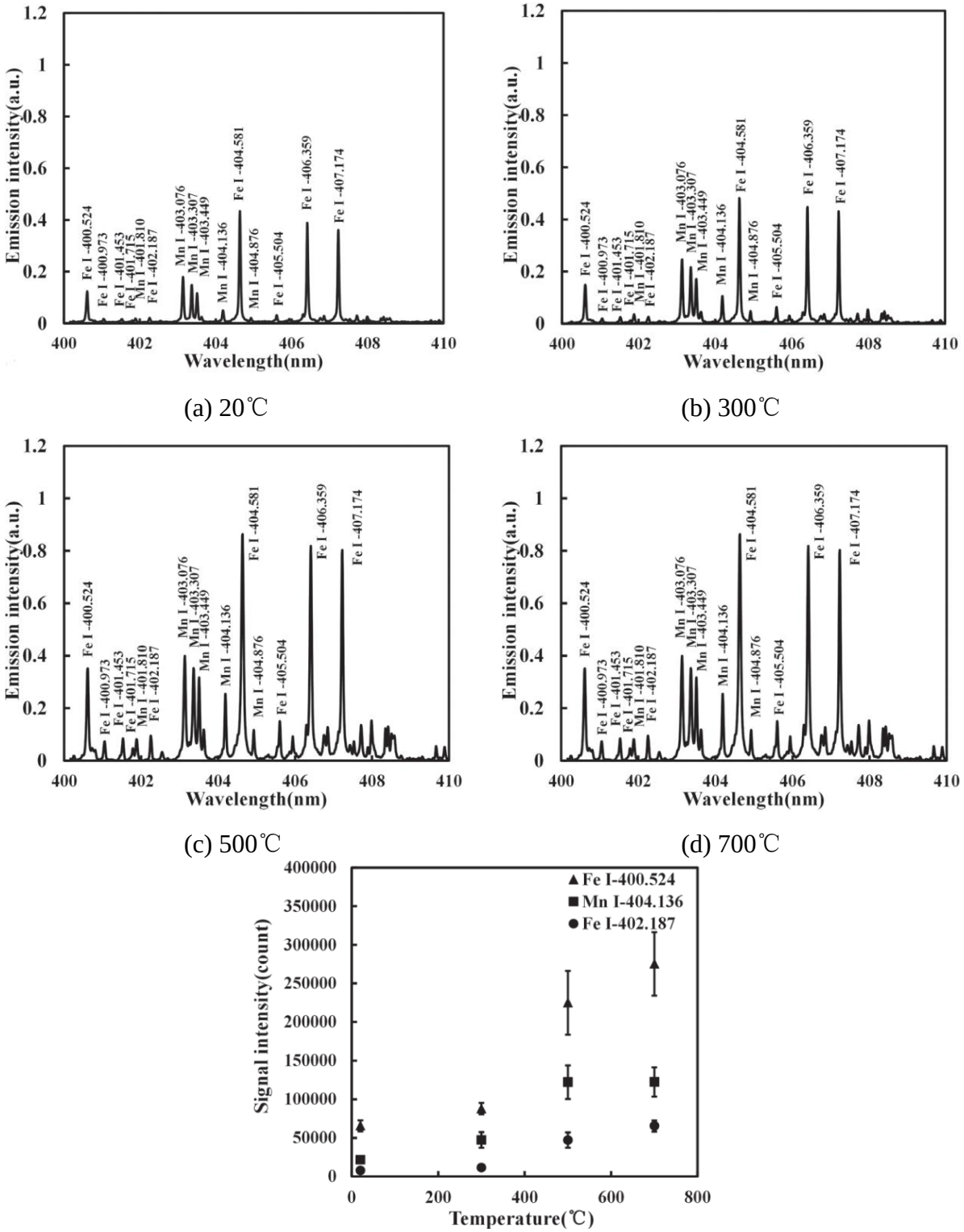

(e) Signal intensity of Fe I 400.524 nm, Mn I 404.136 nm, Fe I 402.187 nm

Fig.5-1 Measured results at different sample temperature by SP-LIBS

It can be seen from the Eq.(5-1) that increasing the initial sample temperature T_0 under the same conditions can effectively increase the amount of laser energy used for ablation of the sample. Therefore, less laser energy is required to heat the sample under high sample temperature condition and high sample temperature can enhance the ablation amount of the sample. More energy in the laser pulse is also used for the plasma evolution process, including

electron impact ionization process and inverse bremsstrahlung absorption process. Therefore, signal intensity will increase with sample temperature.

5.2 Characteristics of Plasma using Long-Short DP-LIBS

Variations in sample temperature have an impact on the signal strength of SP-LIBS, which will affect the accuracy of quantitative analysis. Long and short DP-LIBS method is an effective method to improve plasma stability and signal strength. Therefore, the collinear length DP-LIBS method was used to measure the standard steel sample, and the influence of sample temperature was further analyzed. Fig.5-2 shows the measurement results at different sample temperatures using long and short DP-LIBS. The measured spectrum is the average of the five measurements and normalized by the maximum signal measured by long and short DP-LIBS, as shown in Figure 5-2(a), (b), (c) and (d). By observing the spectra, it can be clearly seen that the emission spectra at different sample temperatures are almost overlapped, and the variation is not as sharp as SP-LIBS. The results show that long and short DP-LIBS can obtain relatively stable measurement results at different sample temperatures. Fig.5-2(e) shows the variation trend of emission spectrum intensity with sample temperature. Compared with SP-LIBS, the signal intensities of Fe 400.524nm, Mn 404.136nm and Fe 402.187nm measured by long and short DP-LIBS tend to be stable at different sample temperatures. The results show that the long and short DP-LIBS method can reduce the influence of sample temperature on signal intensity, which is mainly due to the heating effect of long pulses in long and short DP-LIBS. In the long and short DP-LIBS process, the long pulse irradiates the sample first. Due to the low peak power of the long pulse, the sample absorbs the energy of the long pulse to increase the temperature without generating plasma. After short pulse radiation, the sample heated by long pulse will be atomized and evaporated to generate plasma. Therefore, the short pulse will irradiate the sample under relatively stable conditions.

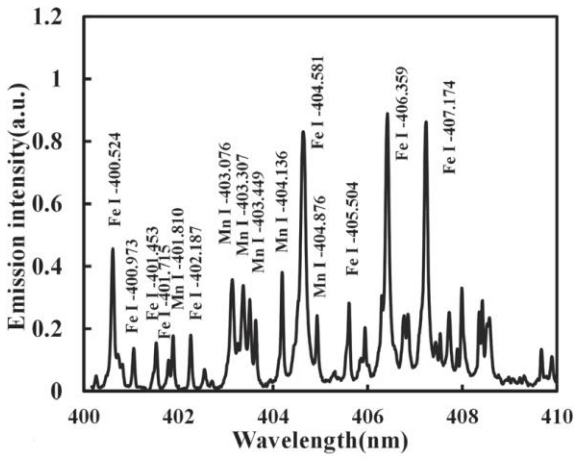

(a) 20℃

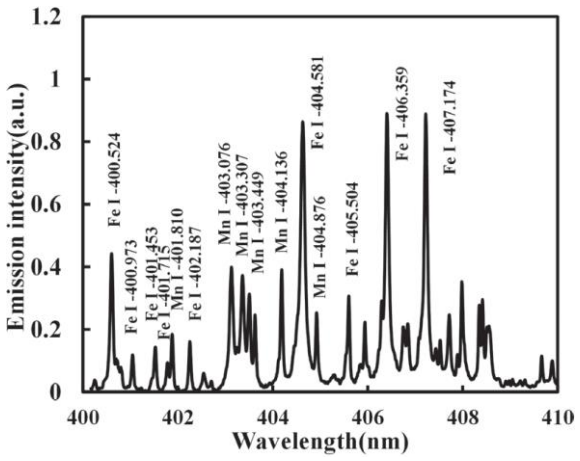

(b) 300℃

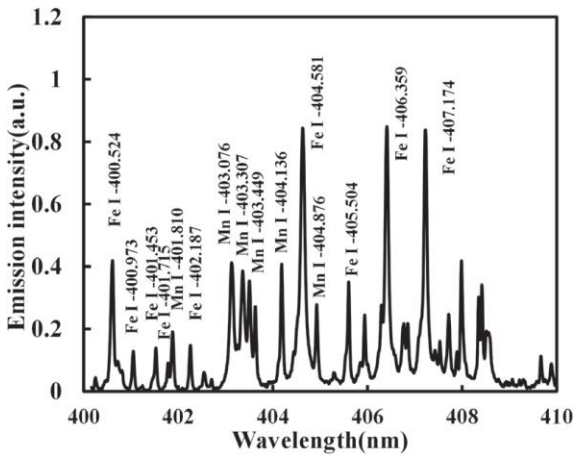

(c) 500℃

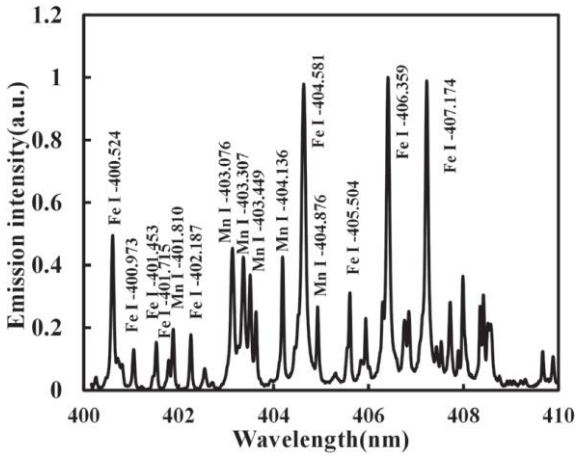

(d) 700℃

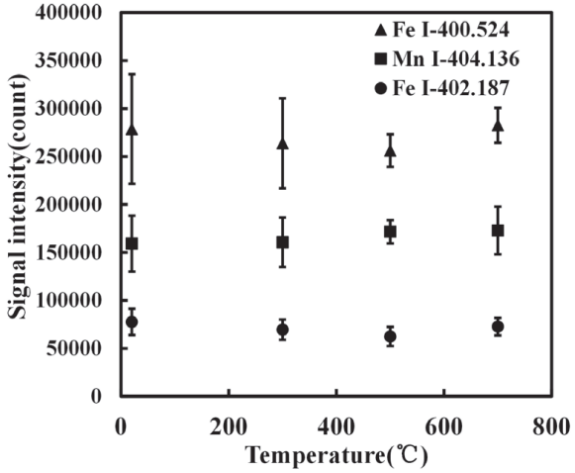

(e) Signal intensity of Fe I 400.524 nm, Mn I 404.136 nm, Fe I 402.187 nm

Fig.5-2 Measured results at different sample temperature by long-short DP-LIBS

5.2.1 Delay Time Effect

In order to clarify the sample temperature effect using long-short DP-LIBS, the intensity ratio of Mn 404.136nm/Fe 400.524nm and Fe 402.187nm/Fe 400.524nm were discussed in detail under different delay time conditions. The main reason for using ratio of Mn 404.136nm/Fe 400.524nm is to eliminate the variations caused by the fluctuations of the laser energy between each shot and the ratio with an internal standard also is a common method for normalizing calibration spectra. For the same atom with different upper level energy, the emission intensity from upper level with higher energy is more sensitive to plasma temperature compared with that from lower energy. Therefore, Fe 402.187nm/Fe 400.524nm was employed as the plasma temperature indicator to discuss the detection features. Fig.5-3 shows the effect of the delay time on Mn 404.136nm/Fe 400.524nm at sample temperature of 300°C. It can be seen that Mn 404.136nm/Fe 400.524nm of SP-LIBS fluctuated sharply with the delay time and had large error bar. So the signal measured by SP-LIBS showed poor signal stability with delay time, which will lead to low repeatability and accuracy. Compared with SP-LIBS, Mn 404.136nm/Fe 400.524nm of long-short DP-LIBS was higher and more stable with delay time and had smaller error bar. This phenomenon indicates that the signal intensity measured by

long-short DP-LIBS can be stabilized for a period of time, which can effectively improve measurement repeatability and accuracy. Fig.5-4 shows the variation of intensity ratio of Fe 402.187nm/Fe 400.524nm with delay time for long-short DP-LIBS and SP-LIBS at sample temperature of 300°C. Fe 402.187nm/Fe 400.524nm of SP-LIBS also fluctuated when increasing the delay time due to the unstable plasma. Theoretically Fe 402.187nm/Fe 400.524nm has a tendency to decrease as the delay time increases in SP-LIBS, but the results didn't show this tendency because of the unstable plasma. However, long-short DP-LIBS can get higher and more stable value of Fe 402.187nm/Fe 400.524nm than that using SP-LIBS when increasing the delay time, which means the plasma temperature was maintained at a higher level using long-short DP-LIBS. As the delay time increased, the Fe 402.187nm/Fe 400.524nm of long-short DP-LIBS displayed remarkable stabilization compared with that using SP-LIBS. The long-short DP-LIBS can maintain plasma stability and the plasma decay was deferred to extend the plasma lifetime. The main reason is the long pulse width laser of long-short DP-LIBS can control cooling process of plasma and plasma can maintain higher temperature and more stable state.

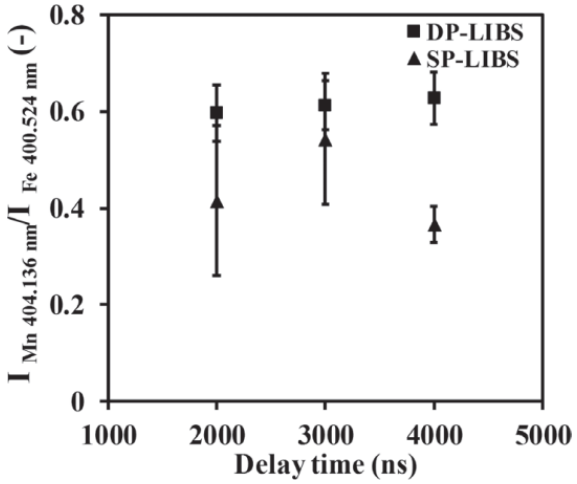

Fig.5-3 Variation of intensity ratio of Mn I 404.136 nm/Fe I 400.524 nm with delay time for long-short DP-LIBS and SP-LIBS at sample temperature of 300°C

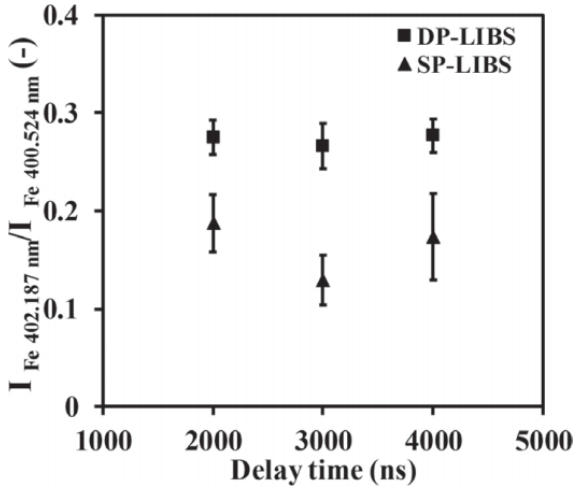

Fig.5-4 Variation of intensity ratio of Fe I 402.187 nm/Fe I 400.524nm with delay time for long-short DP-LIBS and SP-LIBS at sample temperature of 300°C

5.2.2 Sample Temperature Effect

According to the above comparison of measured spectra using SP-LIBS and long-short DP-LIBS, the signal was enhanced and became stable using long-short DP-LIBS. The detection features at different sample temperature were discussed here.Fig.5-5 shows the variation of intensity ratio of Mn 404.136nm/Fe 400.524nm with sample temperature for long-short DP-LIBS and SP-LIBS in delay time of 3000ns. Due to the variation of sample ablation mass, Mn 404.136 nm/Fe 400.524nm of SP-LIBS fluctuated sharply with the sample temperature. Compared with SP-LIBS, long-short DP-LIBS can also obtain higher and more stable ratio under different sample temperature conditions. This phenomenon indicates that long-short DP-LIBS can enhance the signal intensity and keep signal intensity stable at different sample temperature. Long pulse width laser heats and softens the sample before the short pulse irradiation, and short pulse laser will generate a relatively stable ablation mass. Therefore, the signal intensity can be maintained in a stable situation. Plasma temperature indictor Fe 402.187nm/Fe 400.524nm was employed to compare the plasma temperature at different sample temperature using SP-LIBS and long-short DP-LIBS in delay time of 3000ns, as shows in Fig.5-6. Fe 402.187nm has a higher upper energy than that of Fe 400.524nm. With the increased sample temperature, Fe 402.187nm/Fe 400.524nm of SP-LIBS had a trend of continuous increased. Therefore, plasma temperature had continuously changes with the sample temperature, which means plasma of SP-LIBS can be affected by sample temperature. However, there was quite different phenomenon for long-short DP-LIBS, as shows in Fig.5-6(b). Fe 402.187nm/Fe 400.524nm of long-short DP-LIBS was higher and more stable than that of SP-LIBS at different sample temperature, which means plasma with higher and more stable temperature can also be obtained by long-short DP-LIBS under different sample temperature conditions. In LIBS process, a part of pulse laser energy was used to heat the material before the material was evaporated and vaporized to produce plasma, so the laser energy involved in the plasma generation process was affected by the initial temperature of sample. For long-short DP-LIBS, because of the pre-heat process of the long pulse, the short pulse produces the plasma at relatively stable surface temperature. Thus, for long-short DP-LIBS, the laser energy involved in the plasma generation process was basically same in different sample temperature conditions. So long-short DP-LIBS technique can reduce the effect of initial sample temperature and improve the detection capability for steel in complex environment. In addition, when comparing Fig.5-5(a) and (b), Fig.5-6(a) and (b), ratios at same sample temperature also presented the smaller error bar in long-short DP-LIBS condition, which means that long-short DP-LIBS can achieve a better measurement repeatability than SP-LIBS and further proves that long-short DP-LIBS can achieve more stable plasma state.

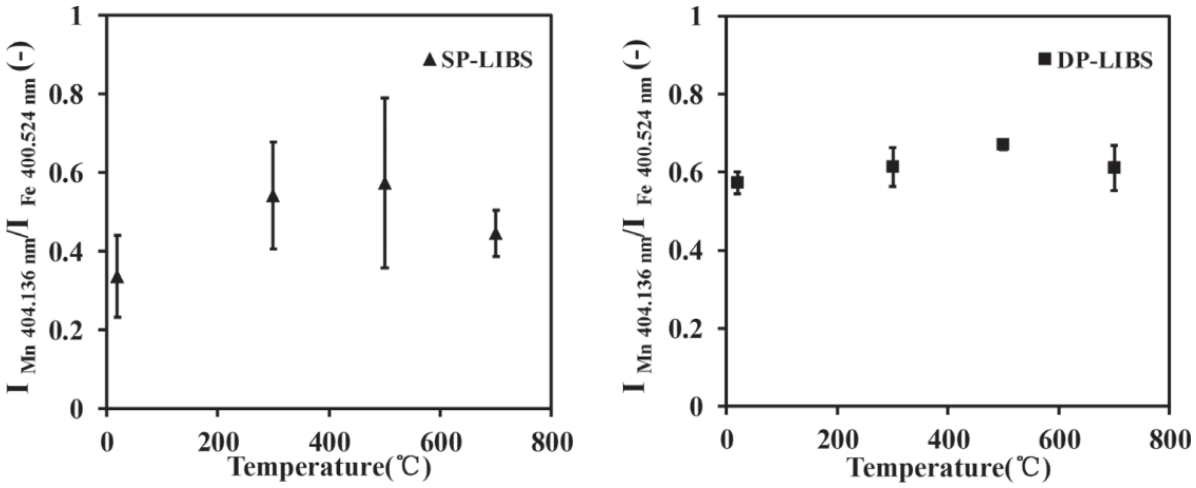

(a) SP-LIBS (b) long-short DP-LIBS

Fig.5-5 Variation of intensity ratio of Mn I 404.136nm/Fe I 400.524nm with sample temperature for long-short DPLIBS and SP-LIBS in delay time of 3000ns

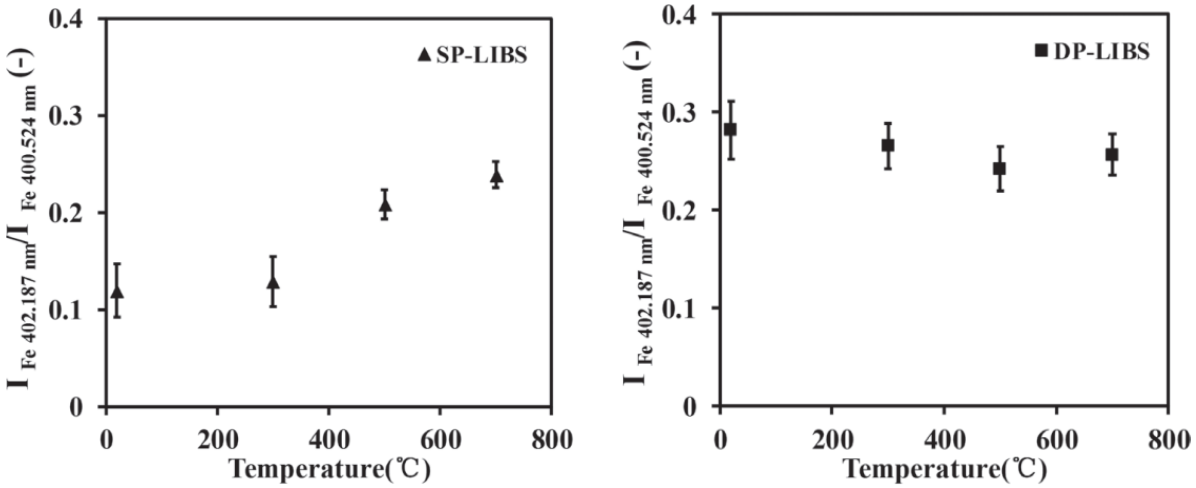

(a) SP-LIBS (b) long-short DP-LIBS

Fig.5-6 Variation of intensity ratio of FeI 402.187nm/FeI 400.524nm with sample temperature for long-short DP-LIBS and SP-LIBS in delay time of 3000ns

5.2.3 Plasma Temperature Correction

In order to reduce the influence of sample temperature on the measurement results, the plasma temperature correction method was applied to analyze the detection characteristics of long-short DP-LIBS and SP-LIBS at different sample temperature. In LIBS process, the emission intensity is a function of concentration of species and plasma temperature. Due to the plasma and plasma temperature are not stable and uniform, the emission intensity for each element will fluctuates with plasma temperature, which will affect the accuracy of quantitative analysis. Therefore, a plasma temperature correction method was proposed to improve the quantitative analysis capability of LIBS signal by our group, which was described in the previous work. Theoretical analysis shows that the dependence of emission intensity on plasma temperature can be corrected using the plasma temperature correction factor according to the temperature indicator which is the intensity ratio of different spectral lines from the same

element. In the actual process, the plasma from LIBS process is inhomogeneous and complex. The plasma temperature correction factor depends on the experimental conditions include the experimental system, environment temperature and so on, which should be determined under actual experimental conditions. In this study, the emission intensity ratio of FeI402.187nm/FeI400.524nm was used as temperature indictor for the determination of the plasma temperature correction factor. After plasma temperature correction, the variation trend of Mn404.136nm/Fe400.524nm for long-short DP-LIBS and SP-LIBS with sample temperature in delay time of 3000ns as shows in Fig.5-7. It can be seen from Fig.5-5(a) and Fig.5-7(a), after the plasma temperature correction, the Mn404.136nm/Fe400.524nm ratio for SP-LIBS still fluctuates sharply with the sample temperature. The relative standard deviations of Mn404.136nm/Fe400.524nm for SP-LIBS before the plasma temperature correction in Fig.5-5(a) and after the plasma temperature correction in Fig.5-7(a) were 22.56% and 21.86% respectively, which was not obviously optimized. It indicates that the temperature correction method could not significantly reduce the effect of sample temperature on measurement results of SP-LIBS. However, it can be seen from Figs.5-5(b) and Fig.5-7(b) that there was different result for long-short DP-LIBS. After the plasma temperature correction, Mn404.136nm/Fe400.524nm of long-short DP-LIBS was significantly more stable with the different sample temperature than that before the plasma temperature correction. The relative standard deviations of Mn404.136nm/Fe400.524nm for long-short DP-LIBS before the plasma temperature correction in Fig.5-5(b) and after the plasma temperature correction in Fig.5-7(b) were 6.46% and 1.78% respectively, which was significantly reduced by plasma temperature correction. Therefore, when employing the plasma temperature correction method, the change of plasma temperature caused by different sample temperature was corrected and the signal of long-short DP-LIBS becomes quite stable with the sample temperature compared to the measurement without plasma temperature correction. Therefore, the accuracy of the element content reflected by the spectral intensity can be significantly improved.

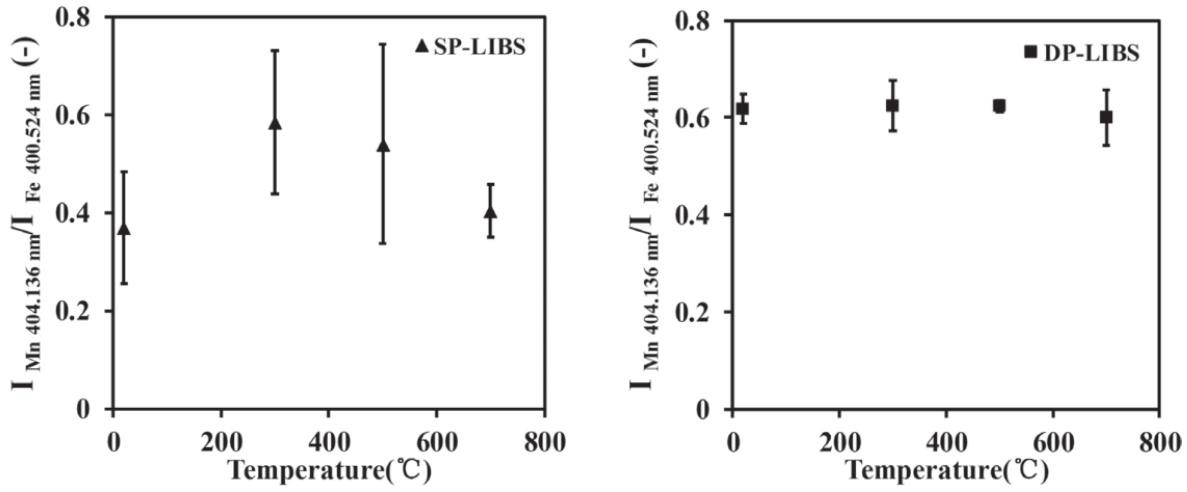

(a) SP-LIBS (b) long-short DP-LIBS

Fig.5-7 Plasma temperature correction result for long-short DP-LIBS and SP-LIBS in delay time of 3000ns

For practical industrial applications, it is preferred that the correction is based on the LIBS signals only, for in this way the on-line measurement is more efficient, and the measurement system is simpler. Besides, the laser-induced plasma has some fluctuations time to time, the other methods, such as infrared temperature measurement, cannot help to evaluate the fluctuations.

5.3 Comparison of SP-LIBS and Long-Short DP-LIBS in Boltzmann Plot

The more detail analysis of plasma states were adopted by Boltzmann Plot. According to discussion in secession 4.4, Fe lines during 400-410nm regions are difficult for Boltzmann Plot analysis. Besides, some Fe lines, such as Fe9, Fe11, Fe13 have high intensity, which has the danger of self-absorption. And the low backgrounds noise makes it easier for Mn lines identifications, as shown in Fig.5-1 and Fig.5-2. So the Boltzmann Plot based on Mn lines are reasonable.

For pure iron sample, the Boltzmann Plot at different conditions are listed in Fig.5-8. As it can be observed, R^2 is larger than 0.95, so the analysis is reliable. For the intercepts, no matter using SP-LIBS or long-short DP-LIBS, they kept at a stable levels. When sample temperature increased, intercepts increased. When delay time increased, intercepts decreased. It means the breakdown of samples increased as sample temperature increased, while the number of Mn atoms decreased when delay time decreased. But comparing SP-LIBS and long-short DP-LIBS, the intercepts didn't have obvious change, it means the atom number in plasma doesn't have obvious change in these two methods. For plasma temperature, it has obvious increase with sample temperature using SP-LIBS. Plasma temperature didn't have obvious increase with sample temperature using long-short DP-LIBS. Besides, plasma temperature at room temperature under long-short DP-LIBS is higher than that at 500℃ under SP-LIBS. It indicates that long-short DP-LIBS has more obvious effects on heating plasma than the sample temperature. Considering that the long pulse laser beam just exists with a small area on the sample surface, its heating efficiency is much more obvious. Therefore, long-short DP-LIBS doesn't help to increase the breakdown amount of the sample, but help to reheat the plasma, making a more obvious and stable signals.

The summary of the plasma temperature at different sample temperature under different laser configurations are shown in Fig.5-9, which is calculated based on Boltzmann Plot of Mn lines.

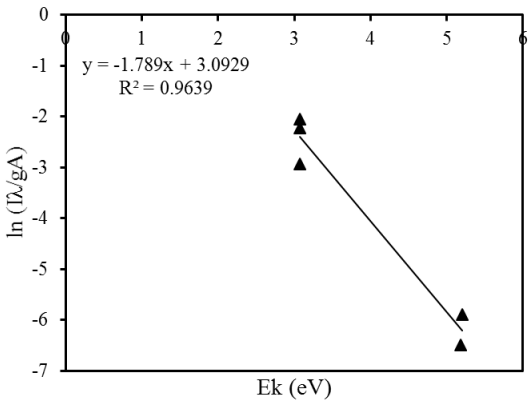

(a) SP-LIBS 20C D2000ns

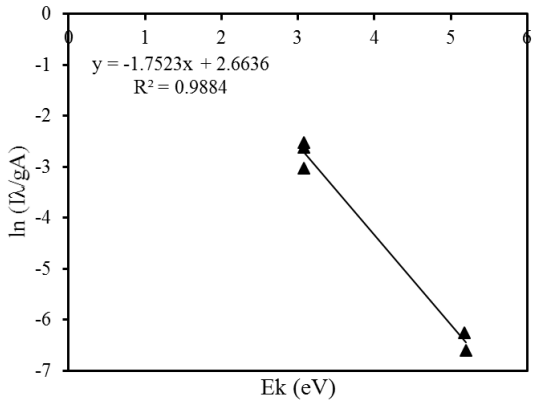

(b) SP-LIBS 20C D3000ns

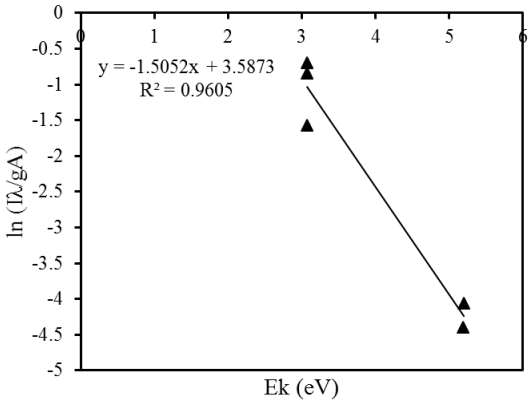

(c) SP-LIBS 500C D2000ns

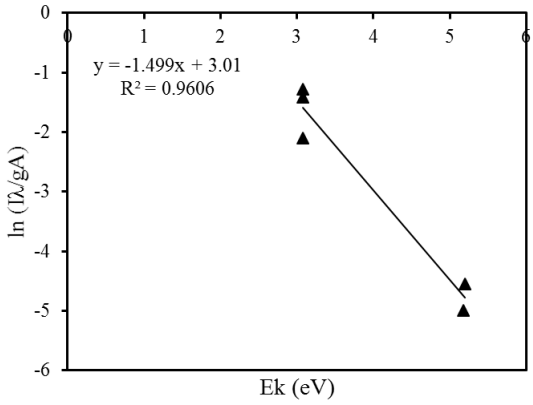

(d) SP-LIBS 500C D3000ns

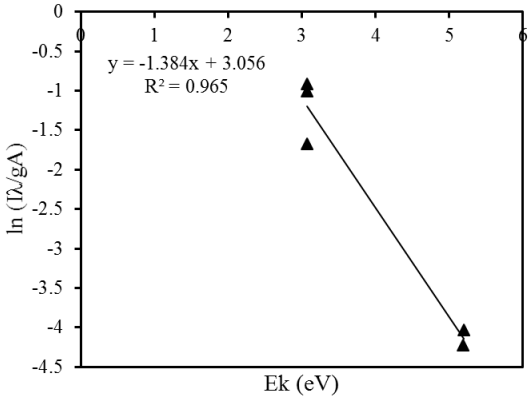

(e) long-short DP-LIBS 20C D2000ns

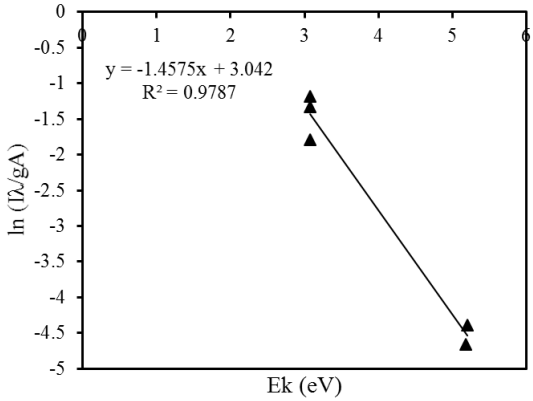

(f) long-short SP-LIBS 20C D3000ns

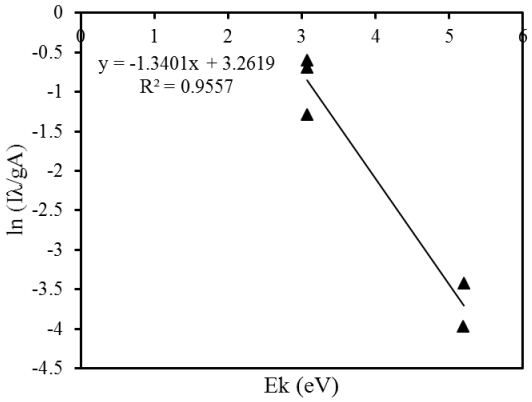

(g) long-short DP-LIBS 500C D2000ns

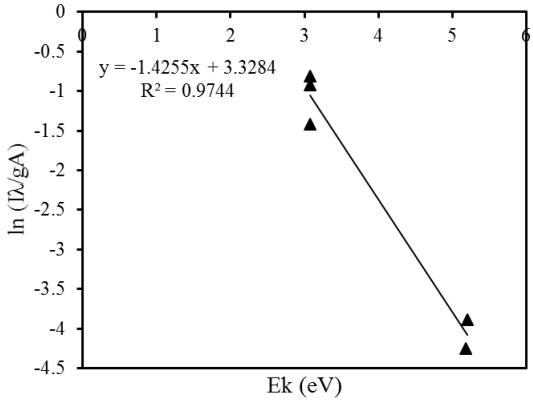

(h) long-short SP-LIBS 500C D3000ns

Fig.5-8 Boltzmann Plot using Mn lines of pure irons at different conditions

As it is summarized in Fig.5-9, For SP-LIBS, there is an obvious increase of plasma temperature with the increase of sample temperature. For long-short DP-LIBS, plasma temperature at different sample temperature had less difference. Besides, For SP-LIBS, the plasma temperature at different delay time are more scattered. Therefore, it has testified that, long-short DP-LIBS helps to stabilize plasma temperature, inducing the plasma with less interference from sample temperature, and slower cooling down speed of it.

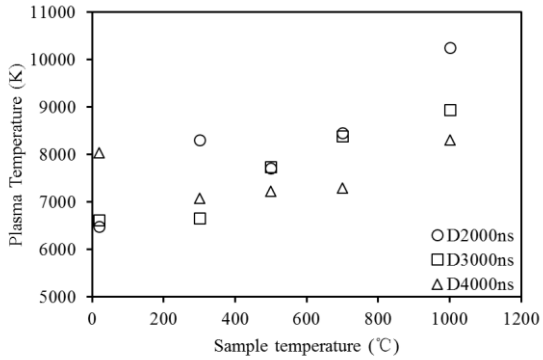

(a) Pure iron, SP-LIBS

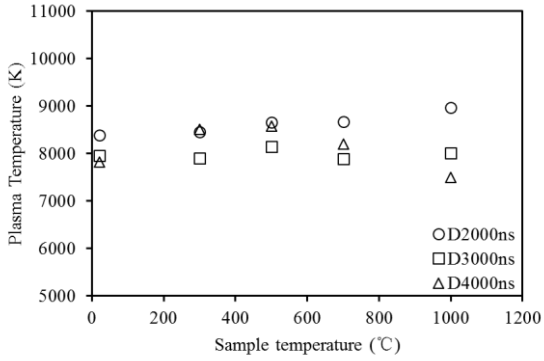

(b) Pure iron, long-short DP-LIBS

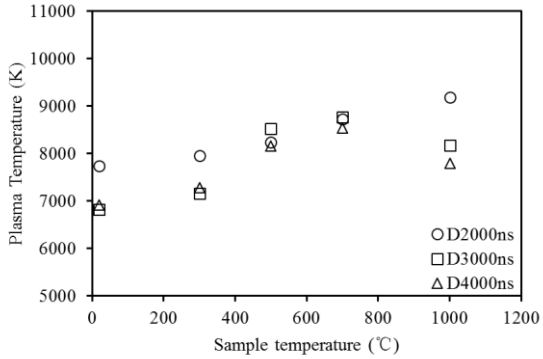

(a) ZG10#, SP-LIBS

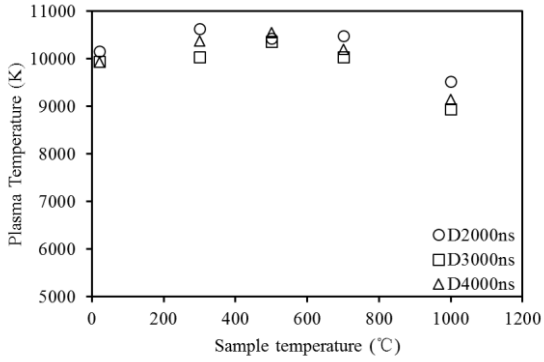

(b) ZG10#, long-short DP-LIBS

Fig.5-9 plasma temperature at different sample temperature under SP-LIBS and long-short DP-LIBS (Boltzmann Plot using Mn lines)

5.4 Quantitative Analysis of Mn using SP-LIBS and Long-Short DP-LIBS

5.4.1 Basic Calibration Curve between Component Ratio and Intensity Ratio

To compare the results of SP-LIBS and long-short DP-LIBS, the ratios of Mn* and Fe5 signal are calculated in each temperature. Fig.5-9, Fig.5-10, Fig.5-11, Fig.5-12, Fig.5-13 show the quantitative analysis results of Mn composition using SP-LIBS and long-short DP-LIBS at different sample temperature respectively.

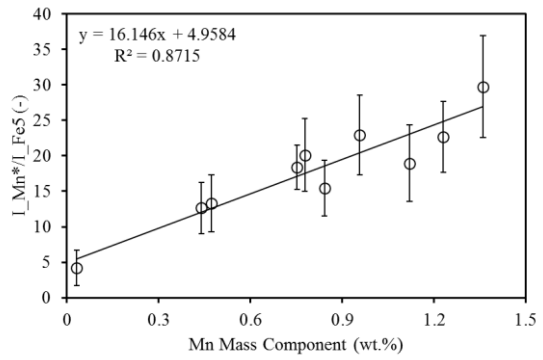

(a) SP-LIBS, D2000ns

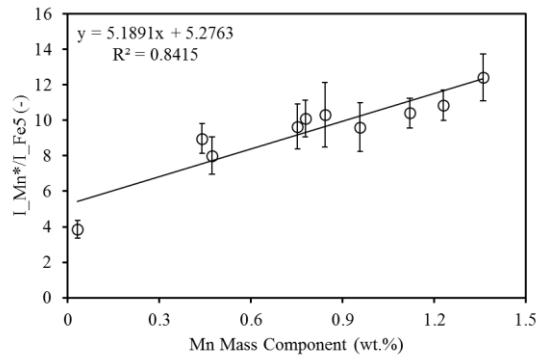

(b) long-short DP-LIBS, D2000ns

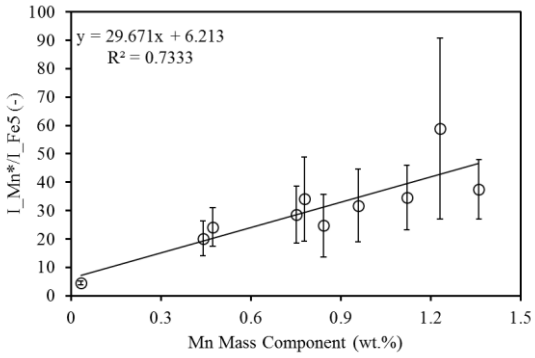

(c) SP-LIBS, D3000ns

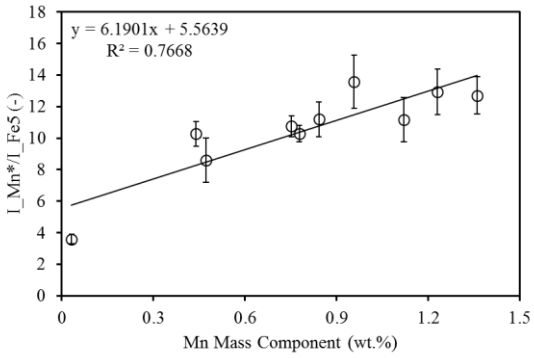

(d) long-short DP-LIBS, D3000ns

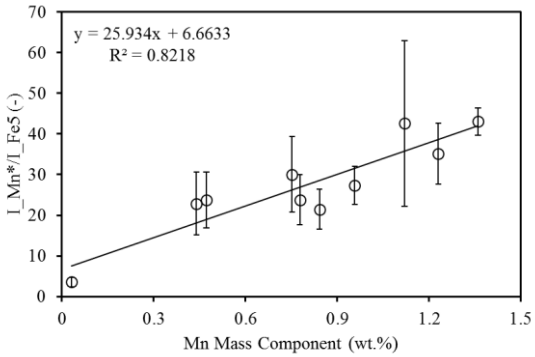

(e) SP-LIBS, D4000ns

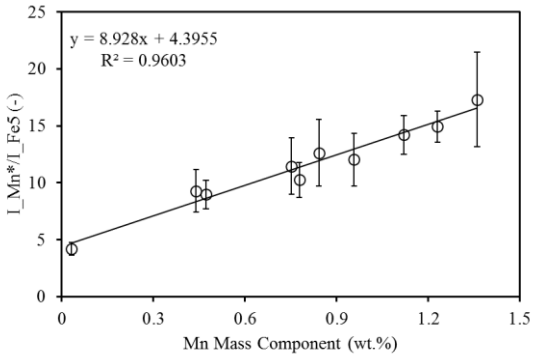

(f) long-short DP-LIBS, D4000ns

Fig.5-9 Mn calibration curves (Mn*/Fe5) for quantitative analysis at 20℃

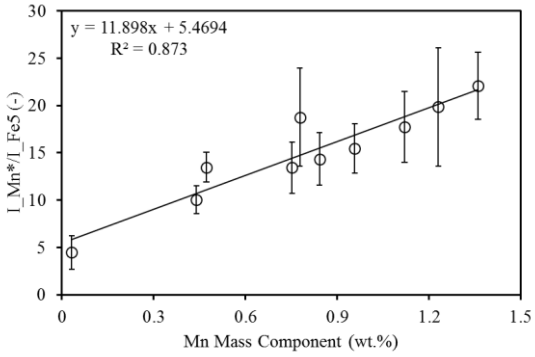

(a) SP-LIBS, D2000ns

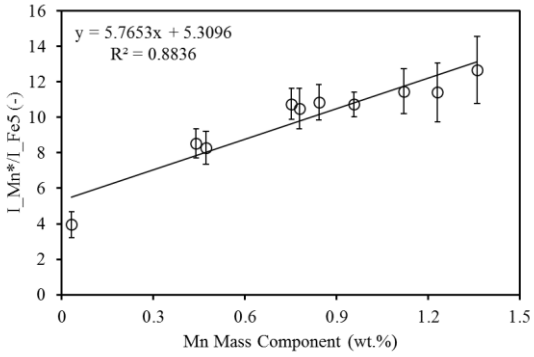

(b) long-short DP-LIBS, D2000ns

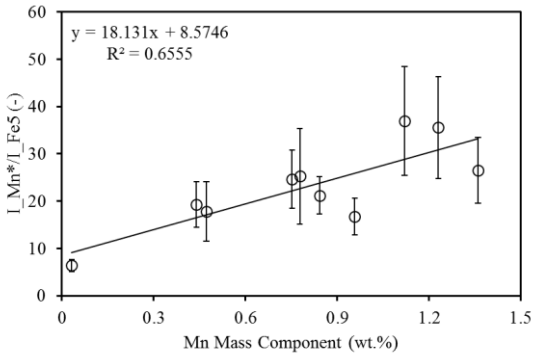

(c) SP-LIBS, D3000ns

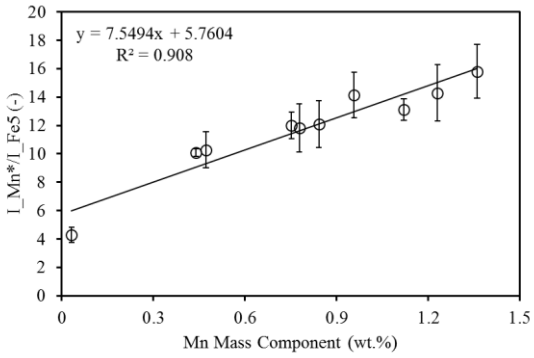

(d) long-short DP-LIBS, D3000ns

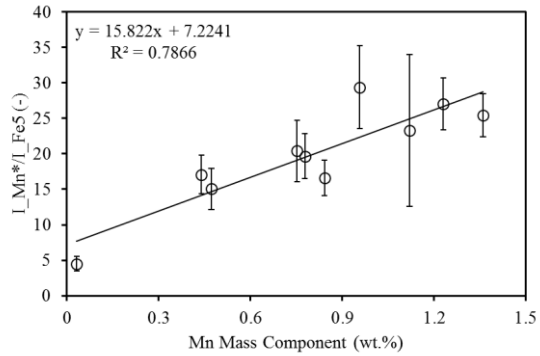

(e) SP-LIBS, D4000ns

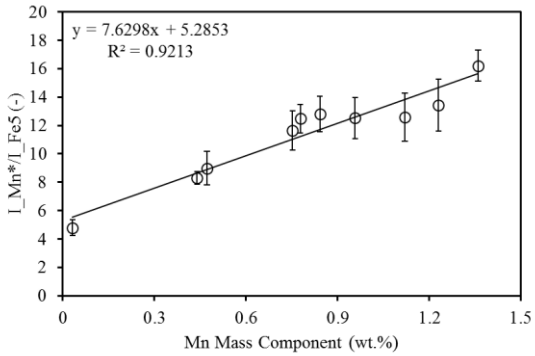

(f) long-short DP-LIBS, D4000ns

Fig.5-10 Mn calibration curves (Mn*/Fe5) for quantitative analysis at 300℃

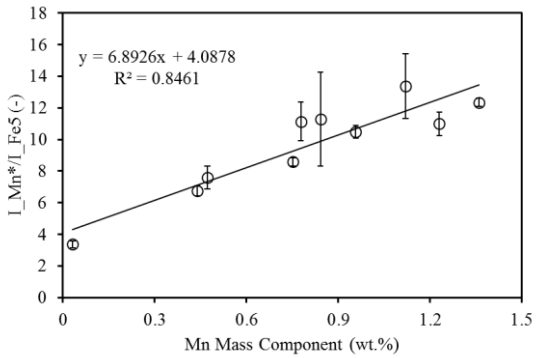

(a) SP-LIBS, D2000ns

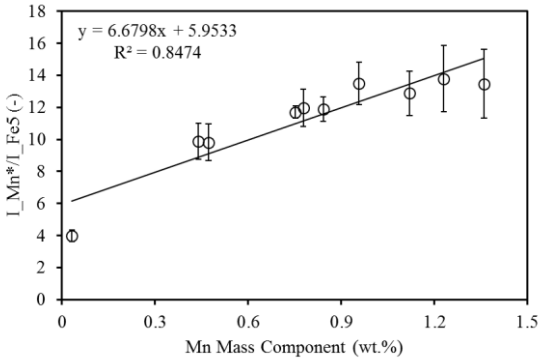

(b) long-short DP-LIBS, D2000ns

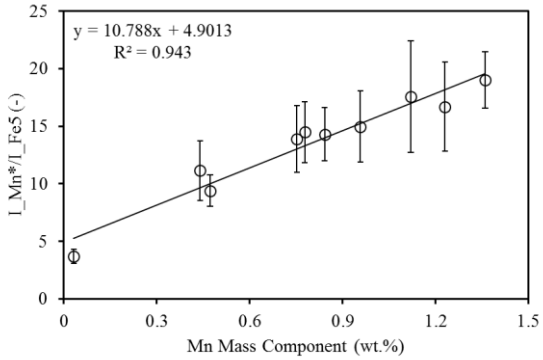

(c) SP-LIBS, D3000ns

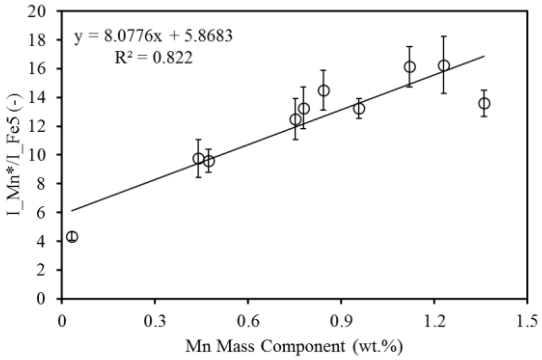

(d) long-short DP-LIBS, D3000ns

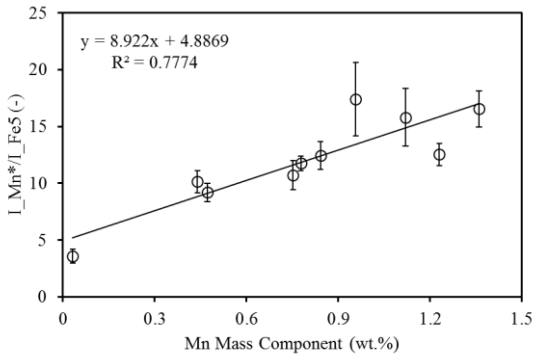

(e) SP-LIBS, D4000ns

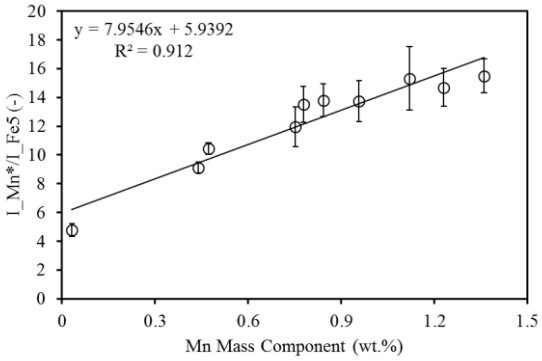

(f) long-short DP-LIBS, D4000ns

Fig.5-11 Mn calibration curves (Mn*/Fe5) for quantitative analysis at 500℃

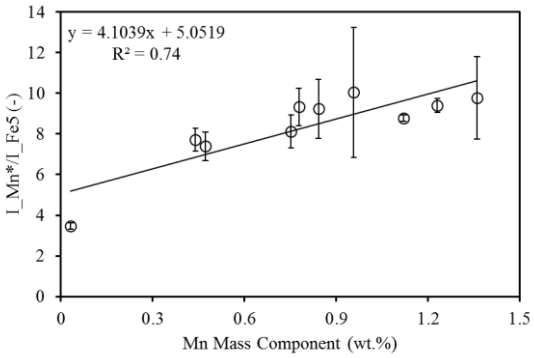

(a) SP-LIBS, D2000ns

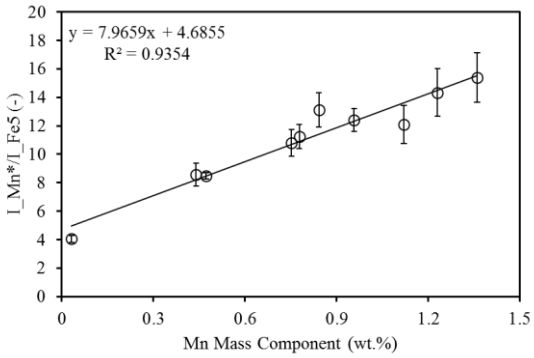

(b) long-short DP-LIBS, D2000ns

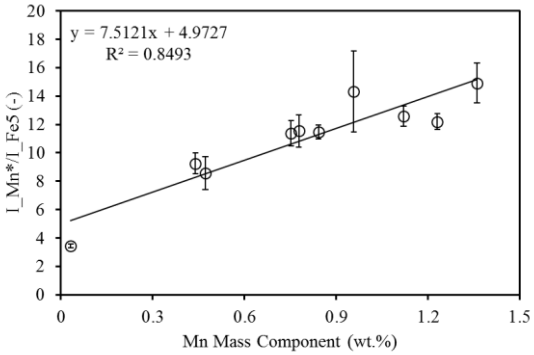

(c) SP-LIBS, D3000ns

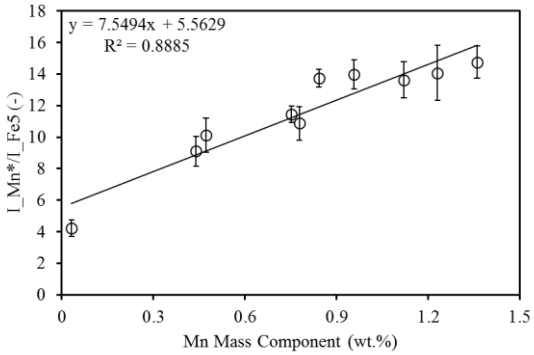

(d) long-short DP-LIBS, D3000ns

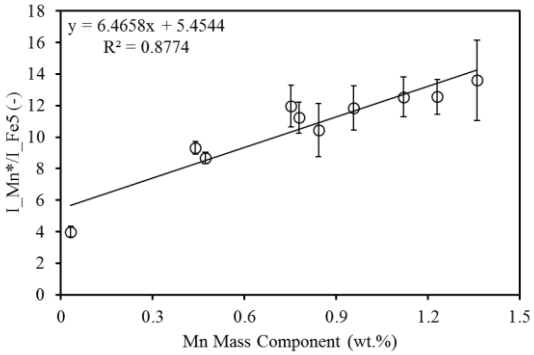

(e) SP-LIBS, D4000ns

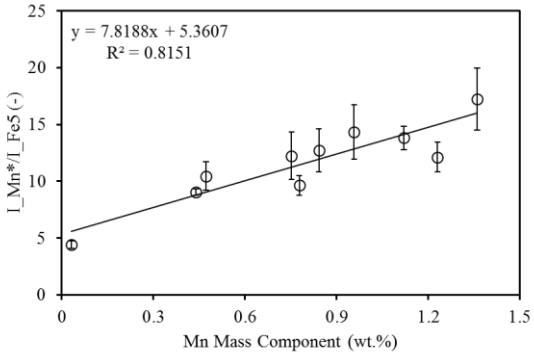

(f) long-short DP-LIBS, D4000ns

Fig.5-12 Mn calibration curves (Mn*/Fe5) for quantitative analysis at 700℃

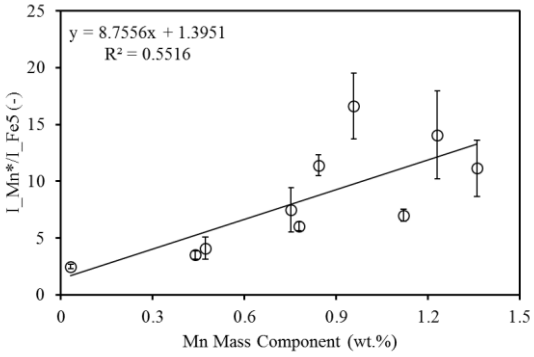

(a) SP-LIBS, D2000ns

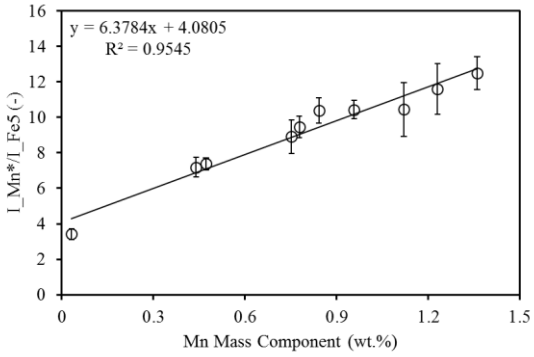

(b) long-short DP-LIBS, D2000ns

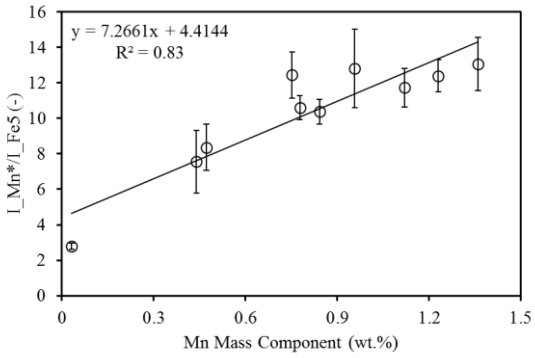

(c) SP-LIBS, D3000ns

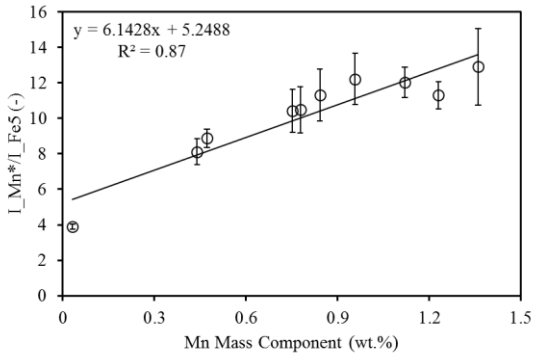

(d) long-short DP-LIBS, D3000ns

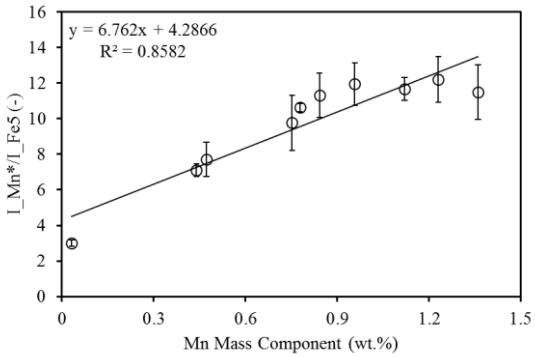

(e) SP-LIBS, D4000ns

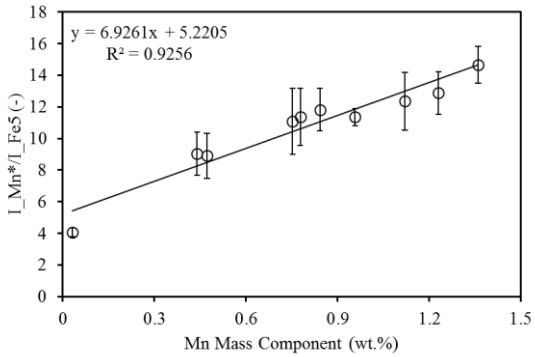

(f) long-short DP-LIBS, D4000ns

Fig.5-13 Mn calibration curves (Mn*/Fe5) for quantitative analysis at 1000℃

As it can be observed in above 5 figures, sample temperature has obvious effects on quantitative measurement, and long-short DP-LIBS have obvious different effects on quantitative measurement with SP-LIBS.

When using SP-LIBS, at room temperature, the calibration curves have low linear correlation under. As sample temperature increased, the linear correlation had somehow increased. But the increase of linear correlation is not stable, and the slope of the calibration curves decreased, which means the Mn signal becomes less sensitive to the Mn component. These results are consistent with the results in Fig.4-19. The error bars in SP-LIBS is usually big, meaning the unstable measurement of the samples. It is difficult to find which sample has higher possibility for unstable measurement, and big error bars occurred at different sample temperatures, so the LIBS measurement quality is challenged when using SP-LIBS.

When using long-short DP-LIBS, calibration curves mainly had a relative high levels of linear correlation, and the error bars at different sample temperature and different sample species are limited to a relative stable. This is very good for quantitative measurement, and it has testified long-short DP-LIBS method is good for signals quality control, which also good for the quantitative measurement. Besides, compared with SP-LIBS, the linear correlation and the slopes of calibration curves kept relative stable as delay time increased. It means the plasma is more stable in this delay time regions, which is also good for measurement.

For long-short DP-LIBS, the slope of the calibration curve is smaller than SP-LIBS measurement, and the intercepts kept high. For ideal measurement, it hopes the slope is high, so the sensitivity is high and the limit of detection (LOD) is low. The intercept should be zero, because when there is no element component, the signal should be zero. But for practical

measurement, the intercepts are usually not zero. Up to now, some researchers points out that the breakdown process of surrounding gas and the limitation of spectrometer precision. For quantitative measurement, the results of long-short DP-LIBS is preferred. Because the big error bars means the unstable and uncontrollable errors may occur, and it is difficult to calibrate. The unstable calibration curves at different delay time means the measurement conditions should be carefully selected. Therefore, long-short DP-LIBS is preferred for quantitative measurement.

The long-short DP-LIBS have both the more stable LIBS signals and quantitative models. The phenomenon could be explained as the result of power supply from long laser pulse. In LIBS process, the core of plasma is first produced by the absorption of the incident laser energy, such as multi-photon ionization process. Once the initial free electrons are produced, laser photons are strongly absorbed through inverse bremsstrahlung absorption to induce rapid expansion of plasma. When introducing the external energy from the long pulse laser in the plasma cooling process, the inverse bremsstrahlung absorption can appear in this process to maintain the plasma at higher temperature and extend its lifetime. Therefore the stability of plasma can be improved using DP-LIBS.

Besides, at high sample temperature, the calibration curves between SP-LIBS and long-short DP-LIBS became similar. It testified that the long pulse laser has the heating effects on sample surface, and when sample temperature increased, the heating effects from laser beam becomes not so obvious.

The calibration curves show a remarkable different according to the sample temperature. As the sample temperature increasing, the slope of the calibration curves decreased. However, the phenomenon is quite different when using long-short DP-LIBS. The slope of the calibration curves is relative stable when the sample temperature changed. The results indicate that the long-short DP-LIBS can generate a stable plasma condition in the different sample temperature conditions. Even though the slope is not big, but it can be optimized through machine learning method, so the stability of the slope is more important. In the plant conditions, the temperature of measured target is usually unknown. Thus, if we want to apply LIBS technique to the real plant, an improved LIBS method is necessary. Long-short DP-LIBS seems a good choice for the measurement of steel products on the production line.

5.4.2 Quantitative SVM Model using Long-Short DP-LIBS

The calibration curves in secession 5.4.1 points out that, the quantitative measurement based on only one spectral line is not enough, so the quantitative models based on multiple variates are also necessary for long-short DP-LIBS.

In Chapter 4, different types of quantitative models have been discussed. PLS model is limited by the relations structure of linear regression, BPNN method is influenced by the training process, which is difficult to control. In this secession, SVM method is proposed for steel measurement, because it has the merits of non-linear regression ability, and the regression results is not affected by the training processes [66]. Therefore, SVM method is proposed to replace PLS and BPNN in this secession. SVM quantitative models using SP-LIBS and long-short DP-LIBS were established respectively.

To determination of the quantitative model structure parameters, including the input vectors and the input vectors compositions and the model types. The change of input vector influencing

the model quality is presented in Fig.5-14. As it can be observed, Mn lines are important, if there is no Mn lines, the quantitative model cannot work, as shown in (b). But only based on Mn lines are also not enough, the backgrounds are also important. When both Mn and Fe lines are included, the more spectral lines is, the better the model is. Even though some spectral lines of Mn have weak intensity, such as Mn5, it also helps to improve the quality. It is because when the spectral line can be distinguished from the backgrounds noises, the spectral line contains the information of the target element. The more information the model obtains, the more accurate it will be.

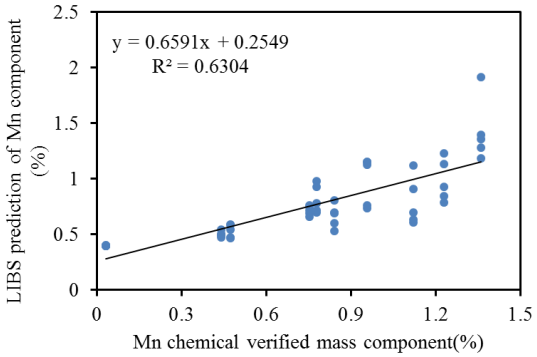

(a) All Mn lines (4 lines)

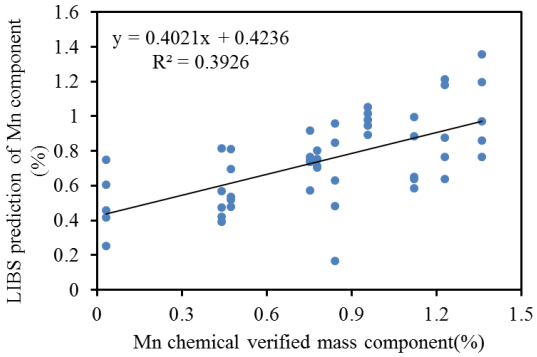

(b) All Fe lines (8 lines)

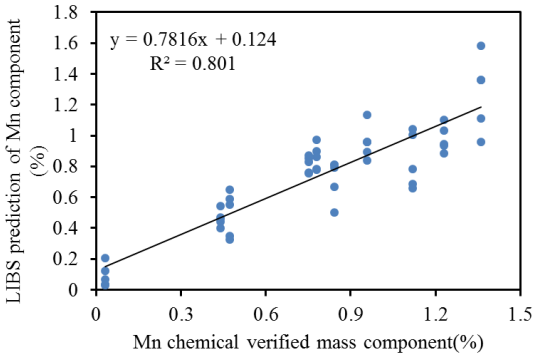

(c) Fe1, Mn1, Mn*

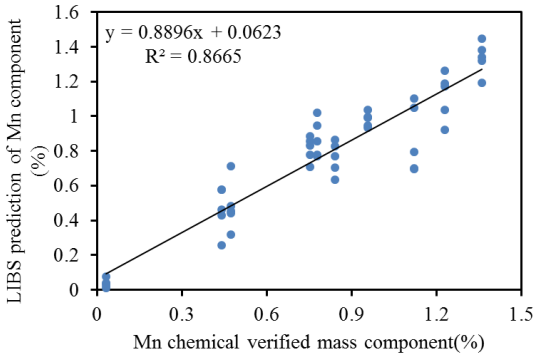

(d) Fe5, Fe9, Fe11 Mn1, Mn*

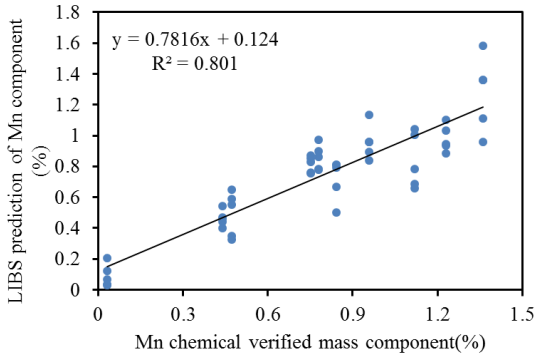

(e) All spectral lines in Table 4-4

Fig.5-14 The change of input vector influencing the model quality (20℃, SP-LIBS, delay time: 2000ns)

The model structure also have the influence on quantitative models. SVM has the special structure of kernel function, which consists of three commonly used types. The kernel function influence on quantitative models are shown in Fig.5-15.

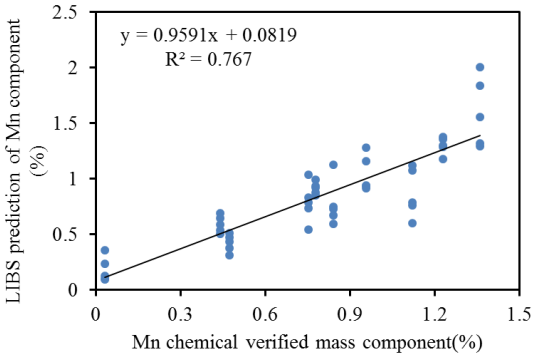

(a) Linear

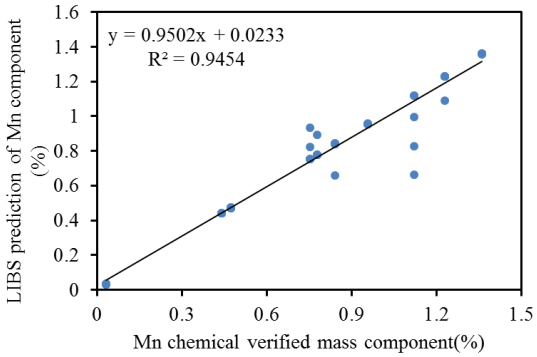

(b) Radial basis function

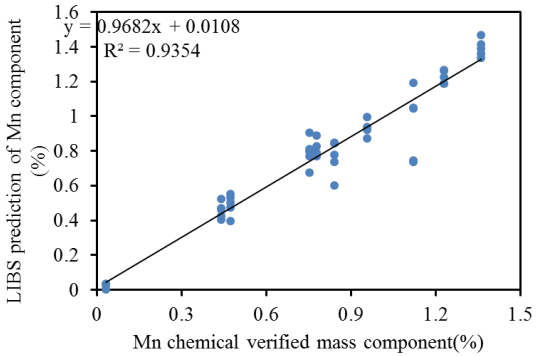

(c) Polynomial

Fig.5-15 The kernel function influence on quantitative models (20℃, SP-LIBS, delay time: 2000ns)

As it can be observed, the linear kernel function has not good results, it is consistent with the analysis before that the plasma is not a linear system. The radial basis function has a relative good result, but it is not proposed. Because some of the samples have no error fluctuations, such kind of phenomena calls over-fitting, which is bad for the model to expand its application regions, to measure the sample it didn't meet in training. In this way, polynomial kernel function is preferred, which is (0.03*u'*v)^3. It is determined after a series of attempts. The determination of the kernel function testified SVM model is also good for non-linear regression.

Different delay time corresponds to different plasma cooling stage. The models set up based on the signals at different delay time is presented in Fig.5-16.

Different from the common image, when long-short DP-LIBS can obtain more stable and obvious signals, the quantitative model is not better. On the contrast, at delay time of 3000ns in (d), the model was serious scattered. Besides, it is not the hotter plasma states the better, delay time 4000ns for SP-LIBS and long-short DP-LIBS was better. When plasma is hot, the background emissions are also strong, and the cooling speed is sharper, which are all not good for stable and robust LIBS signals measurement. Therefore, in this system, the delay time of

4000ns are better. Therefore, it is necessary to be careful and select an appropriate measurement conditions for quantitative models establishment.

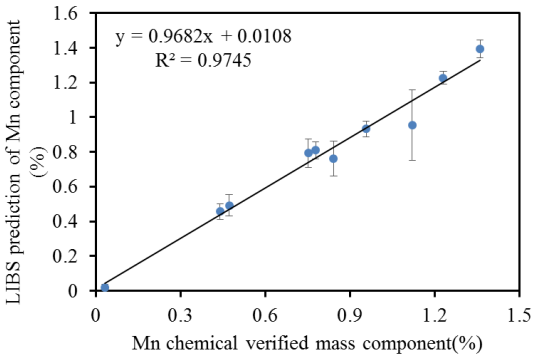

(a) SP-LIBS D2000ns

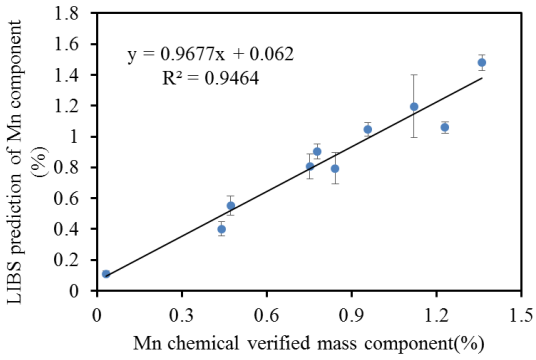

(b) long-short DP-LIBS D2000ns

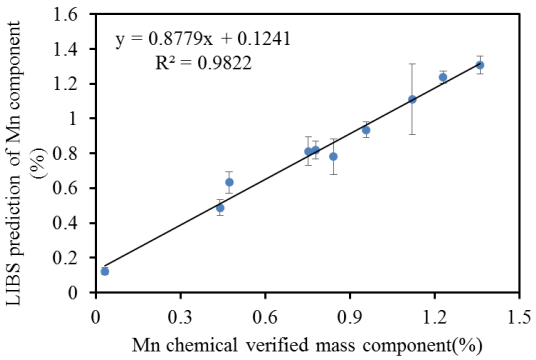

(c) SP-LIBS D3000ns

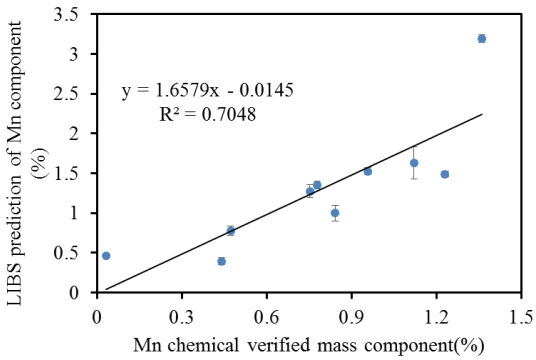

(d) long-short DP-LIBS D3000ns

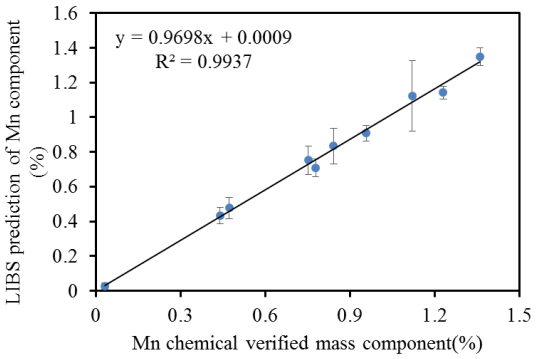

(e) SP-LIBS D4000ns

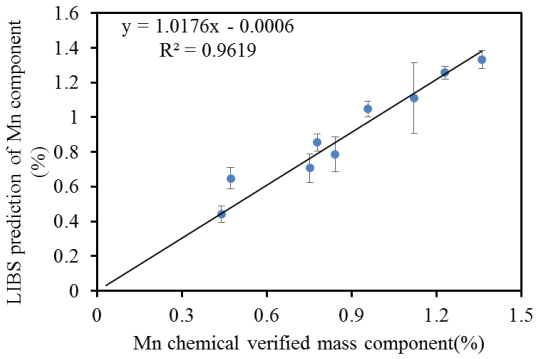

(f) long-short DP-LIBS D4000ns

Fig.5-16 The SVM models set up based on the signals at different delay time

5.5 Summary

Sample temperature effect on steel measurement using SP-LIBS and collinear long-short DP-LIBS was experimentally investigated to improve the application ability of LIBS technique for steel on-line inspection in this study. Standard steel sample was measured by SP-LIBS and long-short DP-LIBS at different sample temperature of 20°C, 300°C, 500°C, and 700°C.

Long-short DP-LIBS has changed the plasma formation process of steel. The signals is more stable with less fluctuations. Besides, when the sample temperature changed, the signals under

SP-LIBS have more variations than that under long-short DP-LIBS. Through observing the measurement results of SP-LIBS and collinear long-short DP-LIBS at different sample temperature, the results show that the sample temperature has significantly effect on signal intensity measured by SP-LIBS. For long-short DP-LIBS, measured spectra at each sample temperature did not change obviously and the signal intensity tend to be more stable at different sample temperature. Long-short DP-LIBS can reduce the influence of sample temperature on the measurement results

Under long-short DP-LIBS, the cooling down speed of plasma become slower. Plasma temperature decreased slower and the signals kept more stable along delay time.

The more stable plasma and signals is good for quantitative models. Under long-short DP-LIBS, the calibration curves are also more stable at different sample temperature and delay time. This is good for the signals quality control of quantitative models. Because the calibration curves under long-short DP-LIBS have high intercepts and relative low slopes, quantitative models are necessary. The quantitative models should consider the non-linear characteristics of plasma and the selection of model structure, the input signals at different delay time should also be considered.

6 Conclusions and Outlooks

6.1 Conclusions

When sample temperature is elevated from room temperature, the general plasma temperature doesn't have obvious increase, while the total Fe atoms and Fe^+ ions numbers are improved. The plasma temperature calculated from Fe atoms is lower than that from Fe^+ ions, while the number of Fe atoms is much bigger than Fe^+ ions. Which is consistent with the thermal theory, while it indicates the inhomogeneity inside plasma. When sample temperatures change, the change of each Fe line is also not uniform, which can be observed in Boltzmann Plot.

For Mn quantitative analysis, Mn atom line is more robust than Mn ion line. The Mn atom line has less interference with Fe lines, and it is sensitive to the components at evaluated sample temperature. Through the discussion of PLS model, the Mn lines have non-linear relation with the component, which is different from the theory equations, but it is reasonable for the complicity of plasma. Based on Mn atom lines, the multi-variates PLS using 2^{nd} order has higher accuracy, it means that the plasma is a non-linear system, and put more information with less interference in to the quantitative models help to increase the accuracy. Plasma is a non-linear system, and the emission of elements are also not following just a simple linear theory. Based on the 2^{nd} order PLS, the accuracy of the model increased. When adding the plasma temperature factor Fe5/Fe1 and electron number density factor FWHM of Fe9, the quantitative model increased the quantitative quality.

Because the plasma is non-linear system, BPNN method is also good for the quantitative model regression. The results shows that it can obtain the better regression accuracy. However, BPNN method accuracy relies on not only the training dataset, but also the training processes. There is no general theory for the most correct training processes, so the BPNN model may have the danger to be in bad regression, which is not good for quantitative measurement.

Sample temperature effect on steel measurement using SP-LIBS and collinear long-short DP-LIBS was experimentally investigated to improve the application ability of LIBS technique for steel on-line inspection in this study. Standard steel sample was measured by SP-LIBS and long-short DP-LIBS at different sample temperature of 20°C, 300°C, 500°C, and 700°C.

Long-short DP-LIBS has changed the plasma formation process of steel. The signals is more stable with less fluctuations. Besides, when the sample temperature changed, the signals under SP-LIBS have more variations than that under long-short DP-LIBS. Through observing the measurement results of SP-LIBS and collinear long-short DP-LIBS at different sample temperature, the results show that the sample temperature has significantly effect on signal intensity measured by SP-LIBS. For long-short DP-LIBS, measured spectra at each sample temperature did not change obviously and the signal intensity tend to be more stable at different sample temperature. Long-short DP-LIBS can reduce the influence of sample temperature on the measurement results

Under long-short DP-LIBS, the cooling down speed of plasma become slower. Plasma temperature decreased slower and the signals kept more stable along delay time.

The more stable plasma and signals is good for quantitative models. Under long-short DP-LIBS, the calibration curves are also more stable at different sample temperature and delay

time. This is good for the signals quality control of quantitative models. Because the calibration curves under long-short DP-LIBS have high intercepts and relative low slopes, quantitative models are necessary. The quantitative models should consider the non-linear characteristics of plasma and the selection of model structure, the input signals at different delay time should also be considered.

In general, there are two innovations in this paper:

1) Long-short DP-LIBS method has obvious merits on steel measurement. The signals were stabilized with less fluctuations. Plasma states became more stable. Sample temperatures have less interference on steel measurement, for surface situations are more stabilized. The quantitative measurement using long-short DP-LIBS has higher accuracy than that of SP-LIBS.
2) Plasma is a non-linear system, so the signal intensity is usually not linear with the element content. The quantitative models help to increase the accuracy of measurement, and it should consider the plasma states change. Plasma temperature factor and width of the spectral lines can somehow reflect the sample temperature change. When adding these information into the model, the model increased it accuracy at different sample temperature.

6.2 Outlooks

In this study, the temperature characteristics of steel measured by LIBS are seriously discussed, and long-short DP-LIBS method is proposed. For the further research, long-short DP-LIBS deserves much progress.

1) For plasma physics, how plasma is influenced by long-short DP-LIBS should be considered. Whether it has obvious effects on metal materials only or also on oxide materials such as fly ash and ceramics, is also an important target of LIBS.

2) For long-short DP-LIBS, it is a very good method for plasma stabilization and quantitative measurement. Whether it is good for different surface situations can be more studied. The chemical standard steel samples measured in this study has rough surface situations, which introduced errors to measurement. Whether long-short DP-LIBS can solve the surface roughness effects, more experiments should be adopted.

3) For applications, how to set up the system for industrial should be considered. For steel industry, the remote measurement is necessary. Whether the laser beam configuration works in a long distance should be considered.

References

[1] Z.Z. Wang, Y. Deguchi, F. Shiou, J.J. Yan, J.P. Liu: Application of Laser-Induced Breakdown Spectroscopy to Real-Time Elemental Monitoring of Iron and Steel Making Processes [J]. ISIJ Int., 56 (2016), 5.

[2] B.H. Smith, S.Szyniszewski, J.H. Hajjar, B.W. Schafer, S.R. Arwade: Steel foam for structures: A review of applications, manufacturing and material properties [J]. J. Constructional Steel Research, 71 (2012), 1.

[3] Y.N. Singhbabu, B. Sivakumar, J.K. Singh, H. Bapari, A.K. Pramanick, R.K.Sahu: Efficient anti-corrosive coating of cold-rolled steel in a seawater environment using an oil-based graphene oxide ink [J]. Nanoscale, 7 (2015), 17.

[4] M.E. Medhat, Y.F. Wang: Investigation on radiation shielding parameters of oxide dispersion strengthened steels used in high temperature nuclear reactor applications [J]. Annals of Nuclear Energy, 80 (2015), 1.

[5] M. Darabara, L. Bourithis, S. Zinelis, G.D. Papadimitriou: Assessment of elemental composition, microstructure, and hardness of stainless steel endodontic files and reamers [J]. J. Endodontics, 30 (2004), 7.

[6] R.Sarkar, A. Sengupta, V. Kumar, S.K.Choudhary: Effects of Alloying Elements on the Ferrite Potential of Peritectic and Ultra-Low Carbon Steels [J]. ISIJ Int., 55 (2015), 4.

[7] Noll R , Bette H , Brysch A , et al. Laser-induced breakdown spectrometry - Applications for production control and quality assurance in the steel industry [J]. Spectrochimica Acta Part B Atomic Spectroscopy, (2001), 56(6):637-649.

[8] Williamson D.L., Davis J.A., Wilbur P.J.: Effect of austenitic stainless steel composition on low-energy, high-flux, nitrogen ion beam processing [J]. Surface and Coatings Technology, (1998), 103-104(none):178-184.

[9] Yoshihiro Deguchi. Industrial Applications of Laser Diagnostics, CRC Press (Taylor & Francis group) [M], (2012).

[10] Sheta S, Afgan M S, Hou Z, et al. Coal analysis by laser-induced breakdown spectroscopy: A tutorial review[J]. Journal of Analytical Atomic Spectrometry, (2019).

[11] Renwei Liu, Kai Rong, Zhenzhen Wang, ea al. Sample Temperature Effect on Steel Measurement Using SP-LIBS and Collinear Long-short DP-LIBS[J]. ISIJ International, Vol.60, No.8, January, (2020).

[12] Wang Zhe, Yuan TingBi, Hou ZongYu, et al. Laser-induced breakdown spectroscopy in China [J]. Frontiers of physics, 2014, 9(4):419-438.

[13] Wang ZhenZhen, Deguchi Yoshihiro, Zhang ZhenZhen, et al. Laser-induced breakdown spectroscopy in Asia [J]. Frontiers of Physics, 2016, 11(6).

[14] Lin Xu. A study of iron ore classification based on chemometrics methods and laser-induced breakdown spectroscopy [D]. Nothwest University, (2015).

[15] Guo Guangmeng. Development of Compact Laser-induced Breakdown Spectroscopy (LIBS) Instrument and Analysis Methods of Solutions and Soils [D]. Jilin University, (2019).

[16] Takahashi Tomoko, Yoshino Soichi, Takaya Yutaro, et al. Quantitative in situ mapping of elements in deep-sea hydrothermal vents using laser-induced breakdown spectroscopy and

multivariate analysis [J]. Deep–Sea Research I (2020), prepublish.
[17] Fang Fang. Distribution Regularity of Typical Heavy Metal Elements in Peel an Pulp of Gannan Navel Orange [D]. Jiangxi Agricultural University, (2018).
[18] Cisewski J., Snyder E., Hannig J., et al. Support vector machine classification of suspect powders using laser-induced breakdown spectroscopy (LIBS) spectral data [J]. Journal of Chemometrics, (2012), 26: 143-149.
[19] Jennifer L. Gottfried, Frank C. De Lucia, Jr, et al. Strategies for residue explosives detection using laser-induced breakdown spectroscopy [J]. Journal of Analytical Atomic Spectrometry, (2008), 23: 205-216.
[20] Botto A, Campanella B, Legnaioli S, et al. Applications of laser-induced breakdown spectroscopy in cultural heritage and archaeology: a critical review [J]. Journal of Analytical Atomic Spectrometry, 2019, 34: 81-103.
[21] Sturm V , Vrenegor J , Noll R , et al. Bulk analysis of steel samples with surface scale layers by enhanced laser ablation and LIBS analysis of C, P, S, Al, Cr, Cu, Mn and Mo[J]. Journal of Analytical Atomic Spectrometry, 19 (2004):451.
[22] Aragón C, Aguilera J A, Campos J. Determination of Carbon Content in Molten Steel Using Laser-Induced Breakdown Spectroscopy [J]. (1993), 47(5):606-608.
[23] Palanco, S, Conesa, S, Laserna, J. J. Analytical control of liquid steel in an induction melting furnace using a remote laser induced plasma spectrometer[J]. Journal of Analytical Atomic Spectrometry, (2004) (4):462.
[24] Sun Lanxiang, Yu Haibin, Cong Zhibo, et al. Quantitative Analysis of Mn and Si of Steels by LaserInduced Breakdown Spectroscopy Combined with Neural Networks [J]. Acta Optica Sinica, (2010), 30 (9):2757-2765.
[25] Yi, R. X, Guo, L. B, Zou, X. H, et al. Background removal in soil analysis using laser-induced breakdown spectroscopy combined with standard addition method [J]. Optics Express, (2014), 24(3):2607.
[26] Popov A M , Colao F , Fantoni R . Enhancement of LIBS signal by spatially confining the laser-induced plasma[J]. Journal of Analytical Atomic Spectrometry, (2009), 24(5):602.
[27] Sobral H, Robledo-Martinez A. Signal enhancement in laser-induced breakdown spectroscopy using fast square-pulse discharges [J]. Spectrochimica Acta Part B: Atomic Spectroscopy, (2016).
[28] Palanco. S, Cabalin. L. M, Romero. D, et al. Infrared laser ablation and atomic emission spectrometry of stainless steel at high temperatures [J]. J.anal.at.spectrom, (1999) 14(12):1883-1887.
[29] Leonid V. Zhigilei, Elodie Leveugle, Barbara J. Garrison, et al. Computer Simulations of Laser Ablation of Molecular Substrates [J]. Cheminform, (2003), 34.
[30] Eschlbõck-Fuchs.S, Haslinger.M.J, Hinterreiter.A, et al. Influence of sample temperature on the expansion dynamics and the optical emission of laser-induced plasma [J]. Spectrochimica Acta Part B Atomic Spectroscopy, (2013), 87:36-42.
[31] Tavassoli S.H., Gragossian A.: Effect of sample temperature on laser-induced breakdown spectroscopy [J]. Optics and Laser Technology, (2009), 41(4):481-485.
[32] Rauschenbach I., Lazic V., Pavlov S.G., et al: Laser induced breakdown spectroscopy on soils and rocks: Influence of the sample temperature, moisture and roughness [J]. Spectrochimica Acta Part B Atomic Spectroscopy, (2008), 63(10):1205-1215.

[33] Scaffidi J., Pearman W., Carter J.C., et al. Effects of Sample Temperature in Femtosecond Single-Pulse Laser-Induced Breakdown Spectroscopy [J]. Applied optics, (2004), 43(13):2786-91.

[34] Jiang. X, Hayden. P, Laasch. R, et al. Inter-pulse delay optimization in dual-pulse laser induced breakdown vacuum ultraviolet spectroscopy of a steel sample in ambient gases at low pressure [J]. Spectrochimica Acta Part B Atomic Spectroscopy, (2013), 86:66-74.

[35] Lu Y, Zorba V, Mao X, et al. UV fs–ns double-pulse laser induced breakdown spectroscopy for high spatial resolution chemical analysis [J]. Journal of Analytical Atomic Spectrometry, (2013), 28.

[36] Ahmed R., Baig M. A.. A comparative study of single and double pulse laser induced breakdown spectroscopy [J]. Journal of Applied Physics, (2009), 106(3).

[37] Babushok V.I., Delucia F.C., Gottfried J.L., et al. Double pulse laser ablation and plasma: Laser induced breakdown spectroscopy signal enhancement [J]. Spectrochimica Acta Part B Atomic Spectroscopy, (2006), 61(9):999-1014.

[38] R. Sanginés, Sobral H , Alvarez-Zauco E . The effect of sample temperature on the emission line intensification mechanisms in orthogonal double-pulse Laser Induced Breakdown Spectroscopy [J]. Spectrochimica Acta Part B, (2012), 68: 40-45.

[39] R. Noll. Laser-Induced Breakdown Spectroscopy Fundamentals and Applications [J]. Springer LLC. , (2011).

[40] J.A. Aguilera, C. Aragón: Characterization of a laser-induced plasma by spatially resolved spectroscopy of neutral atom and ion emissions. Comparison of local and spatially integrated measurements [J]. Spectrochimica Acta Part B Atomic Spectroscopy, 59 (2004), 12.

[41] Ü. Aydin, P. Roth, D.G. Gehlen, R. Noll: Spectral line selection for time-resolved investigations of laser-induced plasmas by an iterative Boltzmann plot method [J]. Spectrochimica Acta Part B Atomic Spectroscopy, 63 (2008), 10.

[42] J.A Aguilera, C. Aragón: Multi-element Saha–Boltzmann and Boltzmann plots in laser-induced plasmas [J]. Spectrochimica Acta Part B Atomic Spectroscopy, 62 (2007), 4.

[43] M.A. Ismail, H. Imam, A. Elhassan, W.T. Youniss, M.A. Hairth: LIBS limit of detection and plasma parameters of some elements in two different metallic matrices [J]. Journal of Analytical Atomic Spectrometry, 19 (2004), 4.

[44] Z.C. Wang: Thermodynamics· Statistical Physics [M]. Higher Education Press (China), Third Edition (2003).

[45] J.A. Bottencourt: Fundamentals of Plasma Physics [M]. Springer LLC. & Word Book LNC. (China), (2004).

[46] Darbani S M R , Ghezelbash M , Majd A E , et al. Temperature effect on the optical emission intensity in laser induced breakdown spectroscopy of super alloys [J]. Journal of the European Optical Society Rapid Publications, (2014).

[47] Aguilera J A, C. Aragón, Madurga V, et al. Study of matrix effects in laser induced breakdown spectroscopy on metallic samples using plasma characterization by emission spectroscopy [J]. Spectrochimica Acta Part B Atomic Spectroscopy, (2009), 64(10):993-998.

[48] Wang Z.Z., Deguchi Y., Liu R.W., et al. Emission Characteristics of Laser-Induced Plasma Using Collinear Long and Short Dual-Pulse Laser-Induced Breakdown Spectroscopy

(LIBS) [J]. Applied Spectroscopy, 71 (2017), 2187.
[49] Cui M.C., Deguchi Y., Wang Z.Z., et al. Enhancement and stabilization of plasma using collinear long-short double-pulse laser-induced breakdown spectroscopy [J]. Spectrochimica Acta Part B-Atomic Spectroscopy, 142 (2018), 14.
[50] Yoshihiro D., Minchao C., Zhenzhen W., et al. EXPRESS: Improvement of the Analysis of Manganese in Steel Samples Using Collinear Long-Short Double Pulse Laser-Induced Breakdown Spectroscopy (LIBS) [J]. Appl. Spectrosc., 73 (2019), 152.
[51] J. Vrenegor, R. Noll, V. Sturm: Investigation of matrix effects in laser-induced breakdown spectroscopy plasmas of high-alloy steel for matrix and minor elements [J]. Spectrochimica Acta Part B Atomic Spectroscopy, 60 (2005), 7-8.
[52] V. Sturm, J. Vrenegor, R. Noll, M. Hemmerlin: Bulk analysis of steel samples with surface scale layers by enhanced laser ablation and LIBS analysis of C, P, S, Al, Cr, Cu, Mn and Mo [J]. Journal of Analytical Atomic Spectrometry, 19 (2004), 4.
[53] I. Bassiotis, A. Diamantopoulou, A. Giannoudakos, F. Roubani-Kalantzopouliu, M. Kompitsas: Effects of experimental parameters in quantitative analysis of steel alloy by laser-induced breakdown spectroscopy [J]. Spectrochimica Acta Part B Atomic Spectroscopy, 56 (2001), 6.
[54] L. Peter, V. Sturm, R. Noll: Liquid steel analysis with laser-induced breakdown spectrometry in the vacuum ultraviolet [J]. Applied Optics, 42 (2003), 30.
[55] L.X. Sun, H.B. Yu, Z.B. Cong, Y. Xin: On-line semi-quantitative analysis of molten steel composition using laser-induced breakdown spectroscopy. Chinese Journal of Scientific Instrument [J], 32 (2011), 11.
[56] G. Hubmer, R. Kitzberger, K. Mörwald: Application of LIBS to the in-line process control of liquid high-alloy steel under pressure [J]. Analytical & Bioanalytical Chemistry, 385 (2006), 2.
[57] J. Gruber, J. Heitz, H. Strasser, D. Bauerle, N. Ramaseder: Rapid in-situ analysis of liquid steel by laser-induced breakdown spectroscopy [J]. Spectrochimica Acta Part B Atomic Spectroscopy, 56 (2001), 6.
[58] H. Balzer, M. Hoehne, R. Noll, V. Sturm: New approach to online monitoring of the Al depth profile of the hot-dip galvanised sheet steel using LIBS [J]. Analytical & Bioanalytical Chemistry, 385 (2006), 2.
[59] H. Balzer, S. Hölters, V. Sturm, R. Noll: Systematic line selection for online coating thickness measurements of galvanised sheet steel using LIBS [J]. Analytical & Bioanalytical Chemistry, 385 (2006), 2.
[60] Mermet J M , Mauchien P , Lacour J L . Processing of shot-to-shot raw data to improve precision in laser-induced breakdown spectrometry microprobe [J]. Spectrochimica Acta Part B: Atomic Spectroscopy, (2008), 63(10).
[61] Qianqian Wang, Xutai Cui, Geer Teng, et al. Evaluation and improvement of model robustness for plastics samples classification by laser-induced breakdown spectroscopy [J]. Optics and Laser Technology, (2020), prepublish.
[62] Li X , Wang Z , Lui S L , et al. A partial least squares based spectrum normalization method for uncertainty reduction for laser-induced breakdown spectroscopy measurements [J]. Spectrochimica Acta Part B Atomic Spectroscopy, (2013), 88:180-185.
[63] Jie, Feng, Zhe, et al. A PLS model based on dominant factor for coal analysis using laser-

induced breakdown spectroscopy [J]. Analytical and Bioanalytical Chemistry, (2011).
[64] Yao S , Lu J , Dong M , et al. Extracting Coal Ash Content from Laser-Induced Breakdown Spectroscopy (LIBS) Spectra by Multivariate Analysis [J]. Analytical Abstracts, (2012), 65(10):1197.
[65] Asgill M E, Groh S, Niemax K, et al. The use of multi-element aerosol particles for determining temporal variations in temperature and electron density in laser-induced plasmas in support of quantitative laser-induced breakdown spectroscopy [J]. Spectrochimica Acta Part B Atomic Spectroscopy, (2015), 109:1-7.
[66] Yun Liu, Jie Lian, Michael R. Bartolacci, et al. Density-Based Penalty Parameter Optimization on C-SVM [J]. Scientific World Journal, (2014), 2014: 1-9.
[67] Dong Wang, Xiangbin Wu, Dongmei Lin. Two heuristic strategies for searching optimal hyper parameters of C-SVM [C].Proceeding of the English International Conference on Machine Learning and Cybernetics, Baoding, (2009).
[68] Prathibha B.N., Sadasivam V. Hybrid transforms domain-based mammogram analysis using C-SVM classifier [J]. International Journal of Medical Engineering & Informatics, (2012), 4: 146-156.
[69] Jiao He, Congyuan Pan, Yongbin Liu, et al. Quantitative Analysis of Carbon with Laser-Induced Breakdown Spectroscopy (LIBS) Using Genetic Algorithm and BP Neural Network Models [J]. Applied Spectroscopy, (2019), 73: 678-686.
[70] Shichen Xie, Tao Xu, Xiaodan Han, et al. Accuracy improvement of quantitative LIBS analysis using wavelet threshold de-noising [J]. Journal of Analytical Atomic Spectrometry, (2017), 32: 629-637.
[71] Kuohu Li, Lianbo Guo, Jiaming Li, et al. Quantitative analysis of steel samples using laser-induced breakdown spectroscopy with an artificial neural network incorporating a genetic algorithm [J]. Applied Optics, (2017), 56: 935-941.
[72] Yang Zhao, Lei Zhang, Shu-Xia Zhao, et al., et al. Review of methodological and experimental LIBS techniques for coal analysis and their application in power plants in China [J]. Frontiers of Physics, (2016), 11: 114211.
[73] Tianlong Zhang, Chunhua Yan, Juan Qi, et al. Classification and discrimination of coal ash by laser-induced breakdown spectroscopy (LIBS) coupled with advanced chemometric methods [J]. Journal of Analytical Atomic Spectrometry, (2017), 32: 1960-1965.
[74] Jiao He, Congyuan Pan, Yongbin Liu, et al. Quantitative Analysis of Carbon with Laser-Induced Breakdown Spectroscopy (LIBS) Using Genetic Algorithm and BP Neural Network Models [J]. Applied Spectroscopy, (2019), 73: 678-686.
[75] Amir Hossein Farhadian, Masoud Kavosh Tehrani, Mohammad Hossein Keshavarz, et al. Energetic materials identification by laser-induced breakdown spectroscopy combined with artificial neural network [J]. Applied Optics, (2017), 56: 3372-3377.
[76] Zhimin Lu, Juehui Mo, Shunchun Yao, et al. Rapid Determination of the Gross Calorific Value of Coal Using Laser-Induced Breakdown Spectroscopy Coupled with Artificial Neural Networks and Genetic Algorithm [J]. Energy & Fuels, (2017), 31: 3849-3855.
[77] Mohammad Vahid Dastjerdi, Seyyed Jabbar Mousavi, Mahmood Soltanolkotabi, et al. Identification and Sorting of PVC Polymer in Recycling Process by Laser-Induced Breakdown Spectroscopy (LIBS) Combined with Support Vector Machine (SVM) Model [J]. Iranian Journal of Science & Technology Transaction and Science, (2018), 42: 959-

965.
[78] Jingjun Lin, Xiaomei Lin, Lianbo Guo,et al. Identification accuracy improvement for steel species using a least squares support vector machine and laser-induced breakdown spectroscopy [J]. Journal of Analytical Atomic Spectrometry, (2018), 33: 1545-1551.
[79] Tianbing Chen, Linying Zhang, Lin Huang, et al. Quantitative analysis of chromium in pork by PSO-SVM chemometrics based on laser induced breakdown spectroscopy [J]. Journal of Analytical Atomic Spectrometry, (2019), 34: 884-890.
[80] Lei Zhang, Yao Gong, Yufang Li, et al. Development of a coal quality analyzer for application to power plants based on laser-induced breakdown spectroscopy [J]. Spectrochimica Acta Part B Atomic Spectroscopy, (2015), 113: 167-173.
[81] Haobin Peng, Guohua Chen, Xiaoxuan Chen, et al. Hybrid classification of coal and biomass by laser-induced breakdown spectroscopy combined with K-means and SVM [J]. Plasma Science and Technology, (2019), 21: 64-72.
[82] Kramida, A.; Ralchenko, Y.; Reader, J.; NIST ASD Team. NIST Atomic Spectra Database (ver. 5.6.1), [Online]. Available: https://physics.nist.gov/asd; National Institute of Standards and Technology: Gaithersburg, MD, (2018).
[83] Rifai K , Laville S , Vidal F , et al. Quantitative analysis of metallic traces in water-based liquids by UV-IR double-pulse laser-induced breakdown spectroscopy [J]. Journal of Analytical Atomic Spectrometry, (2012), 27: 276-283.
[84] Caneve L , Colao F , Fantoni R , et al. Laser ablation of copper based alloys by single and double pulse laser induced breakdown spectroscopy[J]. Applied Physics. A, Materials Science & Processing, (2006), 85: 151-157.
[85] Tognoni E , Cristoforetti G . Basic mechanisms of signal enhancement in ns double-pulse laser-induced breakdown spectroscopy in a gas environment[J]. Journal of Analytical Atomic Spectrometry, (2014), 29:1318-1338.
[86] Andrew J. Effenberger, Jill R. Scott. Effect of atmosphere on collinear double-pulse laser-induced breakdown spectroscopy [J]. Analytical and Bioanalytical Chemistry, (2011), 400: 3217-3227.
[87] Nicolodelli G , Senesi G S , Perazzoli I L D O , et al. Double pulse laser induced breakdown spectroscopy: A potential tool for the analysis of contaminants and macro/micronutrients in organic mineral fertilizers [J]. Thence of the Total Environment, (2016), 565: 1116-1123.

Acknowledgements

It is very important for me to have the opportunity to study in Xi'an Jiaotong University and Tokushima University, for double degree courses. I have learned a lot about how to do the research during this period. The understanding of society and the research work has been improved.

Thanks Prof. Yoshihiro Deguchi for his kind and serious supervision, and the help to the experiments setup and the paper publication. In the period that I studied in Japan, he has given me a lot of caring about the life also. He has taught me how to control the plasma process and states based on the change of laser beam pulse width. For fly ash powder flow measurement, Prof. Deguchi has taught me using 1ns pulse width laser to decrease the interference of surrounding CO_2. For steel measurement, Prof. Deguchi has firstly proposed the long-short DP-LIBS method to pretreat the sample surface and stabilize plasma, which greatly increased the behavior of LIBS measurement on steel.

Thanks Prof. Zhenzhen Wang for her detail supervision. As for the conference and journal paper submission, there are many points I have learned from her. During the years when I was studying for my Ph.D., she gave me lots of unselfish help.

Thanks Prof. Jiping Liu and Prof. Junjie Yan, for their kind caring and budget support, which give me the chance to enlarge the research on fly ash LIBS measurement, which is important for my Chinese dissertation.

Thanks Minchao Cui, Akihiro Ikutomo and Kai Rong, I have worked with them for the steel measurement, and there are great help from them to establish the experimental systems and finish the journal paper.

Thanks Weigang Nan, Shunpei Katsumori and Ruomu Hu for the research of fly ash, which is the important thesis for my Chinese dissertation.

Finally, thanks my parents for a long-time support!

Achievements

[1] **Renwei Liu**, Kai Rong, Zhenzhen Wang, Minchao Cui, Yoshihiro Deguchi, Seiya Tanaka, Junjie Yan, and Jiping Liu. Sample Temperature Effect on Steel Measurement Using SP-LIBS and Collinear Long-short DP-LIBS. ISIJ International, (2020), Vol.60, No.8.

[2] **Renwei Liu**, Yoshihiro Deguchi, Weigang Nan, Ruomu Hu, Zhenzhen Wang, Yuki Fujita, Seiya Tanaka, Kazuki Tainaka, Kenji Tanno, Hiroaki Watanabe, Jiping Liu, Junjie Yan. Unburned carbon measurement in fly ash using laser-induced breakdown spectroscopy with short nanosecond pulse width laser. Advanced Powder Technology, (2019), Vol.30, Page.1210-1218.

[3] Zhenzhen Wang, Yoshihiro Deguchi, **Renwei Liu**, Akihiro Ikutomo, Zhenzhen Zhang, Daotong Chong, Junjie Yan, Jiping Liu, and Fang-Jung Shiou. Emission Characteristics of Laser-Induced Plasma Using Collinear Long and Short Dual-Pulse Laser-Induced Breakdown Spectroscopy (LIBS). Applied Spectroscopy, (2017), Vol.7, No.9, Page.2187-2198.

[4] Minchao Cui, Yoshihiro Deguchi, Zhenzhen Wang, Yuki Fujita, **Renwei Liu**, Fang-Jung Shiou, Shengdun Zhao. Enhancement and stabilization of plasma using collinear long-short double-pulse laser-induced breakdown spectroscopy. Spectrochimica Acta Part B-Atomic Spectroscopy, (2018), Vol.142, Page.14-22.

[5] Zhenzhen Wang, **Renwei Liu**, Yoshihiro Deguchi, Seiya Tanaka, Kazuki Tainaka, Kenji Tanno, Hiroaki Watanabe, Junjie Yan, and Jiping Liu. Detection Improvement of Unburned Carbon Content in Fly Ash Flow Using LIBS with a Two-Stage Cyclone Measurement System. Energy &Fuels, (2019), Vol.30, No.8, Page.7805-7812.